

FOR REFERENCE ONLY

41 0640196 4



ProQuest Number: 10182980

All rights reserved

INFORMATION TO ALL USERS

The quality of this reproduction is dependent upon the quality of the copy submitted.

In the unlikely event that the author did not send a complete manuscript and there are missing pages, these will be noted. Also, if material had to be removed, a note will indicate the deletion.



ProQuest 10182980

Published by ProQuest LLC (2017). Copyright of the Dissertation is held by the Author.

All rights reserved.

This work is protected against unauthorized copying under Title 17, United States Code  
Microform Edition © ProQuest LLC.

ProQuest LLC.  
789 East Eisenhower Parkway  
P.O. Box 1346  
Ann Arbor, MI 48106 – 1346

326613

THE NOTTINGHAM TRENT UNIVERSITY LLR	
Short loan	PH D/BNS/04
Ref	Sim

# Mitochondrial biochemistry and its role in apoptosis

by

Tracy Dawn Simmons B.Sc. (Hons)

The school of biomedical and natural sciences  
Nottingham Trent University

A thesis presented in accordance with the regulations governing the  
award of the degree of Doctor of Philosophy in the Nottingham Trent  
University

September 2004

**Tracy Dawn Simmons**

**A thesis presented in accordance with the regulations governing the award of the degree of Doctor of Philosophy in the Nottingham Trent University**

**Mitochondrial biochemistry and its role in apoptosis  
Abstract**

Apoptosis is a form of programmed cell death that occurs throughout the lifespan of all living creatures. It is morphologically distinct from that of necrosis where one of the main distinguishing features between these two types of death is the maintenance of the plasma cell membrane during apoptosis and the avoidance of an inflammatory response. Many human disorders occur when the regulation of apoptosis fails and tissue homeostasis is lost.

Markers of apoptosis and necrosis include externalisation of phosphatidyl serine from the inner to the outer plasma cell membrane, loss of mitochondrial transmembrane potential, release of apoptogenic factors into the cytosol such as cytochrome c, DNA fragmentation and loss of plasma membrane integrity. These indicators of apoptosis and necrosis can be measured using flow cytometry or fluorescence microscopy. These methods are usually quite subjective and can involve lengthy procedures for their measurement.

This thesis describes the use of bioluminescent technology to measure the levels of ATP and ADP within samples of cells to assess cell viability, early and late apoptosis and necrosis. The bioluminescent ATP kit Vialight HS was able to measure a 96 well white plate in 5 minutes showing sensitivity and reliability over the ATP standard range and also down to 50 cells per well giving  $R^2$  values of 0.999 and 0.996 respectively. The ATP/ADP detection assay ApoGlow™ was found to correlate well with the traditional methods of measuring both apoptosis and necrosis. Bioluminescent technology was able to distinguish between apoptosis and necrosis when ApoGlow™ was used in conjunction with the ToxiLight assay, which measures the loss of the plasma membrane and thus dead cells with the release of adenylate kinase (AK) from the cell.

The ApoGlow™ assay would lend itself particularly well for use as a screening assay during testing of potentially cytotoxic drugs. Those drugs showing a response could then be investigated in more depth with other assays to confirm apoptosis and necrosis.

For Ezekiel

## **Acknowledgements**

I would like to thank the Haematology department at the Nottingham City Hospital for the staining of the cytopsin preparations.

I would also like to thank my supervisor, Dr Claire Scholfield, for her friendship and support throughout my thesis and Dr Ian Daniels at the David Evan's medical research centre, Nottingham City Hospital for his invaluable advice and encouragement throughout my studies and also for the staining of the cytopsin preparations for cytochrome c analysis.

Finally I would like to thank Ezekiel Simmons and Anthony Pitt for always being there.

## ***Abbreviations***

<b>ADP-CR</b>	ADP Converting Reagent
<b>AIF</b>	Apoptosis inducing factor
<b>AK</b>	Adenylate kinase
<b>AK-DR</b>	Adenylate Kinase Detection Reagent
<b>AMR</b>	ATP Monitoring Reagent
<b>ANT</b>	Adenine nucleotide translocator
<b>Apaf-1</b>	Apoptotic protease activating factor 1
<b>Ara-C</b>	1- $\beta$ -D-Arabinofuranosylcytosine
<b>BH</b>	Bcl-2 homology domain
<b>CAD</b>	caspase activated deoxyribonuclease
<b>CAM</b>	Camptothecin
<b>CARD</b>	Caspase activation and recruitment domain
<b>Caspase</b>	Cysteine aspartate –specific protease
<b>CED</b>	Cell death defective
<b>CM</b>	Complete media
<b>CrmA</b>	Cowpox virus product cytokine response modifier A
<b>DED</b>	Death effector domain
<b>DEX</b>	Dexamethasone
<b>FADD</b>	Fas associated death domain
<b>FLIPs</b>	Fas associated death domain like ICE inhibitory proteins
<b>IAP</b>	Inhibitor of apoptosis
<b>ICAD</b>	Inhibitor of CAD
<b>ICE</b>	Interleukin-1 $\beta$ converting enzyme
<b>JC-1</b>	5,5',6,6'-tetrachloro-1,1',3,3'-tetraethylbenzimidazolcarbocyanine iodide
<b>LDH</b>	Lactate dehydrogenase
<b>NMR</b>	Nucleotide Monitoring Reagent
<b>NRR</b>	Nucleotide Releasing Reagent
<b>PARP</b>	Poly (ADP-ribose) polymerase



<b>PI</b>	Propidium iodide
<b>PMT</b>	Photomultiplier tube
<b>PS</b>	Phosphatidyl serine
<b>PT</b>	Permeability transition
<b>RLU</b>	Relative light units
<b>Smac Diablo</b>	Second mitoderived activator of caspases direct IAP binding protein with low pl
<b>TAB</b>	Tris Acetate Buffer
<b>TNF</b>	Tumour necrosis factor
<b>VDAC</b>	Voltage dependent anion channel
<b>Z-VAD-FMK</b>	<i>N</i> -benzyloxycarbonyl-Val-Ala-Asp-fluoromethyketone
$\Delta\Psi_m$	Mitochondrial transmembrane potential

# Contents

	Page Number
Title	i
Abstract	ii
Dedication	iii
Acknowledgements	iv
Abbreviations	v
Contents	vii
<b>Chapter 1 – Introduction</b>	<b>1</b>
1.1 Cell death	1
1.1.1 The morphology of necrosis	2
1.1.2 The morphology of apoptosis	2
1.2 The machinery of apoptosis and its regulators	5
1.2.1 The discovery of genes encoding apoptosis	5
1.2.2 Caspases	5
1.2.2.1 Initiator caspases, caspase 8 and caspase 9	8
1.2.2.2 Effector caspase, caspase 3	11
1.2.2.3 Caspase inhibition	12
1.2.3 Involvement of the mitochondria	14
1.2.4 Regulation of apoptosis through the Bcl-2 family of proteins	18
1.3 Mitochondria	20
1.3.1 Structure	20
1.3.2 Metabolism of glucose for the synthesis of ATP	22
1.3.3 Glycolysis	23
1.3.4 Citric acid cycle	24
1.3.5 Electron transport chain	26
1.4 Bioluminescence	28
1.4.1 Measuring bioluminescence	30
1.4.2 Bioluminescent assays	31
1.4.2.1 ViaLight HS	31
1.4.2.2 ApoGlow™	32
1.5 Flow cytometry	34
1.6 Aims of the study	39

<b>Chapter 2 – Materials and methods</b>	<b>40</b>
2.1 Materials	40
2.2 Cell lines	42
2.2.1 Suspension cells	42
2.2.2 Culturing suspension cells	42
2.2.3 Adherent cells	43
2.2.4 Culturing Adherent cells	43
2.3 Counting cells	44
2.4 The structure, mechanism and preparation of the apoptosis inducing agents	45
2.4.1 Structure and mechanism of apoptosis induction	45
2.4.2 Preparation of the apoptosis inducing agents	48
2.4.3 Preparation of the caspase inhibitor	48
2.5 Preparation of apoptotic models	49
2.5.1 Preparation of suspension cell apoptotic models	51
2.5.2 Preparation of washing experiments	50
2.5.3 Preparation of apoptotic models with the general caspase inhibitor caspase inhibitor I (Z-VAD-FMK)	51
2.5.4 Preparation of Met B neomycin and Met B Bcl-2 apoptotic models	52
2.6 Preparation of Necrotic model	52
2.7 Cell number curve	53
2.8 Preparation of Standards	54
2.8.1 ATP standards	54
2.8.2 ADP standards	55
2.9 Preparation of buffers, stains and kits	56
2.9.1 Preparation of buffers	56
2.9.2 Preparation of buffers required during Western blotting	58
2.9.3 Preparation of stains	57
2.9.4 Preparation of kits	58
2.10 Methods	61
2.10.1 Assessing cell morphology	61
2.10.1.1 Romanovsky stained cytospin preparations	61
2.10.2 Measurement of cell viability	61
2.10.2.1 Uptake of propidium iodide (PI)	61
2.10.2.2 Uptake of Trypan Blue	62
2.10.2.3 Measurement of ATP as a viability marker (ViaLight HS)	62

2.10.3 Assessment of apoptosis and necrosis within a cell population	63
2.10.3.1 Annexin V and PI.	63
2.10.3.2 The measurement of ATP and ADP (ApoGlow).	63
2.10.4 Measurement of percentage hypodiploid and cell cycle analysis using propidium iodide	64
2.10.5 Measurement of the change in mitochondrial transmembrane potential ( $\Delta\Psi_m$ )	64
2.10.6 Detection of Cytolysis	65
2.10.6.1 ToxiLight	65
2.10.6.2 CytoTox-ONE (Promega)	65
2.10.7 Measurement of Cytochrome c	66
2.10.8 Western blotting	67
2.10.8.1 DC Protein assay	69
2.10.9 Statistics	69
<b>Chapter 3 - Bioluminescent measurement of Adenosine nucleotides</b>	<b>70</b>
3.1 Introduction	70
3.2 Results	73
3.2.1 Measuring ATP using the ViaLight HS protocol	73
3.2.2 ATP standards	73
3.2.3 Measuring ATP within cells	76
3.2.4 Measuring the mitochondrial transmembrane potential ( $\Delta\Psi_m$ )	79
3.2.5 Development of the ApoGlow bioassay	91
3.2.6 Measuring apoptosis and necrosis	93
3.3 Discussion	99
<b>Chapter 4 – The comparison of bioluminescence with conventional methods of detecting apoptosis and necrosis</b>	<b>104</b>
4.1 Introduction	104
4.2 Results	107
4.2.1 Changes in apoptotic and necrotic cell morphology	107
4.2.2 Measuring apoptosis	108
4.2.3 Early indicators of apoptosis	108
4.2.3.1 Phosphatidyl serine 'flip' from the inner to the outer cell membrane	108
4.2.3.2 Detecting changes in the $\Delta\Psi_m$ with the dual emission potential sensitive probe JC-1	114
4.2.3.3 Measuring cytochrome c release from the inner mitochondrial membrane to the cytosol	121

4.2.4 Measuring later indicators of apoptosis	127
4.2.4.1 Detection of DNA fragmentation by the sub G <sub>0</sub> peak with the DNA binding probe propidium iodide	127
4.2.4.2 Detection of Cytolysis	136
4.2.5 Summary of results	138
4.3 Discussion	140
<b>Chapter 5 – The cells commitment to programmed cell death</b>	<b>146</b>
5.1 Introduction	146
5.2 Results	149
5.2.1 The apoptotic cascade and the cells commitment to apoptosis	149
5.2.2 The involvement of the caspases	155
5.2.3 Cytochrome c release	163
5.2.4 Apoptotic regulators	167
5.3 Discussion	169
<b>Chapter 6 – General Discussion</b>	<b>172</b>
<b>References</b>	

## **Chapter 1 – Introduction**

### **1.1 Cell death**

The general feeling around the concept of death is one of a tragic event, but death at the cellular level can mean the survival of the organism as a whole. It is essential that all cells within a multicellular organism function amicably with one another to maintain tissue homeostasis. Many human disorders occur when this balance between the life and death of individual cells breaks down (*McCarthy (2002), Miller and Marx (1998), Olson and Kornbluth (2001) and Zörnig (2001)*). Inappropriate increases in either cell survival or cell death can lead to diseases such as cancer, autoimmune disorders and Alzheimer's disease (*McCarthy (2002), Miller and Marx (1998), Olson and Kornbluth (2001) and Zörnig (2001)*). So it is not surprising to find that cell death and cell survival are closely regulated within multicellular organisms.

Some recognised forms of cell death are apoptosis, a multistep and highly organised process which avoids an immune reaction by the activation of phagocytic cells (*McCarthy (2002)*), autophagy, which involves bulk degradation of cellular proteins, a process essential during both the growth and development of the organism (*Zörnig (2001)*), oncosis, an accidental form of cell death caused by the failure of the ionic pumps of the plasma membrane resulting in swelling (*Majno and Joris (1995)*) and necrosis, a violent form of cell death producing cellular debris and the induction of an immune response within the organism (*McCarthy (2002)*). The immune response is one of the main distinguishing factors between the apoptotic and necrotic forms of cell death (*Morris et al (1984), Trump et al (1973), Wyllie et al (1980; 1987)*) where these two forms of death will be observed in more detail within this study.

The severity of the initial insult to the cell is usually the deciding factor between a necrotic or apoptotic death where both types of death have

been observed to occur within the same cell culture (*Shimizu et al (1996)*). This finding suggests a common pathway initially between these two modes of death until they are eventually triggered towards either a necrotic or apoptotic demise. It has been proposed that cells exposed to the same stimulus undergo a necrotic death as opposed to an apoptotic death when ATP stores are depleted (*Leist et al (1997)*, *Tsujimoto (1997)*).

### **1.1.1 The morphology of necrosis**

The first visual indicator of necrosis is an increase in cell size as the organelles become disorganised (*McCarthy (2002)*). The mitochondria are seen to swell as the mitochondrial inner membrane shrinks away from the outer membrane during accumulation of lipid rich particles inside the mitochondria. Initially there is little change observed in the chromatin, which disperses and becomes flocculent after cell structure has been lost and proteases, nucleases and lysosomal contents have been released. Eventually the cell membrane ruptures causing an inflammatory response as toxins are released into the surrounding area *in-vivo* (*Morris et al (1984)*, *Trump et al (1973)*, *Wyllie et al (1980; 1987)*). This permeability of the cell membrane allows for the entry of cell viability dyes such as propidium iodide (PI), which binds proportionally to DNA, so therefore the amount of fluorescence detected is proportional to the amount of DNA present and acts as a defining marker of necrotic cell death (*Ormerod (1998)*).

### **1.1.2 The morphology of apoptosis**

The machinery of apoptosis occurs in phases beginning with the initial insult to the cell and passing through into the commitment phase where the death signals received are believed to be no longer reversible (*Slee et al (1999)*, *Takahashi et al (1996)* and *Zamzami et al (2002)*). This commitment phase seems to coincide with the release of apoptogenic factors from the mitochondria to the cytosol (*Slee et al (1999)*) and a loss

of mitochondrial transmembrane potential (*Kroemer et al (1997) and Susin et al (1998)*). The activation of the caspases initiates the amplification phase of apoptosis and the eventual passage into the execution phase where the morphological characteristics of apoptosis can be observed (*Slee et al (1999), Takahashi et al (1996) and Zamzami et al (2002)*). In contrast to necrotic cells apoptotic cells show a decrease in the volume of the cell and the nuclear chromatin becomes greatly compressed early in the apoptotic cascade (*McCarthy et al (2002)*). The organelles within the cell are found to maintain a relatively normal appearance although there is dilation of the endoplasmic reticulum and slight swelling of the mitochondria. As the apoptotic pathway progresses internucleosomal cleavage of DNA occurs, which gives rise to the characteristic 'ladder' appearance on DNA electrophoresis gels (*Kerr and Currie (1972) and Wyllie et al (1980; 1984)*). DNA cleavage has been shown to be a relatively late event in the apoptotic cascade (*Tomei et al (1993)*). Other late morphological markers of apoptosis include the outer cell (plasma) membrane, which is seen to take on a convoluted appearance otherwise known as 'blebbing' as can be seen figure 1.01. This illustrates a cytopsin preparation of the human leukaemia cell line HL60. The slide shows a cell with normal appearance progressing into apoptosis with evidence of blebbing and chromatin condensation. Eventually membrane bound vesicles or apoptotic bodies are released from the cell.

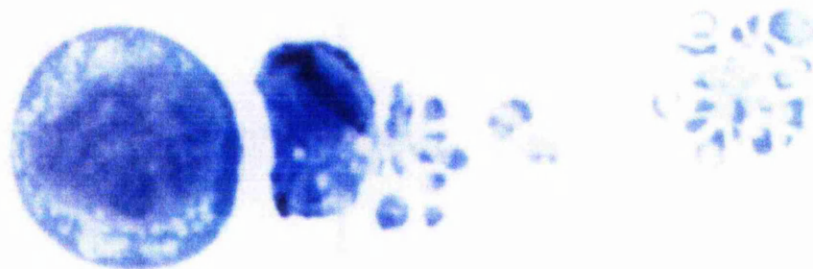


**Figure 1.01.** Cytospin preparations of HL60 cells stained and examined by light microscopy. The slide shows a cell with normal appearance progressing into apoptosis. Picture taken from 'Techniques in Apoptosis; a users guide' (*Gorman et al (1994)*).



It is believed at this stage *in-vivo* that it is the exposure of phosphatidyl serine (PS), that normally resides within the inner cell membrane, that allows for the phagocytosis of these apoptotic cells either by their neighbouring cells or professional macrophages (*Fadok et al (1992) and Savill et al (1993)*). It is this clean up of apoptotic cells whilst plasma membrane integrity has been maintained that stops the necessity of an inflammatory response. (*Morris et al (1984), Trump et al (1973) and Wyllie et al (1980; 1987)*). As phagocytosis of apoptotic cells does not occur *in-vitro* these cells are seen to eventually lose membrane integrity and become permeable to PI (*Ormerod (1998)*), this process as been termed secondary necrosis.

## 1.2 The machinery of apoptosis and its regulators

### 1.2.1 The discovery of genes encoding apoptosis

Much of our understanding of apoptosis at the genetic level came from studies carried out on the nematode worm *Caenorhabditis elegans* (*C. elegans*). Three genes were found to control the 131 cell deaths that occur to produce the adult worm, cell death defective (*ced*)-3, *ced*-4 and *ced*-9 (Ellis and Horvitz (1986) and Horvitz (1999)). Both the genes *ced*-3 and *ced*-4 were found to promote apoptosis whilst *ced*-9 was found to protect the cell from apoptosis (Zörnig et al (2001)). These regulators of the apoptotic death pathway are highly conserved within all multicellular organisms (McCarthy (2002) and Zörnig et al (2001)). The equivalent genetic homologues within mammalian cells have been identified as apoptotic protease activating factor 1 (*apaf*-1) for *ced*-4 and the *bcl*-2 family of proteins for *ced*-9 (McCarthy (2002) and Zörnig et al (2001)). Most attention in mammalian models has focused on the *ced*-3 gene where the equivalent genetic homologue to this gene in mammalian cells was found to be the interleukin-1 (IL-1)-converting enzyme (ICE)-like proteases or caspases, where some 14 other mammalian caspases have now been identified (Cohen (1997) and Wolf and Green (1999)).

### 1.2.2 Caspases

The name 'caspase' comes from the 'c' denoting a cysteine protease and the 'aspase' referring to the ability of these enzymes to cleave after an aspartic (Asp) acid residue (Nicholson (1999)). Caspases are produced as inactive zymogens and become activated following cleavage at aspartic acid residues, they consist of a large and small subunit and a prodomain (Nicholson (1999)). Figure 1.02 shows the typical structure of a procaspase.

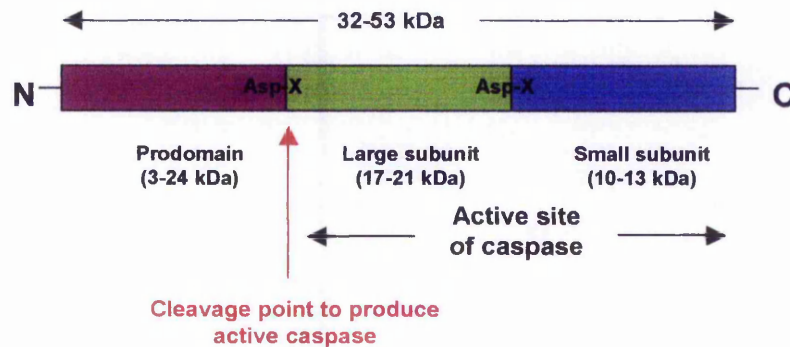


**Figure 1.02.** Structure of a procaspase, (*Nicholson (1999)*).

The caspase family of proteins can be divided into two major subfamilies these are the ICE subfamily and the ced-3 subfamily (*Nicholson (1999)*), where further divisions can be made depending upon the length of their prodomain. Only caspases 3, 6 and 7 have been found to have short prodomains below 10kDa in length (*Nicholson (1999)*). An alternative method for the grouping of the caspases involves their substrate specificities where caspases recognise a tetrapeptide motif. Conserved throughout the caspases is the necessary requirement for aspartic acid at  $P_1$  (*Cohen (1997)* and *Nicholson (1999)*) they are promiscuous at the sites of  $P_2$  and  $P_3$  (*Nicholson (1999)*) and can contain either a hydrophobic, aspartic acid or aliphatic residue at the site of  $p_4$  (*Nicholson (1999)*). The ICE family contains the group I caspases involved in inflammation requiring a hydrophobic residue at  $p_4$ , this group of caspases contains caspase 1, caspase 4, caspase 5 and caspase 13 (*Nicholson (1999)*). The ced-3 family contains both the group II and group III caspases both involved in apoptosis. The group II caspases have a specific requirement for a aspartic acid residue at  $p_4$  and contains the effector caspases which are caspase 2, caspase 3 and caspase 7. Group III contains the initiator caspases such as caspase 6, caspase 8, caspase 9 and caspase 10 where these caspases require a aliphatic residue at  $p_4$ , (*Nicholson (1999)* and *Roy and Cardone (2002)*), During apoptosis the initiator caspases activate the effector caspases in a

caspase cascade (*Nicholson (1999) and Roy and Cardone (2002)*). Although exceptions to this grouping do exist as in some apoptotic models caspase 2 has been found to be self activating and caspase 6 to be a down stream effector caspase (*Nicholson (1999)*).

The structure and function of the prodomain varies greatly between the caspases, those with large prodomains such as procaspases 2, 8, 9 and 10 are thought to be involved in the recruitment of the procaspase to the activation complex (*Nicholson (1999)*). The active caspase consists of the large and small subunits where the active sites of the cysteine and histidine residues are situated only on the large subunit whilst P<sub>1</sub> and its subsite S<sub>1</sub> are situated on both (*Nicholson (1999)*). X-ray crystal structures carried out on caspase 1 and caspase 3 have shown the structure of these two caspases to be similar (*Nicholson (1999)*), suggesting the structure to be conserved throughout the caspase family. Caspase structure was found to consist of a tetramer comprised of a large subunit, homodimer and a small subunit heterodimer (*Nicholson (1999)*). The two dimers orientate themselves in a configuration whereby the two active sites are opposed to one another (*Nicholson (1999)*).

Activation of the procaspase can be achieved through a number of mechanisms such as recruitment activation (or oligomerisation) and transactivation (*Nicholson (1999) and Roy and Cardone (2002)*). Recruitment activation seems to involve the activation of the initiator caspases and depending upon the stimulus received occurs at either the membrane during death receptor mediated activation or within the cytosol during cytotoxic insult (*Roy and Cardone (2002) and Zheng et al (1999)*). Two of the caspases observed within this study, caspase 8 and caspase 9, are activated via this mechanism. Another form of activation, transactivation, utilises the fact that all caspases contain asp artic acid in their P<sub>1</sub> site and therefore once activated can themselves then activate other procaspases thus giving rise to the caspase cascade (*Zheng et al (1999)*). This form of activation is evident during activation of caspase 9 (*Nijhawan et al (1997), Srinivasula et al (1998) and Hirata et al (1998)*).

Upon activation caspase 9 transactivates caspases 3 and 7 forming an amplification loop as activated caspase 3 can itself cleave procaspase 9 (Slee *et al* (1999)). Caspase 3 is believed to be involved in the proteolysis of other important molecules during apoptosis such as the cleavage of Poly (ADP-ribose) Polymerase (PARP) (Roy and Cardone (2002)) and ICAD (Clarke (2002)).

### 1.2.2.1 Initiator caspases, caspase 8 and caspase 9

As stated previously the initiator caspases appear to be activated through oligomerisation and formation of activation complexes. Figure 1.03 is a schematic of the induction of apoptosis through either a death receptor mediated pathway via interactions between the death effector domains (DED) or through a cytotoxic pathway via the caspase activation and recruitment domain (CARD).

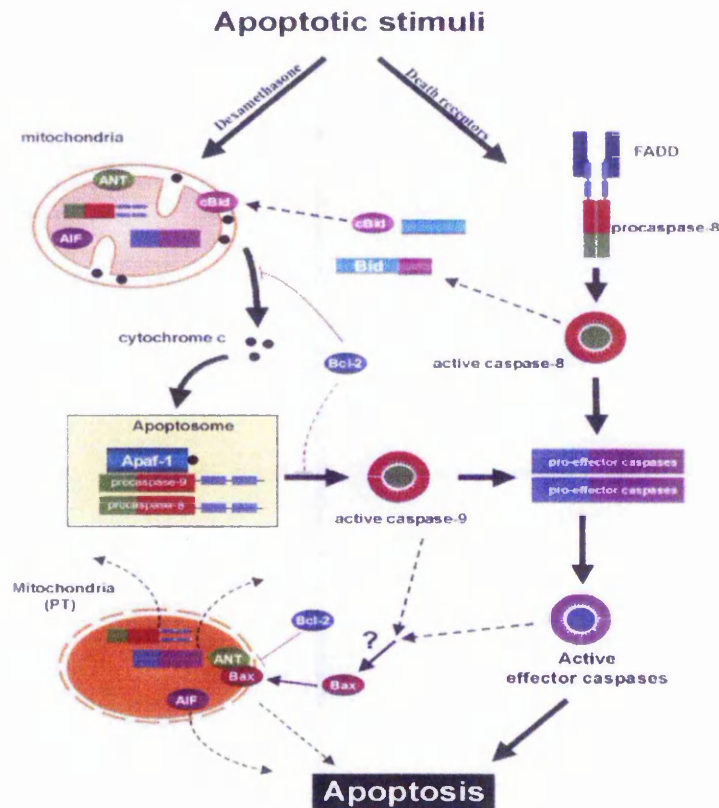


**Figure 1.03.** Apoptotic pathways and caspase activation during death receptor mediated and cytotoxic induced apoptosis (Zheng *et al* (1999)).

The death receptor CD95 (or Fas) belongs to the tumour necrosis factor (TNF) family of receptors. It is expressed on the surface of cells along with its ligand (CD95L / FasL). CD95L causes activation of the receptor upon binding through the formation of a trimeric molecule (*Bajorath and Aruffo (1997)*). Figure 1.04 shows the interactions between the CD95 receptor and its ligand during the activation of caspase 8.

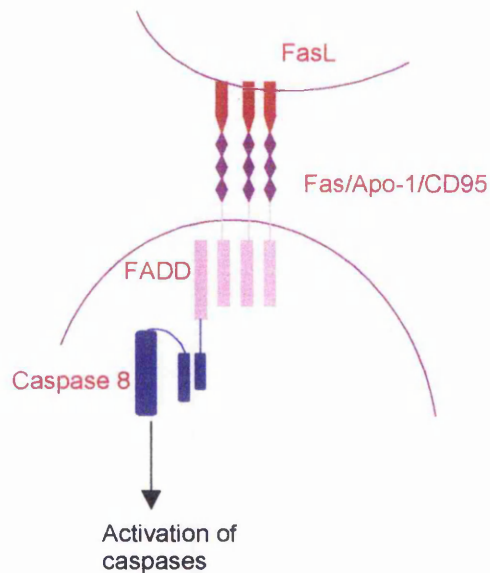


**Figure 1.04.** Mechanism of apoptosis by the interaction between Fas (CD95) and Fas Ligand (CD95L) (*Osborne (1996)*).

Trimerisation of the death receptor CD95 during its association with the ligand recruits the adapter protein FADD (fas associating protein with death domain) where it interacts with the receptor via their death effector domain (DED). Following this the activation complex is formed and caspase 8 is activated upon binding of the procaspase 8 to the complex. Procaspase 8 exists as a 55kDa enzyme and during apoptosis is first cleaved into an intermediate cleavage product of 41kDa and subsequently processed to the 18kDa active form (*Nicholson (1999)*). Active caspase 8 then transactivates the effector caspases such as caspase 3, an important caspase in the initiation of the caspase cascade (*Zheng et al (1999)*) and the eventual demolition of the cell by the proteolysis of other important molecules during apoptosis, such as the

activation of the nuclease CAD (caspase activated deoxyribonuclease) from its inactive form ICAD (inhibitor of CAD), (Clarke (2002)). Caspase 8 contains two DED within its prodomain region, one for the formation of the activation complex and the other is believed to be involved in the stabilisation or homodimerisation of the complex (Kumar (1999)).

Caspase 8 has been found to regulate erythropoiesis and the normal development of the heart (Zheng *et al* 1999)). Mutation of the catalytic cysteine residue of active caspase 8 results in an isoform of caspase 8 with no apoptotic function. Expression of active caspase 8 in the presence of these isoforms resulted in little cell death. Similarly, these isoforms were found to block cell death induced by CD95, suggesting that the isoforms exert a dominant-negative effect and may be important in the regulation of apoptosis *in vivo* (Cohen (1997)).

Activation of procaspase 9 involves the formation of the apoptosome. Upon its release into the cytosol during apoptosis cytochrome c binds to Apaf-1 causing a conformational change exposing its CARD domain. This change is stabilised by the binding of ATP, which in turn allows the joining of seven molecules of Apaf-1 together with cytochrome c and ATP to produce the apoptosome (figure 1.05).

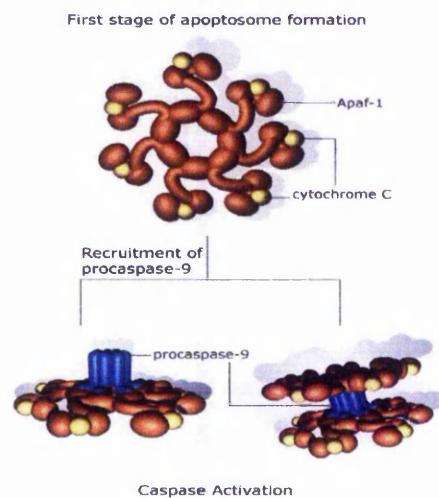


**Figure1.05.** Formation of the apoptosome, (Whitley *et al* (2004)).

This enables the recruitment of seven molecules of procaspase 9 to the apoptosome where they bind to Apaf-1 via their CARD to CARD domains (*Whitley et al (2004)*). Upon binding procaspase 9 is cleaved and activated resulting in the caspase cascade (*Zheng et al (1999)*). Active caspase 9 activates the effector caspase 3 and enters into an amplification loop whereby active caspase 3 can further activate caspase 9 (*Roy and Cardone (2002)*). The activation of caspase 3 by caspase 9 has been found to be an essential apoptotic pathway for the normal development of the brain through neuronal cell death. It has also been demonstrated that granzyme B can activate pro-caspase-9, although to differently sized products than those formed by caspase 3 activation. Inactive caspase 9 has a molecular weight of 46kDa, caspase 3 was found to cleave at Asp-330, generating two products of molecular masses 37 kDa and 10 kDa. Granzyme B however cleaved procaspase-9 with a preference for Asp-315 over Asp-330 thereby generating the active enzyme (*Cohen (1997)*).

#### **1.2.2.2 Effector caspase, caspase 3**

Caspase 3 is classed as an effector caspase and as such is activated downstream in the caspase cascade where its activation by the initiator caspase, caspase 9, has been found to be an absolute requirement of neuronal cell death and normal brain development (*Zheng et al (1999)*). Once activated, caspase 3 can form an amplification loop as activated caspase 3 cleaves procaspase 9 (*Slee et al (1999)*). In its inactive form caspase 3 exists as a 32kDa proenzyme and is cleaved into active subunits of 17kDa and 11kDa early during apoptosis by cleavage at Asp-28–Ser-29 and Asp-175–Ser-176 (*Cohen (1997)*). X-ray crystallography carried out on caspase 3 has shown it to be comprised of a tetramer consisting of a large subunit homodimer and a small subunit heterodimer (*Nicholson (1999)*) which orientate themselves in a configuration whereby the two active sites are opposed to one another (*Nicholson (1999)*).



Caspase 3 can also be known as an execution caspase, cleaving proteins supporting both the nuclear membrane and components of the cytoskeleton allowing for further dismantling of the cell and eventual disposal through phagocytosis. Caspase 3 has been found to be responsible either partially or wholly for the proteolysis of numerous substrates, such as the cleavage of the nuclear enzyme PARP (*Cohen (1997) and Roy and Cardone (2002)*) and DNA-PK<sub>CS</sub> a double strand break DNA repair protein (*Song et al (1996)*). Caspase 3 was found to be the deciding caspase in the proteolytic cleavage of gelsolin and Pak2 substrates responsible for the fragmentation of DNA and nuclear condensation during apoptosis (*Zheng et al (1999)*) and is also responsible for the proteolysis of the active form of CAD from ICAD (*Clarke (2002)*).

#### **1.2.2.3 Caspase inhibition**

The first instance of caspase inhibition was identified during investigations of viral pathogenesis (*Roy and Cardone (2002)*). In order to invade the host cell and to prevent an inflammatory response leading to their demise, viruses were found to encode anti apoptotic genes (*Ekert et al (1999) and Roy and Cardone (2002)*). The cowpox virus was found to contain cowpox virus product cytokine response modifier A (CrmA), a cytokine that inhibits caspase 1, thereby preventing an immune response (*Ekert et al (1999) and Roy and Cardone (2002)*). Further studies with CrmA showed the capabilities of the cytokine to inhibit some of the apoptosis related caspases. Caspase 8 was mostly affected with only slight inhibition of caspase 10. Caspases 3, 6 and 7 were completely unaffected by CrmA (*Cohen (1997) and Ekert et al (1999)*). This data would suggest that CrmA is specific for the initiator caspases, however the finding that CrmA had no affect upon caspase 9 when studied *in vitro* (*Ekert et al (1999)*) would perhaps suggest a interaction between CrmA and the prodomain of the caspase, as both caspases 8 and 10 contain the DED domain and caspase 9 contains a CARD domain. The affects of CrmA were completely lost in caspases with no prodomain.

Viruses have also been found to encode Fas associated death domain like ICE inhibitory proteins (FLIPs) to aid in their survival by manipulation of the CD95 death signalling pathway and cell suicide (*Zornig et al (2001)*). The  $\gamma$ -herpesviruses has been found to interact with FADD to inhibit its recruitment and activation of caspase 8 (*Zornig et al (2001)*).

The inhibitor of apoptosis protein (IAP) exists in all mammalian cells, yeasts, *C. elegans* and *Drosophila* (*Ekert et al (1999)*). It was first discovered by *Miller and Marx (1998)* and identified as a baculoviral product capable of suppressing apoptosis of cells infected with a baculoviral strain containing a p35 deletion (*Crook et al (1993)*). IAP's work by inhibiting selected caspases therefore repressing specific apoptotic pathways (*Roy and Cardone (2002)*). IAP's have been observed to work in two ways by either inhibiting activation of the procaspase in the first place or by inhibiting the activity of the caspase upon activation (*Roy and Cardone (2002)*). The IAP's block mitochondrial pathways by inhibiting the formation of the apoptosome by blocking caspase 9 and Apaf-1 interactions and preventing cleavage and activation of caspase 9 through caspase 3 (*Roy and Cardone (2002)*). By blocking caspase 3 and 7 activity and the formation of the apoptosome the IAP's ensure inhibition of apoptosis in cells undergoing apoptosis via the mitochondrial route and cells bypassing this pathway (*Roy and Cardone (2002)*).

As uncontrolled apoptosis has been identified as the root cause of many human disorders the development of synthetic caspase inhibitors for pharmacological use has gathered momentum (*Ekert et al (1999)*). Synthetic caspase inhibitors are developed based upon the substrate cleavage site of the caspase and as such are competitive inhibitors of this region. Z-VAD-FMK used in this study is an irreversible, general caspase inhibitor, containing three aspartate residues and has been proven useful in many experimental studies to inhibit the effects of apoptosis (*Nicholson (1999)*).

### 1.2.3 Involvement of the mitochondria

The involvement of the mitochondria is pivotal to the regulation of both death signalling and cell survival mechanisms during apoptosis (*Loeffler and Kroemer (2000), Olson and Kornbluth (2001), Susin et al (1996), Wang (2001) and Zamzami et al (2002)*). This is evident in the action of both the anti and promoting members of the Bcl-2 family of proteins upon the mitochondria (*Tsujimoto (2002)*). The irreversible opening of permeability transition (PT) pores has been found to occur early during apoptosis leading to a loss of the mitochondrial transmembrane potential ( $\Delta\Psi_m$ ) (*Susin et al (1996) and Zamzami et al (2002)*). The release of apoptosis promoting proteins from the mitochondria to the cytosol during PT pore formation has also been shown to occur early during apoptosis (*Wang (2001) and Zamzami et al (2002)*).

Mitochondria are the main site of ATP synthesis (*Alberts et al (1989)*) and as all cells have an absolute requirement for ATP its depletion would be an accurate indicator of the viability of the mitochondria and the cell itself (*Crouch et al (1993)*). When ATP stores are depleted it has been proposed that cells exposed to the same stimulus will undergo a necrotic death as opposed to an apoptotic death (*Leist et al (1997)*). This supports the theory that whilst programmed cell death requires ATP it is not necessary during necrosis (*Tsujimoto (1997)*). The  $\Delta\Psi_m$  occurs due to the flow of electrons across the inner mitochondrial membrane during the synthesis of ATP in a process called oxidative phosphorylation (*Alberts et al (1989)*). Energy is released as electrons flow through the complexes of the inner mitochondrial membrane and fall to a lower energy state. This release of energy actively transports  $H^+$  ions from the matrix to the intermembrane space, thus making the matrix negatively charged and the intermembrane space positively charged (*Alberts et al (1989)*). This exchange of ions across the inner mitochondrial membrane can be detected by cationic lipophilic fluorochromes such as 5,5',6,6'-tetrachloro-1,1',3,3'tetraethylbenzimidaz-

zolcarbocyanine iodide (JC-1), 3,3'-dihexyloxacarbocyanine iodide (DiOC<sub>6</sub>) and Rhodamine123 (Rh123) through fluorescent microscopy and flow cytometric analysis (*Ormerod (1998)*). Functioning mitochondria in viable cells have a high  $\Delta\psi_m$  and as a consequence actively uptake the dyes (*Salvioli et al (2000)*). The lack of uptake of these dyes therefore is indicative of a loss of the  $\Delta\psi_m$  and can be used to measure the mitochondrial state. The loss of the  $\Delta\psi_m$  has been found to occur early during apoptosis regardless of cell type and apoptotic stimulus, preceding exposure of PS and DNA fragmentation (*Mignotte and Vayssiere (1998) and Susin et al 1996*)).

One suggestion for the disruption of the  $\Delta\psi_m$  is the irreversible opening of megachannels or permeability transition (PT) pores, which span the inner and outer mitochondrial membranes (*Mignotte and Vayssiere (1998) and Susin et al 1996*)). These pores are necessary for the equilibrium of essential ions between the cytosol and the mitochondrial matrix, two major components of which are the adenine nucleotide translocator (ANT) situated within the inner mitochondrial membrane and the voltage dependent anion channel (VDAC) situated on the outer mitochondrial membrane (*Zörnig et al (2001)*). One theory for the opening of these PT pores is the binding of a pro-apoptotic member of the Bcl-2 family of proteins Bax to the ANT causing depolarisation and permeabilisation of the mitochondria (*Zörnig et al (2001)*). Another model that predicts mitochondrial swelling as the culprit for the eventual loss of the  $\Delta\psi_m$  is the closure of the voltage dependent anion channel (VDAC). Closure of the VDAC would result in disruption of the exchange of ATP and ADP across the mitochondrial membrane leading to hyperpolarisation and subsequent matrix swelling (*Zörnig et al (2001)*). As the inner membrane has an overall larger surface area than the outer membrane due to being folded into cristae, the swelling of the matrix eventually leads to outer membrane rupture (*Susin et al (1996) and Zörnig et al (2001)*). The rupture of the mitochondrial membrane would result not only in the disruption of the  $\Delta\psi_m$  but also in the release of apoptogenic factors from the mitochondria to the

cytosol (*Wang (2001) and Zamzami et al (2002)*). Apoptogenic factors include cytochrome c, apoptosis inducing factor (AIF) and Smac Diablo (second mitoderived activator of caspases direct IAP binding protein with low pI) (*Loeffler and Kroemer (2000), Wang (2001) and Zamzami et al (2002)*). Cytochrome c was the first of these proteins to be identified for its apoptogenic properties where its release into the cytosol is essential during the formation of the apoptosome (*Loeffler and Kroemer (2000), Wang (2001), and Zamzami et al (2002)*). It has been observed that the caspase activating property of cytochrome c is only present when it is in the holocytochrome c form containing a haem group and not in the apocytochrome c form (*Zamzami et al (2002)*). Research has revealed that microinjection of cytochrome c into the cell does not always induce apoptosis (*Garland and Rudin (1998) and Deshmukh and Johnson (1998)*), which would suggest that other factors are required in addition to cytochrome c for the cells commitment to die.

Apoptosis inducing factor (AIF) is a FAD binding flavo protein, whose structure is highly conserved between different species (*Susin et al (1999)*). As isolated AIF showed no nuclease activity in itself it is thought to induce some of the nuclear morphology associated with apoptosis through the activation of nucleases (*Susin et al (1996)*). Its effects on purified mitochondria suggest it works independently of caspases as addition of the broad spectrum caspase inhibitor Z-VAD-FMK does not alter the apoptotic outcome or loss of the  $\Delta\Psi_m$  and release of cytochrome c (*Zamzami et al (2002)*).

There is evidence to suggest that cytochrome c release precedes mitochondrial depolarisation, loss of the  $\Delta\Psi_m$  and mitochondrial rupture (*Finucane et al (1999) and Sanchez-Alcazar et al (2000)*), suggesting an alternative mechanism for the release of these apoptogenic factors from the mitochondria involving the formation of pores. Bax is a prime candidate for the formation of such pores as it has been observed that oligomers of Bax can form large conductance channels showing similarity

to the pore forming properties of the diphtheria toxin (*Muchmore et al (1996)*). Bax can either act alone or in conjunction with the VDAC to form these conducting channels (*Zörnig et al (2001)*). Oligomerisation of Bax is thought to occur through the binding of another member of the Bcl-2 family, Bid. Bid is first cleaved by active caspase 8 where in its truncated form binds to Bax causing a conformational change (*Zornig et al (2001)*). This change in the structure of Bax is believed to expose the NH<sub>2</sub>-terminal domain (*Hsu et al (1997)*) allowing for its oligomerisation and insertion into the mitochondrial membrane (*Eskes et al (2000)* and *Desagher et al (1999)*). The opening of these pores can then lead to the release of cytochrome c (*Desagher et al (1999)*). A candidate for the regulation of the formation of these PT pores seems to be Bcl-2, which is localised to the membranes of the mitochondria, nucleus and endoplasmic reticulum (*Tsujimoto (2002)*). It has been observed that Bcl-2 can recruit other proteins to the mitochondrial membrane such as Raf 1 kinase appearing to reinforce the protective properties of Bcl-2 (*Wang (1996)*). It has been proposed that the sensitivity of leukaemia cells to cytochrome c release due to TNF $\alpha$  exposure, is due to the ratio between the pro and anti apoptotic members of the Bcl-2 family of proteins (*Li Jia et al (1999)*). The CEM/VLB cell line used in this study was shown to contain a higher level of the pro apoptotic proteins Bcl-x<sub>s</sub> and Bad than CEM cells and as a result were found to be more susceptible to apoptosis (*Li Jia et al (1999)*). The protective properties of Bcl-2 have been observed during death receptor mediated apoptosis on type 1 and type 2 cells. In type 1 cells a more direct route is taken which bypasses the involvement of the mitochondria altogether (*Slee et al (1999)*). Apoptosis induced by death receptors in type 2 cells however is routed through the mitochondria. Evidence of these two pathways lies in the observation that the protective properties of Bcl-2 are lost in type 1 cells but not in type 2 cells (*Slee et al (1999)*).

#### 1.2.4 Regulation of apoptosis through the Bcl-2 family of proteins

The Bcl-2 family of proteins, as mentioned earlier, are pivotal to the regulation of apoptosis and seem to exert their influence at the level of the mitochondria. They share four conserved Bcl-2 homology (BH) domains and can either inhibit apoptosis, such as the Bcl-2 and Bcl-x<sub>L</sub> proteins, or be promoters of apoptosis, such as Bax, Bcl-x<sub>s</sub>, Bid and Bad. The regions BH1, BH2 and BH4 have been found to be necessary for the anti apoptotic activity of the protein whereas BH3 is essential to promote apoptosis (*Huang et al (1998) and Chittenden et al (1995)*). The apoptotic properties of the BH3 domain are evident in the apoptosis promoting proteins Bid and Bad, which are BH3 domain only proteins. A key feature of these proteins is their ability to interact with one another for the regulation of apoptosis by the formation of heterodimers and homodimers (*Oltvai et al (1993)*). The neutralisation of both the anti apoptotic and apoptosis promoting effects of Bcl-2 and Bax upon formation of heterodimers has been observed (*Belzacq et al (2003)*). It is thought that it is the ratio of anti apoptotic and apoptosis promoting members of Bcl-2 proteins that decides the cell's fate (*Li Jia et al (1999)*).

The continual presence of Bcl-2 at the mitochondria has two functions; one to prevent non-specific permeabilisation of the mitochondrial membrane and two to maintain the passage of molecules across the mitochondria. Bax however is only translocated to the mitochondria during apoptosis, where a death outcome is favoured only if Bax is in greater supply (*Li Jia et al (1999)*). The oligomerisation of Bax and its translocation to the mitochondria is believed to be as a direct consequence of the binding of the BH3 only protein Bid. Bid is first cleaved by active caspase 8 where in its truncated form binds to Bax causing a conformational change. This change in the structure of Bax is believed to expose the NH<sub>2</sub>- terminal domain (*Hsu et al (1997)*) allowing for the oligomerisation and insertion of Bax into the mitochondrial membrane (*Eskes et al (2000) and Desagher et al (1999)*).

It has been suggested that Bax interacts with either the VDAC or the ANT to irreversibly open PT pores whereas Bcl-2 works to suppress this action (*Brenner et al (2000)*). Upon the opening of PT pores Bcl-x<sub>L</sub> is thought to exert an apoptotic inhibitory effect through interactions with Apaf-1 blocking the formation of the apoptosome upon release of cytochrome c from the mitochondria (*Tsujimoto (2002)*). It has been observed however that Bcl-2 is incapable of blocking apoptosome mediated activation of caspase 9 (*Newmeyer et al (2000)*).



### 1.3 Mitochondria

Mitochondria are sites of high energy production essential to drive the normal activity of the cell (*Alberts et al (1989)*). The positioning of the mitochondria within the cell is unique to each particular cell type, where their association with microtubules seems to determine the orientation and distribution of the mitochondria within the cell (*Alberts et al (1989)*). They become localised to sites of high ATP consumption, such as packed between adjacent myofibrils in a cardiac muscle cell (*Alberts et al (1989)*). They are usually between 0.5 $\mu\text{m}$  and 1.0 $\mu\text{m}$  in diameter and consist of an outer membrane, intermembrane space, inner membrane and matrix (*Alberts et al (1989)*).

#### 1.3.1 Structure

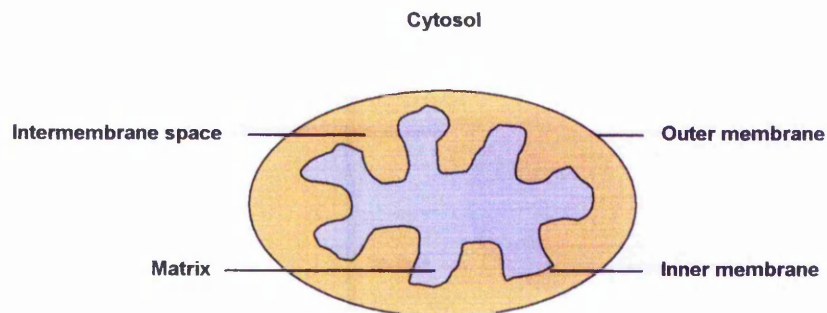


**Figure 1.06.** Structure of a typical mitochondrion (*Alberts et al (1989)*).

The appearance of the outer and inner membranes of the mitochondria are different to one another due to the folding of the inner membrane into cristae, this greatly increases the inner membrane's surface area over that of the outer membrane (*Alberts et al (1989)*). The convoluted appearance and the number of cristae within mitochondria vary between different cell types (*Alberts et al (1989)*), presumably as a reflection of the ATP demand upon that particular cell type. The inner membrane is the main site of synthesis of ATP and contains the proteins necessary for

oxidative phosphorylation (*Spence and Mason (1992)*). As the process of oxidative phosphorylation sets up an electrochemical gradient across the inner membrane, it is essential that the inner membrane is impermeable to most small ions. As a result it contains transport proteins such as the adenine nucleotide translocator (ANT) for the regulation of this (*Alberts et al (1989) and Spence and Mason (1992)*). The enzyme complex ATP synthetase, required for the synthesis of ATP within the matrix, is also contained within the inner membrane (*Alberts et al (1989) and Spence and Mason (1992)*).

As the outer membrane contains the voltage dependent anion channel (VDAC), a large channel forming protein, it is permeable to molecules of up to 10,000 daltons in size. The outer membrane also contains proteins involved in both the synthesis and conversion of lipids, the substrates of which are metabolised within the matrix (*Alberts et al (1989)*).

The intermembrane space is positively charged due to the transport of  $H^+$  ions from the matrix to the intermembrane space, thus making the matrix negatively charged (*Alberts et al (1989)*). The matrix is not only the site of ATP synthesis through the ATP synthetase complex but also contains enzymes critical for the oxidation of pyruvate and fatty acids, essential for the citric acid cycle, a process which takes place within this region (*Alberts et al (1989)*). The ATP produced within the matrix passes into the intermembrane space and is utilised for the phosphorylation of nucleotides. Mitochondrial DNA synthesis is also carried out within the matrix (*Alberts et al (1989)*).

### 1.3.2 Metabolism of glucose for the synthesis of ATP

The cytosol is the point at which the synthesis of ATP begins in a process called glycolysis, whereby glucose is broken down into pyruvic acid and in the presence of oxygen will continue through into the citric acid cycle and the electron transport chain (figure 1.04; *Alberts et al (1989) and Spence and Mason (1992)*).

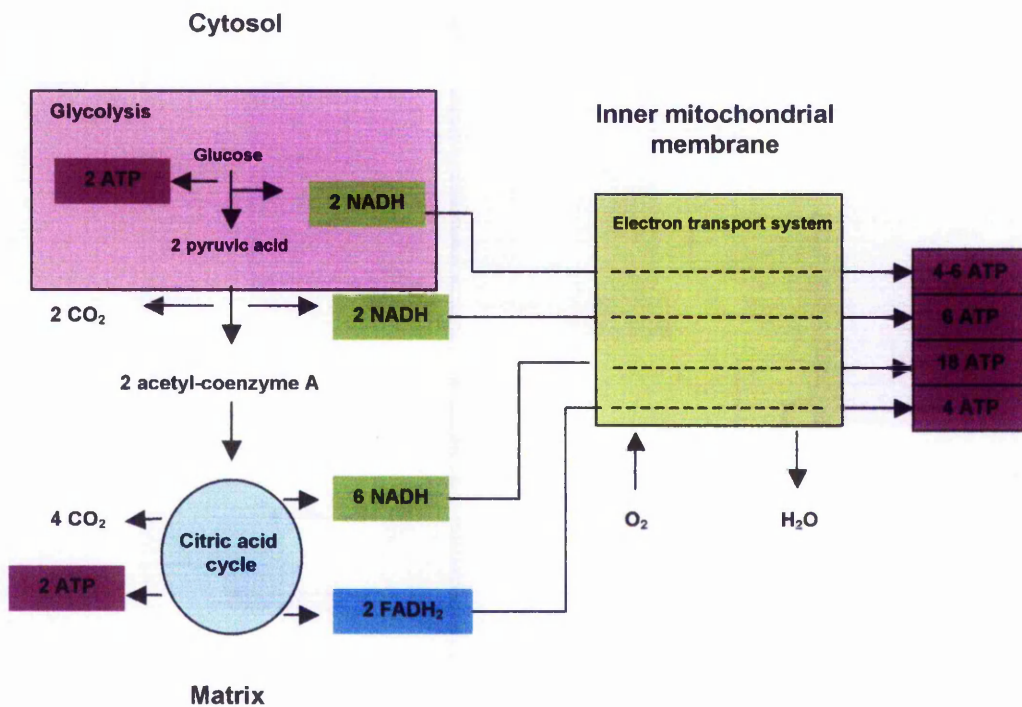


**Figure 1.07.** The pathway of the aerobic breakdown of glucose and its yield of ATP (*Spence and Mason (1992)*)

The process continues through a series of controlled reactions where the product from one process is usually the substrate for the next, eventually yielding 36-38 molecules of ATP. Lack of oxygen will push the breakdown of pyruvic acid towards conversion to lactic acid yielding only a small amount of ATP thus showing the aerobic breakdown of glucose to be the more efficient method.

### 1.3.3 Glycolysis

The glycolytic reaction is an anaerobic one taking place within the cytosol of the cell (*Alberts et al (1989) and Spence and Mason (1992)*). The main features of this reaction are the reduction of two molecules of  $\text{NAD}^+$  to  $\text{NADH}$  and the conversion of two molecules of  $\text{ATP}$  to  $\text{ADP}$  followed by the direct conversion of four  $\text{ADP}$  molecules to an overall yield of two molecules of  $\text{ATP}$  and the generation of two molecules of pyruvic acid (*Alberts et al (1989) and Spence and Mason (1992)*).

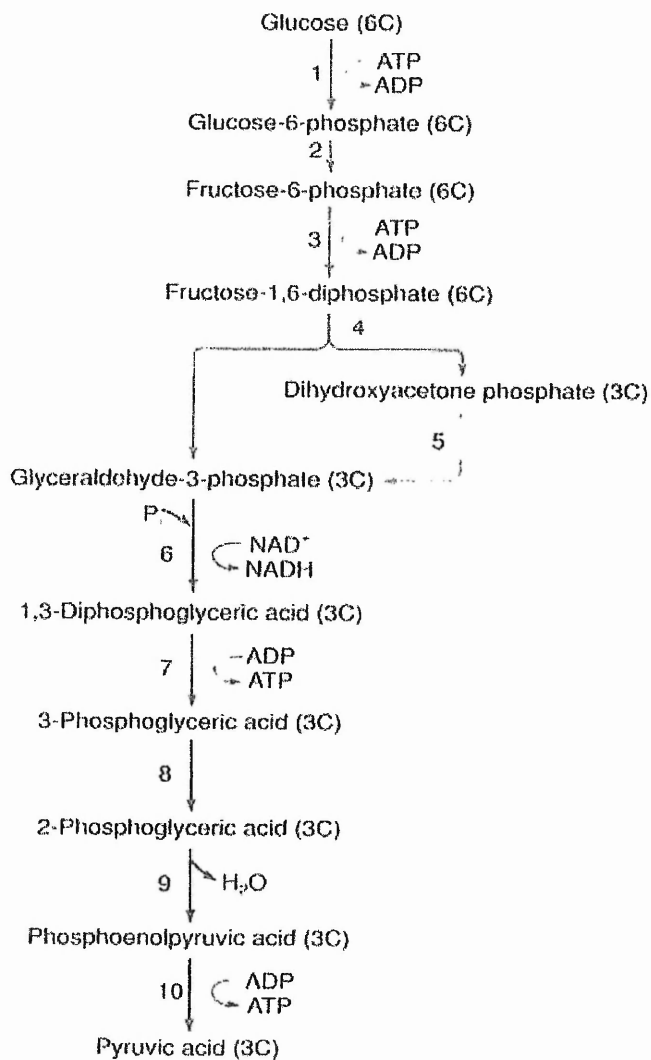


**Figure 1.08.** Glycolysis (*Spence and Mason (1992)*)

### 1.3.4 Citric acid cycle

The citric acid cycle begins when a molecule of pyruvic acid from glycolysis enters the mitochondrion and combines with a molecule of coenzyme A within the matrix of the mitochondria, see figure 1.09, (*Alberts et al (1989) and Spence and Mason (1992)*).

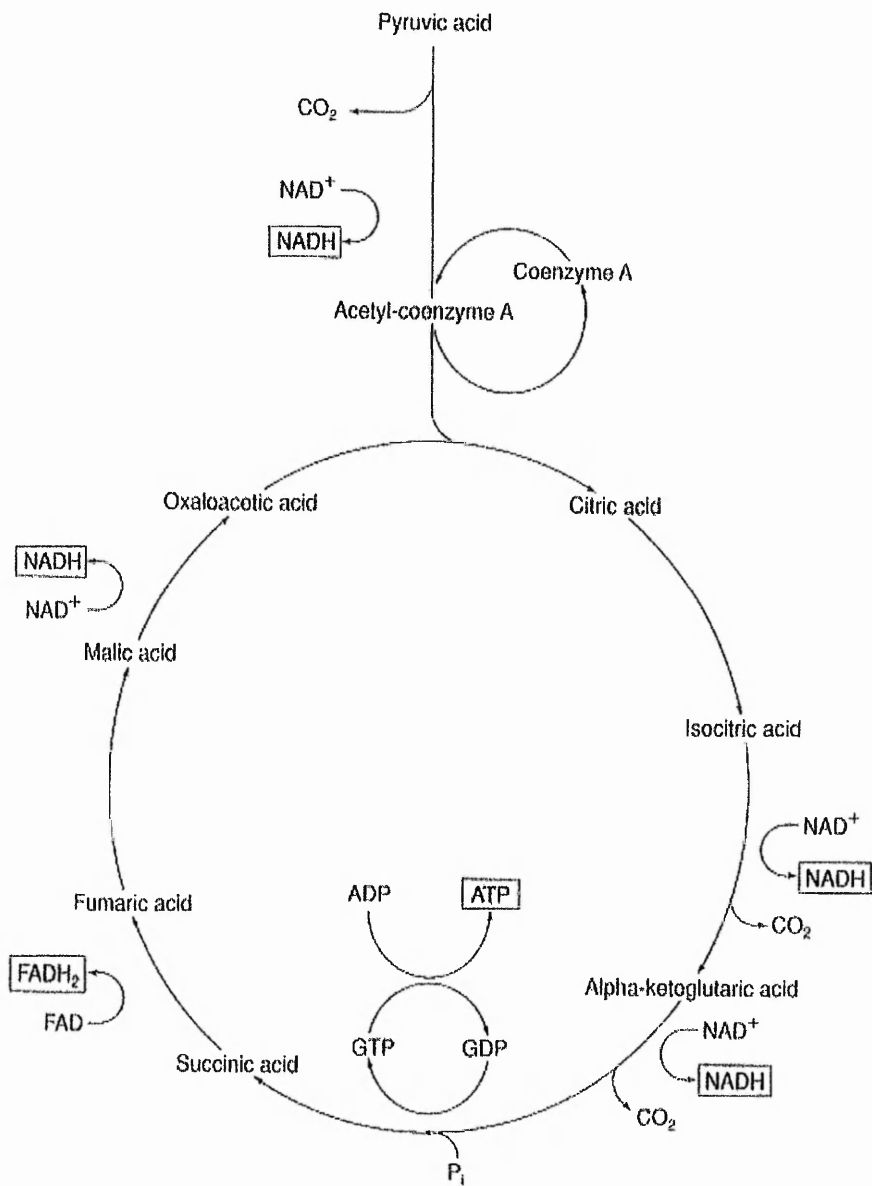


**Figure 1.09.** Citric acid cycle (*Spence and Mason (1992)*)

As glycolysis yields two molecules of pyruvic acid from one glucose molecule the overall yield of the citric acid cycle is eight NADH, six CO<sub>2</sub>, two molecules of FADH<sub>2</sub> and two of ATP (*Alberts et al (1989) and Spence and Mason (1992)*). In order for the metabolism of the next molecule of pyruvic acid and continuation of the citric acid cycle it is essential that the coenzymes NAD<sup>+</sup> and FAD become reduced back to NADH and FADH<sub>2</sub> (*Alberts et al (1989) and Spence and Mason (1992)*). This regeneration of the coenzymes is achieved through their entry into the final stage of ATP synthesis, the electron transport chain (*Alberts et al (1989) and Spence and Mason (1992)*).

### 1.3.5 Electron transport chain

The electron transport chain occurs across the inner mitochondrial membrane yielding a total of 24 molecules of ATP from the eight NADH and 4 ATP from the two FADH<sub>2</sub> produced during the citric acid cycle (Alberts *et al* (1989) and Spence and Mason (1992)). The two NADH molecules produced during glycolysis yield another 4-6 ATP depending upon the shuttle system used during oxidative phosphorylation (Alberts *et al* (1989) and Spence and Mason (1992)).

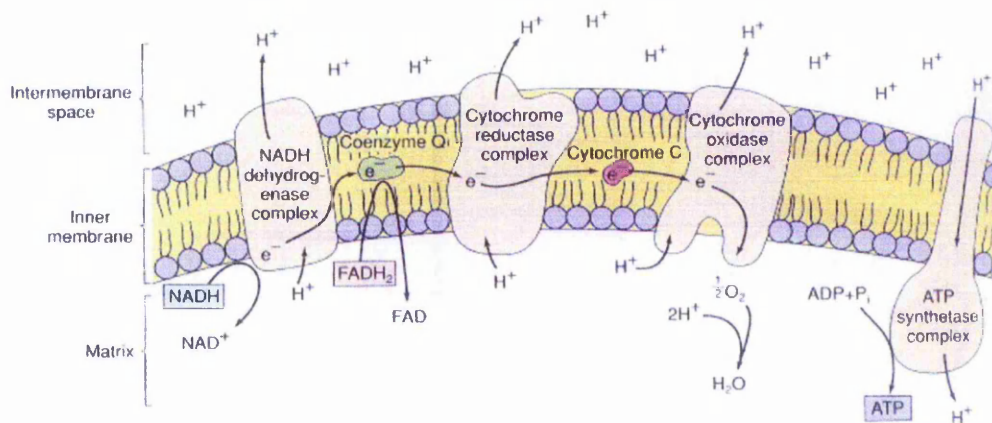


**Figure 1.10.** The electron transport chain, (Spence and Mason (1992)).

The electron transport chain consists of four complexes, the NADH dehydrogenase complex, cytochrome reductase complex, cytochrome oxidase complex and the ATP synthetase complex (Alberts *et al* (1989) and Spence and Mason (1992)). ATP is produced from the donation of H<sup>+</sup> ions from the reduction of NADH and FADH<sub>2</sub>. This results in the regeneration of the coenzymes NAD<sup>+</sup> and FAD for continuation of the citric acid cycle and the transfer of electrons through the four complexes of the electron transport chain (Alberts *et al* (1989) and Spence and Mason (1992)). Electrons are shuttled between the four complexes by either coenzymes also important for the incorporation of vitamins or cytochromes, the haem group of which acts as the electron carrier (Alberts *et al* (1989) and Spence and Mason (1992)). Coenzyme Q ferries

electrons between the complexes NADH dehydrogenase and cytochrome reductase. From here the electron carrier cytochrome c transfers electrons to the third complex cytochrome oxidase and finally the electron is passed to oxygen for the formation of H<sub>2</sub>O (*Alberts et al (1989) and Spence and Mason (1992)*). The passage of the electron through the complexes results in a loss of energy from the electron which is used to transport H<sup>+</sup> ions from the matrix to the intermembrane space thus setting up a electrochemical gradient as the matrix becomes negatively charged and the intermembrane space positively charged (*Alberts et al (1989) and Spence and Mason (1992)*). The passage of H<sup>+</sup> ions from the intermembrane space to the matrix through the ATP synthetase complex results in the formation of ATP driven by the energy released as the H<sup>+</sup> ions move through the complex (*Alberts et al (1989) and Spence and Mason (1992)*).



## 1.4 Bioluminescence

Bioluminescence is the production of light by living organisms. Bioluminescence is used by fireflies to attract mates, anglerfish to lure prey, railroad worms to scare predators and pelagic squid as camouflage (*Pazzagli et al (1988)*). In some higher animals exhibiting bioluminescence, the bioluminescence is actually derived from a symbiotic relationship with bacteria (i.e *Vibrio Fischeri*). It was discovered that bioluminescence is generated by a luciferase-luciferin system by the French scientist Dubois in 1885 (*Biron (2003)*) when studying clams. Dubois found that a crude cold water ground extract of clams would glow for several minutes, after which the glow could be regenerated by the addition of an extract of clams ground in hot water. He designated the cold water extract luciferase and the hot water extract luciferin.

Probably the best known example of bioluminescence is in the North American firefly (*Photinus pyralis*), whose development of a highly efficient bioluminescent system is employed when attracting a mate (*Lundin (1990)*). In 1947 McElroy verified that the firefly bioluminescent reaction was centred around the enzyme luciferase which had an absolute requirement for ATP along with a specific substrate 4,5-Dihydro-(6-hydroxy-2-benzothiazoyl)-4-thiazolecarboxylic acid (D-luciferin). It was established that the firefly bioluminescent reaction was a highly efficient one where 98% of the energy released in the reaction is in the form of light and very little in the way of heat. The quantum yield of the reaction is the highest known of any bioluminescent reaction where nearly one photon of light is generated for every molecule of luciferin oxidised (*Seliger and McElroy (1960)*). The requirement of ATP by the firefly luciferase-luciferin reaction has led to extensive investigations into the use of bioluminescence as a measure of ATP within cells. The only luciferase and luciferin reagents available to the researcher up until the late 1970's and into the early 1980's however were crude protein preparations of homogenised firefly lanterns (*Lundin (1990)*). These crude reagents tended to produce flash reactions rather than a glow

therefore narrowing the time span for measurement. Poor protein purification techniques at that time also meant that these homogenised samples contained high levels of contaminating ATP, adenylate kinase and ATPases leading to extremely high backgrounds (*DeLuca et al (1979)*). The combination of contaminated reagents, poor ATP extraction techniques and lack of commercially available luminometers, led to extensive analytical problems and essentially halted progress within this field (*Lundin (1990)*). The development of a purified luciferase with a stable light emission in the late 1970's however led to bioluminescence becoming the most widely used method of measuring ATP due to its ease, reproducibility and sensitivity over other assays. In the 1990's firefly luciferase was successfully cloned in *E. Coli* leading to a more thermo-robust reagent (*De Wet et al (1985)*).

### 1.4.1 Measuring bioluminescence

A typical detection system for the measurement of ATP using bioluminescence is the luminometer. This consists of a sample chamber, a photomultiplier tube (PMT) for the detection of the light produced and a means of recording the amount of light released. The sample chamber is responsible for receiving and presenting the microplate to the detector. It is important that this is completely sealed to minimise interference from ambient light. In order to produce precise, rapid measurements the sample chamber must be positioned as close to the detector as possible as this positioning gives the optimal signal to noise ratio. The detection system of the luminometer consists of a photomultiplier tube (PMT) where a single photon of light triggers a rapid amplified cascade of electrons. The resulting electrical current created when the photons strike the PMT is measured by the luminometer and expresses this information as arbitrary light units, referred to as relative light units (RLUs). Luminometers can detect an even collection of light from the smallest of samples, obtained by either positioning the PMT side on or end on within the machine (*Turner Biosystems application notes (2004)*).

## 1.4.2 Bioluminescent assays

### 1.4.2.1 ViaLight HS

The bioluminescent ATP assay, ViaLight HS (Cambrex Bio Science), was developed to detect ATP released from cells as an indication of viable cell number. It utilises the following reaction.

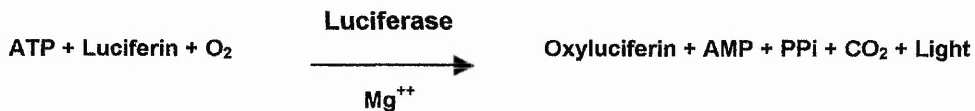


**Figure 1.11.** The reaction resulting in conversion of ATP to light

If all factors in the above reaction mechanism are saturated it can be deduced that the light emission is linearly related to the concentration of ATP present within the sample. The emitted light is then detected by a luminometer and expressed as the relative light units (RLUs).

ATP standard curves can be run in parallel with cell sample preparations in order to determine the concentration of ATP within the sample. It is well established that the luciferase reaction is quenched by intensely coloured mediums such as RPMI 1640 media containing phenol red and foetal bovine serum so therefore ATP standards should be diluted in the same media as the test when making a comparison between the amount of ATP contained within the cell sample. In order to measure ATP within cells, the cells are first gently lysed with a non ionic detergent that punches holes into the cell membrane allowing the release and detection of the nucleotides within the cells. After incubation with this lysis reagent the sample is placed into luminometer and a luciferin-luciferase cocktail is added to the sample and through the reaction in figure 1.11 an ATP/RLU of this sample is obtained.

### 1.4.2.2 ApoGlow™

The recognition of the changes in the relative levels of ATP to ADP during cell death led to the development of the bioluminescent ApoGlow™ (Cambrex Bio Science) assay, that is capable of converting and detecting small amounts of ADP to ATP using the following reaction.

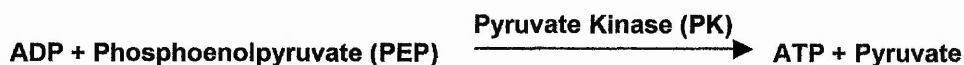


**Figure 1.12.** ADP conversion to ATP.

Whereby the ATP from this reaction is detected and measured as in reaction 1.11.

As in the ViaLight HS method the nucleotides first need to be released from the cells. This is again achieved through the addition of a non ionic detergent that punches holes into the cell membrane allowing the release and detection of the nucleotides within the cells. After incubation with this lysis reagent the sample is placed into a luminometer and a luciferin / luciferase cocktail is added to the sample. Through the reaction in figure 1.11 an ATP/RLU of the amount of ATP within the sample is obtained (reading A) and the ATP RLU's are subsequently allowed to decay for 10 minutes to background levels. ADP Converting Reagent (ADP-CR) is added to the sample and an immediate reading is taken (reading B). This reading shows the background levels of ATP (basal level of ADP prior to any conversion). After a 5 minute incubation to allow for complete conversion of ADP to ATP a third reading is taken (reading C).

The interpretation of the results is based on the relationship between the three readings obtained and these are used to work out the ADP:ATP ratio with the following calculation.

$$\text{ADP:ATP ratio} = \frac{\text{Converted ADP (C)} - \text{Basal ADP (B)}}{\text{Initial ATP (A)}}$$

**Figure 1.13.** Calculation for obtaining the ADP:ATP ratio.

Bioluminescent technology offers many benefits over conventional assays by avoiding the use of radioisotopes and showing greater sensitivity and reproducibility over traditional methods. Bioluminescence has been found to be an excellent alternative method for cell proliferation assays. The luciferin-luciferase assay has been shown to give increased sensitivity over other cell proliferation assays such as the MTT assay on Daudi and CCRF-CEM cell lines (*Petty et al (1995)*) and it has also correlated well with tritiated thymidine in proliferation assays and as a cytotoxicity assay when compared with crystal violet (*Crouch et al (1993)*).

## 1.5 Flow cytometry

The size, granularity and fluorescent properties of a cell can be investigated by the analysis of their forward scatter (FSC-H) indicating cell size, side scatter (SSC-H) showing granularity of the cell and green fluorescent (FL-1) and red fluorescent (FL-2) markers after staining with either one or two fluorometric dyes (*Ormerod (1998) Becton Dickinson (1997)*). Figure 1.14 is representative of the forward scatter and side scatter dot plot for a typical healthy population of cells and also for FL-1 (green) and FL-2 (red) dot plot obtained when analysing for phosphatidyl serine exposure (Green; FL-1) and loss of plasma membrane integrity (red; FL-2), (*R and D systems*). The cells used in this example are healthy Jurkat cells stained with a combination of Annexin V (FL-1) and propidium iodide (FL-2). Each of the dots on the dot plots represents a single cell whereby a percentage of healthy, apoptotic and necrotic populations of cells can be obtained by the use of statistical analysis packages attached to the flow cytometer (*Becton Dickinson (1997)*).

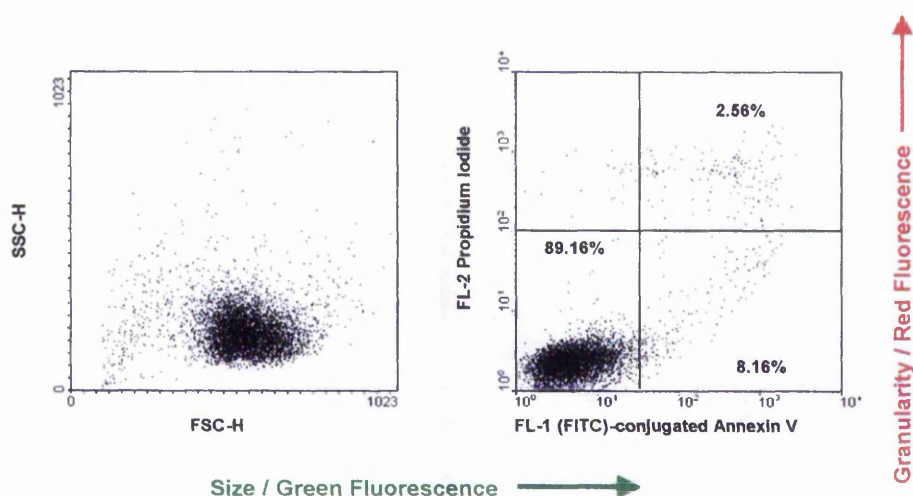


**Figure 1.14.** Forward scatter and side scatter dot plot and FL-1 (green; Annexin V) and FL-2 (red; PI) dot plot showing a typical picture of healthy Jurkat cells stained with a combination of Annexin V and propidium iodide detecting for phosphatidyl serine exposure and loss of plasma membrane integrity, where each dot represents a single cell.

The characteristics of the cell are detected as cells pass in single file in front of a focused laser beam within an isotonic sheath fluid (placed under pressure at approximately 4.5 psi). By the aid of the doublet discriminator the flow cytometer will disregard any cells that have passed by the laser in clumps thereby counting single cells only at a rate of approximately 200 cells per second (*Becton Dickinson (1997)*).

The properties of the cell are clarified by the way in which the cells scatter the incident light and emit fluorescence. Side scatter is measured when the light is reflected at high angles and is detected at 90° to the incident light axis (*Becton Dickinson (1997)*). As cells become apoptotic they are believed to become more granular as their chromatin becomes more condensed (*McCarthy (2002)*) thereby showing an increase in side scatter. The forward scatter of a cell is detected when light is diffracted at angles of between 1 and 10 degrees measured across the axis of the incident light and shows a decrease when cells become apoptotic (*Becton Dickinson (1997)*). FL-1 and FL-2 are detected through the absorbance of energy from the laser by fluorochromes added to the cell sample. This absorbance of energy elevates the fluorochrome to a higher energy level when the cell has passed by the laser this energy is released in the form of a photon of light emitting in the red or green spectra (*Becton Dickinson (1997)*).

A typical flow cytometer will consist of a fluidic system, an optical system and an electronic system all working together to take cells within a FACScan tube and turn them into a visual picture of their relative size, granularity and fluorescent properties on a computer screen. The fluidic system contains an air pump, pressure regulator, sheath fluid reservoir, sample regulator, flow cell and a waste reservoir, where the speed at which the cells pass the laser can be controlled by either increasing or decreasing the pressure (*Becton Dickinson (1997)*). The optical system contains the laser, lenses and prisms to help focus the laser beam and a system of filters and mirrors to guide specific wavelengths to their optical



detector. These optical signals are then converted into electronic signals for computer analysis.

Flow cytometry technology has been used to measure many of the processes during apoptosis and as it measures cells on a per cell basis can be used to obtain a percentage of apoptotic cells within a population (Ormerod (1998)). These cells of interest can be further analysed by the use of cell sorting technology such as the FACScaliber. Many of the proteins involved in apoptosis have been detected and quantified such as the anti apoptotic protein Bcl-2 (Steck *et al* (1996)). The correlation between the expression of Bcl-2 to Bax has also been successfully investigated where peripheral blood lymphocytes from a chronic lymphocytic leukaemia patient were stained with antibodies to Bcl-2, Bax and the general B-cell marker CD19. This data showed the tumour cells to have higher expression of the anti apoptotic protein Bcl-2 (Ormerod (1998)).

The loss of  $\Delta\psi_m$  can be detected by a variety of fluorescent probes such as 5,5',6,6'-tetrachloro-1,1',3,3'-tetraethylbenzimidazolcarbocyanine iodide (JC-1), 3,3'-dihexyloxacarbocyanine iodide (DiOC<sub>6</sub>) and Rhodamine123 (Rh123), (Ormerod (1998), Salvioli *et al* (2000) and Susin *et al* 1996)). Functioning mitochondria in viable cells have a high  $\Delta\psi_m$  and as a consequence actively uptake the dyes (Salvioli *et al* (2000) and Susin *et al* 1996)). The clear dual emission potential sensitive probe JC-1 exists as green monomers when taken in by the cell until concentrated above 1 $\mu$ M inside the mitochondria where red fluorescing J-Aggregates are formed (Salvioli *et al* (2000) and Susin *et al* 1996)). A loss of red fluorescence therefore is indicative of a loss of  $\Delta\psi_m$  and health of the mitochondria. Rh123 is also actively taken up by healthy functioning mitochondria and fluoresces green therefore indicating mitochondrial state by a decrease in green fluorescence (Susin *et al* 1996)). Rh123 can be used in conjunction with the DNA binding probe propidium iodide (PI) where information can be obtained on both mitochondrial and plasma

membrane integrity. Changes in plasma membrane potential can influence the stainability of the mitochondria and can sometimes mimic the changes in the  $\Delta\psi_m$  this has been observed in cells stained with Rh123 (*Salvioli et al (2000)*). One of the benefits of JC-1 staining is that it has been found to be unaffected by agents that depolarise the plasma membrane, whilst it is strongly affected by drugs that dissipate the  $\Delta\psi_m$  such as the drug Valinomycin (*Salvioli et al (2000)*).

The exposure of PS and loss of cell membrane integrity can be assessed using flow cytometry using dual staining with (FITC)-conjugated Annexin V and PI (*Koopman et al (1994) and Martin et al 1995*). This combination of two fluorometric probes allows the researcher to distinguish between cells in the earlier stages of apoptosis and those that have passed into secondary necrosis. PS flip occurs early in the apoptotic cascade where its exposure leads to recognition and clearance of the cell by phagocytosis (*Fadok et al (1992)*). In healthy cells PS remains contained within the cell and plasma membrane remains intact therefore green and red fluorescence is not detected in these cells. Apoptotic cells will fluoresce green as the (FITC)-conjugated Annexin V binds to the PS, necrotic cells will fluoresce both green and red as the cell can no longer exclude PI (*Ormerod (1998)*).

PI can either be used in conjunction with other fluorochromes or alone to assess cell viability (*Ormerod (1998)*). Staining with PI after fixation of the cell sample with 70% (v/v) ethanol (4° C) allows for the analysis of the cell cycle, as the amount of red fluorescence is proportional to the amount of DNA (*Nicoletti et al (1991)*). The four consecutive phases of a typical cell cycle begins with the G<sub>1</sub> phase where the cell contains a full compliment of DNA, followed by S phase (DNA synthesis) then culminating in G<sub>2</sub>/M where cells divide. *Nicoletti et al (1991)* demonstrated how from cell cycle studies the amount of apoptotic cells within a population could be analysed by the study of the sub G<sub>0</sub> peak giving a percentage of hypodiploid.

Flow cytometry is a powerful tool within the apoptosis field and can provide valuable information on the percentage of cells expressing a particular protein for example, although it is unable to tell us the distribution of this protein within the cell. Notwithstanding this flow cytometry has become one of the most widely used and accepted techniques in the study of apoptosis.

## 1.6 Aims of the study

By the avoidance of radioisotopes bioluminescence and the measurement of ATP has proved itself invaluable to the researcher as a quick, safe and highly sensitive alternative to traditional assays such as MTT and tritiated thymidine historically used to measure cell proliferation. Its use as an alternative method for crystal violet used in the investigation of cytotoxicity has also been proven (*Crouch et al (1993) and (Petty et al (1995))*). This study will continue to investigate the use of bioluminescence to assess cytotoxicity and investigate the measurement of ATP as a mitochondrial stress indicator by comparisons with mitochondrial transmembrane potential dyes such as JC-1.

This investigation will also explore the use of bioluminescence as a alternative method for the measurement of apoptosis and necrosis by the bioluminescent assay ApoGlow<sup>TM</sup>. This assay allows for the detection of small quantities of ADP in the presence of high levels of ATP, which is postulated to be sensitive enough to distinguish between necrotic cell death and apoptosis. This theory will be extended to examine the possibility of this assay distinguishing between both early and late apoptosis and using this method as a way of monitoring the transition of a cell populations from viable to apoptotic and finally to secondarily necrotic *in vitro*.

The apoptotic models within this study will be chosen to observe the different death pathways drugs work to induce apoptosis and the speed at which the cells progress through apoptosis into secondary necrosis.

The final investigations of this study will examine the role of ATP and ADP within the apoptotic cascade and try to discover its position in that cascade and how the metabolism of the cell affects the progress and commitment of a cell to die.

## Chapter 2 – Materials and methods

### 2.1 Materials

Material	Supplier
DC protein assay	Amersham International Little Chalfont Buckinghamshire
ECL	
Hyperfilm	
Rainbow Marker	
Anti-Caspase 3 polyclonal antibody	BD Biosciences Between Towns Road Oxford
Anti mouse FITC conjugate	
Anti-human PARP monoclonal antibody	
Blotto	
FACS Flow	
FACScan tubes	
Secondary antibody (Mouse)	
Secondary antibody (Rabbit)	
10% Gel	BIO-RAD Laboratories Ltd Hemel Hempstead Hertfordshire
12% Gel	
15% Gel	
Anti-Human Caspase 8 monoclonal antibody	Biosource Nivelles Belgium
ApoGlow	Cambrex Bio Science Wokingham Berkshire
ATP	
ToxiLight	
ViaLight HS	
5,5',6,6'-tetrachloro-1,1',3,3'- tetraethylbenzimidazolylcarbocyanine iodide (JC-1)	Cambridge Bioscience Newmarket Road Cambridge
Foetal Bovine Serum (FBS)	Harlan Sera Labs Loughborough Leicestershire
ADP	Merck Biosciences LTD Beeston Nottingham
Arabinofuranosyl cytosine	
Camptothecin	
Caspase inhibitor I	
Dexamethasone	
Etoposide	
Ionomycin	
96 well cell culture / luminometer plates (white)	Porvair Sciences Ltd Govett Avenue Sheperton
96 well luminometer plates (white)	
Cytotox One	Promega UK Chilworth Science Park Southampton
TACS Annexin V-FITC	R&D Systems Abingdon Oxford

<b>Cell culture flasks (T25)</b>	<b>Sarstedt Ltd Beaumont Leys Leicestershire</b>
<b>Cell culture flasks (T75)</b>	
<b>Sterile universal (25ml)</b>	
<b>10ml Pipettes</b>	
<b>12 well tissue culture plates</b>	<b>Scientific Laboratory Supplies Wilford Nottingham</b>
<b>Dimethylsulfoxide (DMSO)</b>	<b>Sigma Poole Dorset</b>
<b>Dulbeccos Modified Eagles Medium (DMEM)</b>	
<b>L-Glutamine</b>	
<b>Penicillin / Streptomycin</b>	
<b>Phosphate Buffered Saline tablets (PBS)</b>	
<b>Propidium Iodide</b>	
<b>RPMI 1640</b>	
<b>Trypan blue</b>	
<b>Trypsin EDTA (10X)</b>	
<b>Cytofunnels</b>	<b>Thermo Shandon Astmoor Runcorn</b>
<b>Cytoslides</b>	
<b>Anti Human FAS Activating</b>	<b>Upstate Biotechnology Wolverton Mill South Milton Keynes</b>
<b>Anti-Caspase 9 monoclonal antibody</b>	

**Table 2.01.** List of materials used within this study and their supplier.

## **2.2 Cell lines**

The cell lines used within this study were all obtained from ECACC apart from the stably transfected Met B neomycin and Met B Bcl-2 cell lines, which were a kind gift from Professor Martin Griffin at Nottingham Trent University. The hamster fibrosarcoma cell line Met B is a non-commercially available cell line, which was established from the lung metastases of a parental tumour (HSV-2-333-2-26) and transformed by the herpes simplex virus. The cloned cell lines were given the prefix Met for metastatic variant and a suffix of A to G. 9µg of pSVBcl-2 and 1µg of the selection vector pSVneo was used to transfect the Met B cells with Bcl-2. The Met B neomycin cells were stably transfected with the selection vector, where both cell lines were selected by growth in media containing 400µg/ml of G418. Immunoblotting using commercially available antibody was used to screen for clones expressing the Bcl-2 cDNA.

### **2.2.1 Suspension cells**

**K562** – Human chronic myelogenous leukaemia

**Jurkat** – Human leukaemic T cell lymphoblast

**U937** – Human histiocytic lymphoma

**CEM-7** - Human leukaemic T cell lymphoblast

**HL60** – Human promyelocytic leukaemia

### **2.2.2 Culturing suspension cells**

All suspension cell lines were routinely cultured in 25cm<sup>2</sup> cell culture treated flasks in Roswell Park Memorial Institute (RPMI) 1640 media supplemented with 10% (v/v) heat inactivated foetal bovine serum, 1% (v/v) penicillin (50U ml<sup>-1</sup>) / streptomycin (50µg ml<sup>-1</sup>) and 1% (v/v) L-Glutamine (2mM). Cultures were incubated in a humidified atmosphere of 5% (v/v) CO<sub>2</sub> 95% (v/v) air at a temperature of 37°C. Cells were

passaged twice weekly when they had reached an approximate cell density of  $1 \times 10^6$  cells  $\text{ml}^{-1}$ .

### **2.2.3 Adherent cells**

**Met B neomycin** – Hamster fibrosarcoma, stably transfected with a vector expressing neomycin selection.

**Met B Bcl-2** - Hamster fibrosarcoma, stably transfected with both an expression vector for Bcl-2 and a neomycin selection vector.

### **2.2.4 Culturing Adherent cells**

All of the adherent cell lines were cultured in  $75\text{cm}^2$  cell culture treated flasks in Dulbecco's Modified Eagles Medium (DMEM) media supplemented with 10% (v/v) heat inactivated foetal bovine serum (FBS), 1% (v/v) penicillin ( $50\text{U ml}^{-1}$ ) / streptomycin ( $50\mu\text{g ml}^{-1}$ ) and 1% (v/v) L-Glutamine (2mM). Cultures were incubated in a humidified atmosphere of 5% (v/v)  $\text{CO}_2$  95% (v/v) air at a temperature of  $37^\circ\text{C}$ . They were passaged twice weekly when the cells were confluent. The media was carefully poured off and the cells washed with DMEM to remove traces of FBS and 1ml of (10x) Trypsin EDTA solution (100mg porcine trypsin (v/v), 40mg EDTA (v/v)) was added. The flask was placed at  $37^\circ\text{C}$  in 5%  $\text{CO}_2$  in a humidified atmosphere until the cells detached from the flask. Once detached the cells were placed in a 25ml universal tube with 2mls of FBS and centrifuged at  $400\text{xg}$  for 5 minutes. The supernatant was carefully removed and approximately one third of the cell pellet transferred into a  $75\text{cm}^2$  flask for continued culture.



### 2.3 Counting cells

10 $\mu$ l of trypan blue (0.4% (w/v) solution - 0.81% (w/v) sodium chloride and 0.06% (w/v) potassium phosphate) was placed into a 1.5ml eppendorf tube and mixed with 10 $\mu$ l of cell suspension to give a dilution factor of 2. Enough of the mix was taken to fill the chamber of a haemocytometer and analysed under a light microscope observing for cell number. All of the cells in the four corner squares were counted including any cells touching the top and left borders only and the cell number calculated.

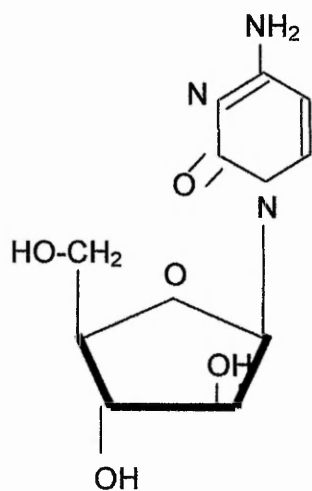
**Cell number (per ml) = mean of 4 squares x dilution factor x10<sup>4</sup>**

**Figure 2.01.** Calculation for the counting of cells (*Sigma*)

## 2.4 The structure, mechanism and preparation of the apoptosis inducing agents and preparation of the caspase inhibitor

### 2.4.1 Structure and mechanism of apoptosis induction

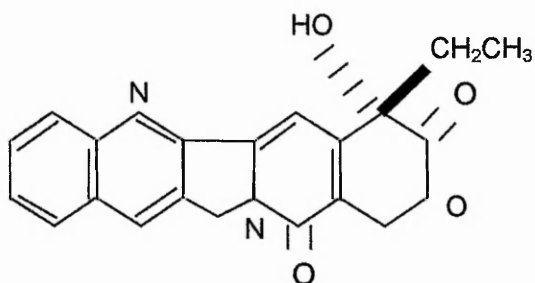
#### 1-β-D-Arabinofuranosylcytosine (Ara-C)



Ara-C is a potent inhibitor of mammalian cell DNA replication and induces apoptosis in human myeloid leukaemia cells by inducing cell cycle arrest in S phase of the cell cycle (*Wills et al (1996) and Decker et al (2003)*).

**Figure 2.02.** Structure of the drug 1-β-D-Arabinofuranosylcytosine (Ara-C) (*Wills et al (1996)*).

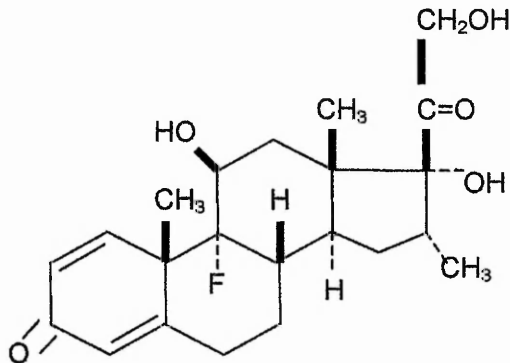
#### Camptothecin (CAM)



Camptothecin binds irreversibly to the DNA – topoisomerase I complex and inhibits the re-association of the DNA strands after cleavage. Camptothecin blocks the cell cycle in S phase at low dosages and induces apoptosis in a large number of normal and tumour cell lines. (*Jones et al (2000)*).

**Figure 2.03.** Structure of the drug camptothecin (CAM) (*Jones et al (2000)*).

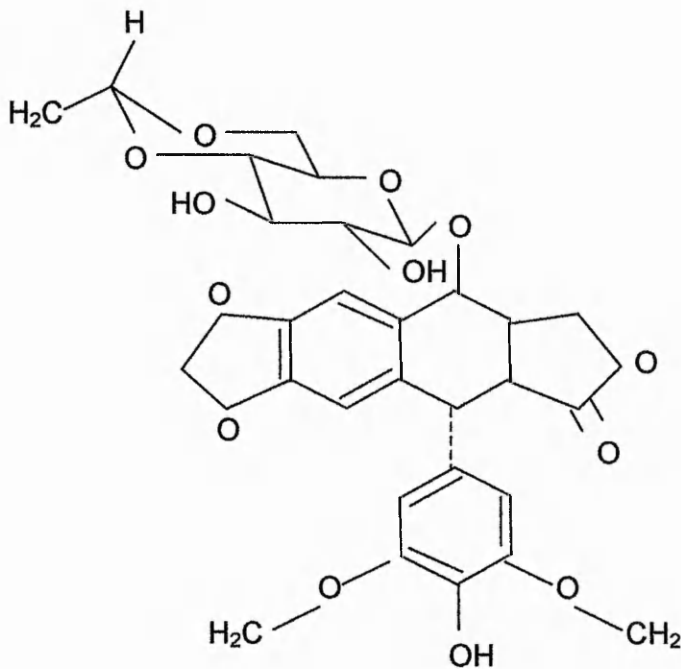
## Dexamethasone (DEX)



The glucocorticoid Dexamethasone shares the general properties of the corticosteroids and is therefore used as an anti inflammatory agent which regulates T cell survival, growth and differentiation. T cells express low levels of Bcl-2 during the G<sub>0</sub> phase of the cell cycle which increases their susceptibility to this agent (Montani et al (1999)).

Figure 2.04. Structure of the drug Dexamethasone (Montani et al (1999)).

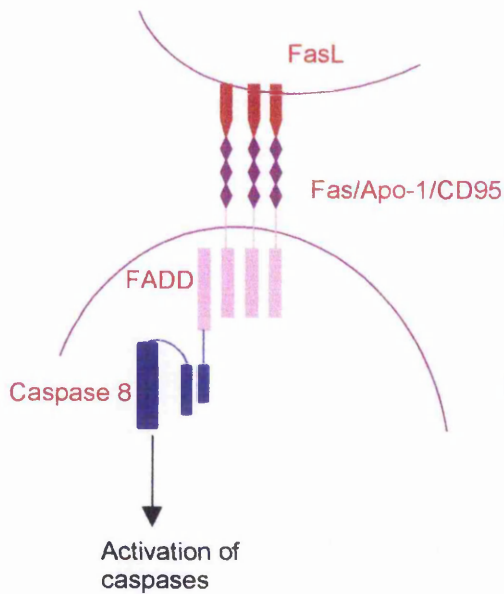
## Etoposide



Etoposide inhibits the reassociation of the double stranded DNA breaks created by topoisomerase II by binding to the topoisomerase II complex and is especially potent during S phase of the cell cycle (De Lange et al (1995)).

Figure 2.05. Structure of the drug Etoposide (De Lange et al (1995)).

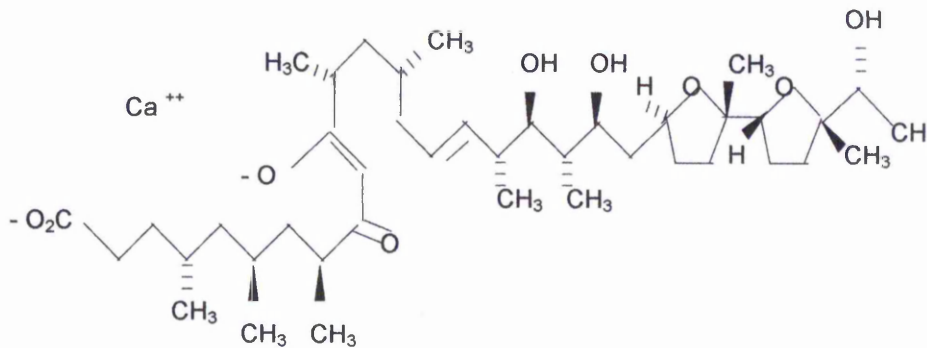
## Anti-Human Fas / CD95 (Activating) IgM CD95



Anti human Fas or IgM CD95 induces apoptosis in human cells via trimerisation of the surface membrane receptor Fas. Association of Fas with FADD by means of the death domain situated on both proteins activates caspase 8 and leads to apoptosis by the recruitment of procaspase 8 to Fas-FADD through the death effector domain. (Osborne *et al* (1996)).

**Figure 2.06.** Mechanism of apoptosis by the interaction between Fas and Fas Ligand (Osborne *et al* (1996))

## Ionomycin



Ionomycin is an antibiotic that acts as a Ca<sup>++</sup> binding ionophore and induces apoptosis by increasing the cells permeability to Ca<sup>++</sup> (Walker *et al* (1997)).

**Figure 2.07.** Structure of the antibiotic Ionomycin (Walker *et al* (1997)).

### 2.4.2 Preparation of the apoptosis inducing agents

All agents were reconstituted in 100% DMSO at the appropriate volume to produce the stock concentrations listed below. The agents were diluted in the required culture media to produce the working concentrations for the studies.

Apoptotic agent	Stock concentration
1- $\beta$ -D-Arabinofuranosylcytosine (Ara-C)	100mM
Camptothecin (CAM)	5mM
Dexamethasone (DEX)	25mM
Etoposide	1mg ml <sup>-1</sup>
Ionomycin	1mM

Table 2.02. Table showing the apoptosis agents and their stock concentrations.

**IgM CD95** – This was reconstituted in RPMI 1640 complete media, to give a stock of 25mg ml<sup>-1</sup> which was further diluted in complete media to give the range of concentrations required.

### 2.4.3 Preparation of the caspase inhibitor

**Caspase inhibitor I** – This was reconstituted in 100% DMSO to give a stock of 5mM.

## 2.5 Preparation of apoptotic models

### 2.5.1 Preparation of suspension cell apoptotic models

In each apoptotic model 3mls of cell suspension ( $5 \times 10^5$  cells  $\text{ml}^{-1}$  apart from K562 which were seeded at  $2.5 \times 10^5$  cells  $\text{ml}^{-1}$ ) were placed in 8 wells of a 12 well tissue culture plate. The cells were dosed with the following concentrations of agent depending upon the model being prepared.

Apototic model	Incubation time (hours)	Dosing range							
		0	0.05	0.1	0.5	1	2	5	10
Jurkat and Ara-C ( $\mu\text{M}$ )	4, 24, 48	0	0.05	0.1	0.5	1	2	5	10
Jurkat and IgM CD95 ( $\text{ng ml}^{-1}$ )	4, 24	0	25	50	100	150	200	250	
U937 and CAM ( $\mu\text{M}$ )	4, 24	0	0.05	0.1	0.5	1	2	5	10
HL60 and CAM ( $\mu\text{M}$ )	4, 24	0	0.05	0.1	0.25	0.5	1	2	5
CEM-7 and DEX (nM)	72	0	10	25	50	75	100	150	200
K562 and Etoposide ( $\mu\text{g ml}^{-1}$ )	72	0	0.5	2	4				

**Table 2.03.** Table showing apoptotic models and the doses used to induce cell death.

Following dosing the cells were incubated at  $37^\circ\text{C}$  in a humidified atmosphere of 5% (v/v)  $\text{CO}_2$ , 95% (v/v) air for the required incubation time indicated above.

## 2.5.2 Preparation of washing experiments

The following apoptotic models were prepared, U937 and CAM, and HL60 and CAM where the drug was removed immediately.

4mls of cell suspension ( $5 \times 10^5$  cells  $\text{ml}^{-1}$ ) were placed in two 25ml universal tubes and dosed with the following concentrations of CAM; 0 (control) and  $5 \mu\text{M}$ . 2mls of each mixture was immediately taken from each universal and plated into a 12 well tissue culture plate. The remainder was centrifuged at 400xg for 5 minutes and the supernatant carefully removed and replaced with 2mls of complete media. This cell suspension was then plated into the 12 well tissue culture plate and incubated at  $37^\circ\text{C}$  in a humidified atmosphere of 5% (v/v)  $\text{CO}_2$ , 95% (v/v) air for 4 hours.

A Jurkat and Ara-C model was set up for drug removal but this time the drug was either removed immediately or after an incubation period of 30 minutes. 8mls of cell suspension ( $5 \times 10^5$  cells  $\text{ml}^{-1}$ ) was split and placed into two 25ml universals in 2ml and 6ml volumes and dosed with either complete media or  $0 \mu\text{M}$  (control-2ml) or  $5 \mu\text{M}$  Ara-C (6ml) where the control and 4mls of drug treated sample were immediately taken and plated into a 12 well tissue culture plate in 2ml volumes. The remainder of the drug treated sample was centrifuged at 400xg for 5 minutes and the supernatant carefully removed and replaced with 2mls of complete media. This cell suspension was then plated into the 12 well tissue culture plate. After an incubation period of 30 minutes at  $37^\circ\text{C}$  in a humidified atmosphere of 5% (v/v)  $\text{CO}_2$ , 95% (v/v) air, one set of drug treated sample was removed and centrifuged at 400xg for 5 minutes and the supernatant carefully removed and replaced with 2mls of complete media. This cell suspension was then plated back into the 12 well tissue culture plate and incubated at  $37^\circ\text{C}$  in a humidified atmosphere in 5% (v/v)  $\text{CO}_2$ , 95% (v/v) air for 48 hours.

### 2.5.3 Preparation of apoptotic models with the general caspase inhibitor caspase inhibitor I (Z-VAD-FMK)

The following apoptotic models were prepared, Jurkat and Ara-C, Jurkat and IgM CD95 and U937 and CAM. 2mls of cell suspension ( $5 \times 10^5$  cells  $\text{ml}^{-1}$ ) were placed in 4 wells of a 12 well tissue culture plate. The cells were dosed with the following concentrations of inhibitor and agent depending upon the model being prepared.

Cell line	Apoptosis inducer	Caspase inhibitor	Incubation time/hours
Jurkat	Ara-C/ $\mu\text{M}$	Z-VAD-FMK/ $\mu\text{M}$	
	0	0	4, 24 and 48
	5	0	4, 24 and 48
	5	50	4, 24 and 48
Jurkat	IgM CD95/ng/ml	Z-VAD-FMK	
	0	0	4, 24
	250	0	4, 24
	250	50	4, 24
HL60	Camptothecin/ $\mu\text{M}$	Z-VAD-FMK/ $\mu\text{M}$	
	0	0	4
	5	0	4
	5	50	4
	0	50	4
U937	Camptothecin/ $\mu\text{M}$	Z-VAD-FMK/ $\mu\text{M}$	
	0	0	4, 24
	5	0	4, 24
	5	50	4, 24
	0	50	4, 24

**Table 2.04.** Table showing the cell line with its apoptosis inducer and caspase inhibitor.

Following dosing the cells were incubated at  $37^\circ\text{C}$  in a humidified atmosphere of 5% (v/v)  $\text{CO}_2$ , 95% (v/v) for the required time period.



#### 2.5.4 Preparation of Met B neomycin and Met B Bcl-2 apoptotic models

Camptothecin and Ionomycin were used independently to induce apoptosis in the two adherent transfected cell lines Met B neomycin and Met B Bcl-2. 100µl of cell suspension ( $1 \times 10^5$  cells ml<sup>-1</sup>; which had been passed gently through a 21G needle to ensure a homogenous suspension) was placed into each well of a 96 well tissue culture plate. 1ml of the cell suspension was also placed into 4 wells of a 12 well tissue culture plate. The plates were incubated for a minimum of 2 hours at 37°C to allow the cells to adhere and spread. The cells were then dosed with either Camptothecin (0 (control), 500, 1000 and 1500µM) or Ionomycin (0 (control), 100, 500 and 1000nM). Following dosing the cells were incubated at 37°C in a humidified atmosphere of 5% (v/v) CO<sub>2</sub>, 95% (v/v) air for 48 hours.

#### 2.6 Preparation of Necrotic model

**Heat treatment of K562 cells** – 2mls of cell suspension ( $1 \times 10^6$  cells ml<sup>-1</sup>) were placed into two 25ml universal tubes. One tube was placed in a water bath at 56°C for one hour to induce necrosis and the other left at room temperature to give healthy control cells. Following the incubation step the healthy and necrotic cells were mixed as shown in table 2.05 to make up 1ml samples and 100µl placed in triplicate into a 96 well white walled bioluminescent plate.

% Necrosis	100	90	80	60	50	30	10	0
Volume necrotic cells (µl)	1000	900	800	600	500	300	100	0
Volume healthy cells (µl)	0	100	200	400	500	700	900	1000

**Table 2.05.** Table showing the volumes required for differing % necrosis samples

## 2.7 Cell number curve

The human leukaemia cell line K562 was diluted 1:10 in RPMI 1640 complete media (see section 2.2.2 for supplements) to produce the cell numbers in table 2.06 where 100µl was placed in triplicate into a 96 well white walled bioluminescent plate. (Section 2.3 for the method of counting cells.)

Cell number (ml <sup>-1</sup> )	1x10 <sup>6</sup>	1x10 <sup>5</sup>	1x10 <sup>4</sup>	1x10 <sup>3</sup>	10	1	0	Blank
Volume C.M (µl)	900	900	900	900	900	900	900	900
Volume of cell suspension (µl)	100µl (1x10 <sup>6</sup> )	100µl (1x10 <sup>5</sup> )	100µl (1x10 <sup>4</sup> )	100µl (1x10 <sup>3</sup> )	100µl (1x10 <sup>2</sup> )	100µl (10)	100µl (1)	100µl (0)

**Table 2.06.** Table showing the volumes required for differing cell numbers

## 2.8 Preparation of Standards

### 2.8.1 ATP standards

ATP standard from a stock concentration of  $10\mu\text{mol ml}^{-1}$  was diluted 1:10 in Tris Acetate Buffer or complete media (see section 2.2.2 for supplements) as shown in table 2.07 to produce the following concentrations of ATP with a blank consisting of Tris Acetate Buffer or complete media. The standards were left on ice throughout the procedure until required when  $100\mu\text{l}$  was placed in triplicate into a 96 well white walled bioluminescent plate.

ATP standard ( $\text{nmol ml}^{-1}$ )	1,000	100	10	1	0.1	0.01	0	Blank
Volume TAB or CM ( $\mu\text{l}$ )	900	900	900	900	900	900	900	900
Volume of ATP ( $\text{nmol ml}^{-1}$ )	100 $\mu\text{l}$ (10,000)	100 $\mu\text{l}$ (1,000)	100 $\mu\text{l}$ (100)	100 $\mu\text{l}$ (10)	100 $\mu\text{l}$ (1)	100 $\mu\text{l}$ (0.1)	100 $\mu\text{l}$ (0)	100 $\mu\text{l}$ (0)

**Table 2.07.** Table showing the dilutions and volumes required for differing ATP standards.

## 2.8.2 ADP standards

ADP standard from a stock concentration of  $100\text{mmol ml}^{-1}$  was diluted to  $10,000\text{nmol ml}^{-1}$  and then diluted 1:10 in Tris Acetate Buffer as shown in table 2.08 to produce the following concentrations of ADP with a blank consisting of Tris Acetate Buffer. The standards were left on ice throughout the procedure until required when  $100\mu\text{l}$  was placed in triplicate into a 96 well white walled bioluminescent plate.

ADP standard ( $\text{nmol ml}^{-1}$ )	1,000	100	10	1	0.1	0.01	0	Blank
Volume TAB ( $\mu\text{l}$ )	900	900	900	900	900	900	900	900
Volume of ADP ( $\text{nmol ml}^{-1}$ )	$100\mu\text{l}$ (10,000)	$100\mu\text{l}$ (1,000)	$100\mu\text{l}$ (100)	$100\mu\text{l}$ (10)	$100\mu\text{l}$ (1)	$100\mu\text{l}$ (0.1)	$100\mu\text{l}$ (0)	$100\mu\text{l}$ (0)

**Table 2.08.** Table showing the dilutions and volumes required for differing ADP standards.

## **2.9 Preparation of buffers, stains and kits**

### **2.9.1 Preparation of buffers**

**Phosphate buffered saline (PBS)** - 1 tablet was dissolved in 200mls of H<sub>2</sub>O to give 0.01M phosphate buffer, 0.0027M potassium chloride and 0.137M sodium chloride at pH 7.4 (25°C).

### **2.9.2 Preparation of buffers required during Western blotting**

**Lysis buffer** – To 5mls of 25mM Tris, 20mM Hepes (pH 7.4 (HCl)) and 0.1% Triton add 1 tablet of complete protease inhibitor and store the buffer on ice.

**Laemmli stopping solution** – 162.5mM Tris-HCl, pH 6.8, 20% (v/v) glycerol, 5% (v/v) β mercaptoethanol, 2% (w/v) SDS and 1% (w/v) bromophenol blue.

**Running buffer** – A stock solution of Running buffer was made as follows, 15g Tris-base, 72g glycine and 5g SDS made up to 1litre in dH<sub>2</sub>O. 120mls of the stock solution was taken and diluted in 480mls of dH<sub>2</sub>O to produce 600mls of working solution.

**Blotting buffer** – A stock solution of Blotting buffer was made as follows, 30.25g Tris-base, 150.25g glycine made up to 1litre in dH<sub>2</sub>O. 100mls of the stock solution was taken and diluted in 700mls of dH<sub>2</sub>O and 200mls of methanol to produce 1000mls of working solution.

### **2.9.3 Preparation of stains**

**5,5',6,6'-tetrachloro-1,1',3,3'tetraethylbenzimidazolcarbocyanine iodide (JC-1)** - JC-1 was reconstituted in neat DMSO to produce a stock solution of 1mg/ml and stored protected from the light at room temperature. The JC-1 was diluted 1:50 prior to use in PBS and filtered through a 0.45 $\mu$ m pore size filter.

**Propidium iodide (PI)** - PI was reconstituted in DMSO to give a stock of 1mg/ml which was diluted 1:20 in PBS (see section 2.8.1 for recipe) to give a working concentration of 50 $\mu$ g/ml.

**Trypan Blue** – Trypan Blue was obtained ready to use at a 0.4% solution (0.81% sodium chloride and 0.06% potassium phosphate).

## 2.9.4 Preparation of kits

### ViaLight HS

- **Nucleotide Releasing Reagent** – Provided ready to use.
- **Tris Acetate Buffer** - Provided ready to use.
- **ATP Monitoring Reagent (AMR)** – AMR was reconstituted by the addition of 10mls of Tris Acetate Buffer to the bottle, this was then allowed to equilibrate for 15 minutes, as to the manufacturers specifications.

### ApoGlow

- **Nucleotide Releasing Reagent** – Provided ready to use.
- **Tris Acetate Buffer** - Provided ready to use.
- **Nucleotide Monitoring Reagent (NMR) (Cambrex)** - NMR was reconstituted by the addition of 10mls of Tris Acetate Buffer to the bottle, this was then allowed to equilibrate for 15 minutes, as to the manufacturers specifications.
- **ADP Converting Reagent (ADP-CR) (Cambrex)** – ADP-CR was reconstituted by the addition of 6mls of Tris Acetate Buffer to the bottle, this was then allowed to equilibrate for 15 minutes, as to the manufacturers specifications.

### ToxiLight

- **AK Assay Buffer** - Provided ready to use.
- **Adenylate Kinase Detection Reagent (AK-DR)** – AK-DR was reconstituted by the addition of 10mls of AK Assay Buffer to the bottle, this was then allowed to equilibrate for 15 minutes, as to the manufacturers specifications.

## TACS™ Annexin V-FITC – Apoptosis detection kit

- **10x binding buffer** – Provided ready to use.
- **1x binding buffer** – Prepared as to the manufacturers specifications by the addition of 500µl of 10x binding buffer to 4.5mls dH<sub>2</sub>O, this is enough for 10 samples.
- **Annexin V and propidium iodide** – Prepared as outlined in table 2.09.

<b>10x binding buffer</b>	<b>100µl stock</b>
<b>Propidium Iodide</b>	<b>100µl stock</b>
<b>Annexin V-FITC</b>	<b>10µl stock</b>
<b>DH<sub>2</sub>O</b>	<b>790µl</b>

**Table 2.09.** Preparation of 1ml of Annexin V-FITC and propidium iodide stain, enough for 10 samples.

## CytoTox-ONE

- **CytoTox-ONE assay buffer** - Provided ready to use.
- **CytoTox-ONE Reagent** – CytoTox-ONE was reconstituted by the addition of 11mls of CytoTox-ONE assay buffer to the bottle, this was then allowed to equilibrate for 15 minutes, as to the manufacturers specifications.
- **Stop solution** – Provided ready to use.



### **DC protein assay**

- **Reagent 1** – Prepared by mixing Reagent S and reagent A as to the manufacturers specifications.
- **Reagent B** - Provided ready for use

### **Enhanced chemiluminescence**

- **ECL** – Prepared by mixing 5mls each of reagents 1 and 2 (1:1).

## **2.10 Methods**

### **2.10.1 Assessing cell morphology**

#### **2.10.1.1 Romanovsky stained cytopsin preparations**

The cytopsin preparations were kindly stained by the Haematology department at the Nottingham City Hospital.

Cytopsin slides were prepared using a Shandon cytopsin 3 centrifuge (200xg for 5 minutes) using disposable cytofunnels where 100 $\mu$ l of sample ( $5 \times 10^5 \text{ ml}^{-1}$ ) was added to the chamber. The cytopsin slides were allowed to air dry and then fixed for 5 minutes in methanol and stained with May Grünwald stain for 5 minutes followed by Giemsa staining for 10 minutes. The slides were differentiated with a series of three washes in Sörensen's buffer. Apoptosis was assessed morphologically in these cells with light microscopy observing for healthy round cells and apoptotic cells with nuclei shrinkage and cell blebbing.

#### **2.10.2 Measurement of cell viability**

The ability of the cell to exclude various dyes indicates the maintenance of the cell membrane integrity and hence the viability of the cell.

##### **2.10.2.1 Uptake of propidium iodide (PI)**

200 $\mu$ l of cell suspension was placed into a round bottom FACs tube and 200 $\mu$ l of PI at 50 $\mu$ g/ml was added to the sample and mixed. The samples were analysed immediately after a 5 minute incubation at room temperature on a Becton Dickinson FACscan Flow Cytometer. The compensation settings were 1.0 and 28.8 where 5,000 events were counted (*Darzynkiewicz et al (1994)*).

### **2.10.2.2 Uptake of Trypan Blue**

10 $\mu$ l of trypan blue was placed in a 1.5ml eppendorf tube and mixed with 10 $\mu$ l of cell suspension to give a dilution factor of 2. Enough of the mix was taken to fill the chamber of a haemocytometer and then analysed under a light microscope. Cell viability was assessed through the number of cells appearing blue under the microscope, which would indicate the loss of the cell membrane integrity (*Gorman et al (1994)*).

### **2.10.2.3 Measurement of ATP as a viability marker (ViaLight HS)**

The intracellular level of ATP is precisely regulated within all metabolically active cells and so therefore when a cell dies the ATP is rapidly lost. This means that ATP is an accurate measurement of living cells within a population. The ATP was measured as outlined in Chapter 1, figure 1.11.

100 $\mu$ l of either cell sample or ATP standard were plated into a 96 well luminometer plate in triplicate. 100 $\mu$ l of the Nucleotide Releasing Reagent (NRR) was added to the wells and left to release the ATP (in the case of cell samples) for 5 minutes. The plate was then placed into a Berthold MPL3 luminometer where 20 $\mu$ l of ATP Monitoring Reagent (AMR) was dispensed into each well and a 1 second integrated reading taken.

### **2.10.3 Assessment of apoptosis and necrosis within a cell population**

#### **2.10.3.1 Annexin V and PI.**

200 $\mu$ l of cell sample ( $5 \times 10^5 \text{ ml}^{-1}$ ) was placed into a round bottom FACs tube. The cells were centrifuged at 400xg for 5 minutes and the supernatant carefully removed. The samples were washed in 500 $\mu$ l of PBS at 4°C and centrifuged at 400xg for 5 minutes. The cells were resuspended in 20 $\mu$ l of the Annexin V + PI mix and incubated for 15 minutes at room temperature protected from the light. 200 $\mu$ l of the 1x binding buffer was added and the samples were analysed within 1 hour of adding the binding buffer on a Becton Dickinson FACscan flow cytometer, where 5,000 events were counted. This technique was modified from the R and D Systems protocol.

#### **2.10.3.2 The measurement of ATP and ADP (ApoGlow™).**

100 $\mu$ l of cell sample was plated out into a 96 well luminometer plate in triplicate. 100 $\mu$ l of the Nucleotide Releasing Reagent (NRR) was added to the wells and left to release the ATP for 5 minutes. The plate was then placed into a luminometer (model specified in results sections, Chapters 3, 4 and 5) where 20 $\mu$ l of Nucleotide Monitoring Reagent (NMR) was dispensed into each well and the initial ATP reading taken (reading A). The ATP RLU's were then allowed to decay to background levels over 10 minutes where afterwards 20 $\mu$ l of the ADP Converting Reagent (ADP-CR) was dispensed and an immediate reading taken (reading B). After a 5 minute incubation to allow for complete conversion of ADP to ATP a third reading was taken (reading C). The three readings were then used to work out the ADP:ATP ratio with the calculation outlined in Chapter 1, figure 1.13, where the ATP and ADP were measured in the reactions outlined in Chapter 1, figures 1.11 and 1.12.

#### **2.10.4 Measurement of percentage hypodiploid and cell cycle analysis using propidium iodide**

Propidium iodide binds proportionally to DNA so therefore can be used as an accurate indicator of DNA levels.

800 $\mu$ l of cell suspension ( $5 \times 10^5$  cells  $\text{ml}^{-1}$ ) was placed into a round bottom FACs tube. The cells were centrifuged at 400xg for 5 minutes and the supernatant carefully removed. The pellet was resuspended in 400 $\mu$ l of 70% (v/v) ethanol ( $4^\circ\text{C}$ ) and incubated for 20 minutes at  $4^\circ\text{C}$ . After this incubation step the samples were washed and centrifuged at 400xg twice with Phosphate Buffered Saline (PBS) and finally resuspended in 400 $\mu$ l of 50 $\mu\text{g ml}^{-1}$  PI. After an incubation of at least 30 minutes at  $4^\circ\text{C}$  the samples were analysed on a Becton Dickinson FACscan Flow Cytometer, where 20,000 events were counted. (The samples could be stored protected from light at  $4^\circ\text{C}$  for up to 48 hours if not analysed the same day).

#### **2.10.5 Measurement of the change in mitochondrial transmembrane potential ( $\Delta\Psi_m$ )**

The stock of 1mg  $\text{ml}^{-1}$  JC-1, was diluted 1:50 prior to use in PBS and filtered with a 0.45 $\mu\text{m}$  pore size filter. 100 $\mu$ l of cell sample ( $5 \times 10^5$   $\text{ml}^{-1}$ ) was placed into a round bottom FACs tube and 200 $\mu$ l of the filtered JC-1 added and mixed. After a 30 minute incubation at  $37^\circ\text{C}$  the samples were analysed immediately on a Becton Dickinson FACscan Flow Cytometer, where 5,000 events were counted. This technique was adapted from Salvioi et al (1997) and Kühnel et al (1997).

## 2.10.6 Detection of Cytolysis

### 2.10.6.1 ToxiLight

20µl volume of experimental supernatant was taken from the culture well and plated out into a 96 well luminometer plate in triplicate. 100µl of Adenylate Kinase Detection Reagent (AK-DR) was added to each well and left for 5 minutes before taking a 1 second integrated reading on a Berthold MPL3 luminometer.

The release of AK into the supernatant was detected in two stages following the reactions outlined in figure 2.08. AK is converted to ATP by the addition of ADP to the sample.

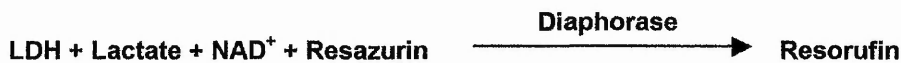


Figure 2.08

The subsequent formation of ATP is then converted to light and measured on a luminometer by the reaction outlined in chapter 1, figure 1.11.

### 2.10.6.2 CytoTox-ONE (Promega)

100µl volume of experimental supernatant was taken from the culture well and plated out into a 96 well luminometer plate in triplicate. 100µl of CytoTox-ONE reagent was added to each well and left at room temperature for an incubation time of 10 minutes. Following this 50µl of stop solution was added and the plate was measured on a Wallac Victor II fluorimeter with an excitation wavelength of 560nm and an emission wavelength of 590nm utilising the following reaction,



**Figure 2.09.** Conversion of Resazurin to fluorescent Resorufin which is proportional to the amount of LDH.

This technique was modified from the Promega protocol.

### 2.10.7 Measurement of Cytochrome c

The cytospin preparations in this procedure were kindly stained by Dr Ian Daniels at the David Evans Medical Research Centre, Nottingham City Hospital.

Cytospin slides were prepared using a Shandon cytospin 3 centrifuge (200xg for 5 minutes) using disposable cytofunnels where 100 $\mu$ l of cell sample ( $5 \times 10^5 \text{ ml}^{-1}$ ) was added to the chamber. The slides were allowed to air dry overnight. The cells were then fixed with 4% (w/v) paraformaldehyde to which 2% (w/v) sucrose had been freshly added for 10 minutes. PBS was used to remove the paraformaldehyde from the slides which were then permeabilised for 15 minutes in Saponin Permeabilisation Buffer (SPB). The SPB was drained and excess carefully removed with tissue from around the cells being careful not to allow the cells to dry out. Antibody to cytochrome c (6H2.B4 (1 in 250 in SPB, 50 $\mu$ l per slide) was immediately added to the slides and incubated in a humidified box for 1 hour at room temperature. The slides were washed four times in SPB for 5 minutes following the incubation step where on the final wash step the slides were drained with care as before. Antimouse FITC conjugate (F0313 (1 in 30 in SPB, 50 $\mu$ l per slide) was immediately added to the slides and incubated in a humidified box for 1 hour at room temperature. The slides were washed three times in SPB for 5 minutes following the incubation step where on the final wash step the slides were drained again as before. A small drop of Vectashield (containing DAPI counterstain) was placed onto a coverslip and the

coverslip carefully placed over the cells being sure not to leave any air bubbles. The edges of the coverslip were then sealed and the slides viewed under a fluorescence microscope observing for blue fluorescing nuclei, showing intact round nuclei in healthy cells and nuclear blebbing in apoptotic cells. Cytochrome c fluoresces green, which in healthy cells gives distinct tight green groups, this becomes dispersed when cytochrome c has been released from the mitochondria.

### **2.10.8 Western blotting**

Approximately  $8 \times 10^6$  cells  $\text{ml}^{-1}$  were washed three times in ice cold PBS. On the final wash the supernatant was carefully removed and the cells resuspended in 100 $\mu\text{l}$  of lysis buffer (section 2.8.1). Cells were disrupted by controlled sonication using a RapiDis 50 cell disruptor. Protein concentrations were determined using the DC protein assay (see below for complete method). Sample and an equal volume of x3 Laemmli stopping solution were heated at 105°C for 5 minutes. 25 $\mu\text{g}$  of each protein sample along with Rainbow marker and an apoptotic model B-JABS and CD95L known to activate the proteins of interest to give a positive control, this positive control was kindly supplied ready for loading on to the gel by Dr Ian Daniels were separated on 10%, 12% or 15% SDS PAGE (Tris-HCl) gels with a 4% stacking gel depending upon protein to be probed. The gels were run at 180mV for 45 minutes in running buffer (section 2.8.1). After the proteins had separated the gels were removed from the glass plate by washing in blotting buffer and transferred to nitrocellulose or PDVF by creating a sandwich as below,

- A piece of sponge was soaked in blotting buffer and placed on transfer cartridge.
- Blotting paper was slid under the gel to capture the gel and placed on top of the sponge.
- Nitrocellulose / PDVF was soaked in blotting buffer and placed on top of the gel.



- Blotting paper was soaked in blotting buffer and placed on top of the gel.
- The gel was gently smoothed using a roller to remove any air bubbles trapped inside.
- A piece of sponge was soaked in blotting buffer and placed on gel.

The cartridge was closed and connected to run at 100mV for 60 minutes in blotting buffer.

The membranes were removed from the cartridge and blocked in PBS containing 0.1% (v/v) Tween 20 and 5% (w/v) milk and probed overnight at 4°C with antibodies to; PARP, caspase 3, caspase 8 and caspase 9 made up as indicated in table 2.10 in 5% blotto. The membranes were washed three times in PBS-Tween and probed with the secondary antibodies made up in 5% Blotto, again as indicated in table 2.10 for 1 hour at room temperature. Bound antibodies were visualised by chemiluminescence using the ECL mix prepared as outlined in section 2.9.4 and immediately exposed to film for 5 minutes.

% Gel	Transfer medium	Primary Antibody	Secondary Antibody
15	PDVF	Caspase 3 1:1000	rabbit 1:1000
12	Nitrocellulose	Caspase 8 2µg ml <sup>-1</sup>	mouse 1:1000
12	Nitrocellulose	Caspase 9 2.5µg ml <sup>-1</sup>	mouse 1:1000
10	nitrocellulose	PARP 2µg ml <sup>-1</sup>	mouse 1:1000

**Table 2.10** Table showing the percentage gel, transfer medium and primary and secondary antibody concentrations required for the western blot analysis of caspase 3, caspase 8, caspase 9 and PARP.

### **2.10.8.1 DC Protein assay**

5 $\mu$ l of each standard was plated out in triplicate, 0.0, 0.2, 0.4, 0.8, 1.0 and 1.5 (mg ml<sup>-1</sup> protein) along with 5 $\mu$ l in triplicate of the cell lysates. 25 $\mu$ l of reagent 1 was added to each well and 200 $\mu$ l of reagent B added. The plate was read immediately on a Rosys Anthos 2001 spectrophotometer and after 15 minutes a further reading was taken.

### **2.10.9 Statistics**

All statistics were undertaken using SPSS version 12.0 or GraphPad instat 3. Correlation was assessed by Spearman's Rho (2 tailed), where significance was taken at  $p < 0.02$ . Wilcoxon matched pairs tests were carried out to show significant difference between samples treated with drug compared to the control, where significance was taken at  $p < 0.05$ . In all of the microtitre plate based assays carried out the experiments were set up in triplicate where the mean and standard Deviation (SD) was calculated for each triplicate, therefore when several experiments were analysed they were expressed as the mean of the triplicate means and the standard error of the mean (SEM) which were calculated using Microsoft Excel 2000. All Flow Cytometry data were analysed on a one tube per sample basis so are therefore expressed as the mean with SD. All graphs were created using Sigma plot version 8.0.

## **Chapter 3 - Bioluminescent measurement of Adenosine nucleotides**

### **3.1 Introduction**

The synthesis of ATP occurs as a result of the flow of electrons across the inner mitochondrial membrane during a process called Oxidative Phosphorylation. Energy is released as electrons flow through the complexes of the inner mitochondrial membrane and fall to a lower energy state. This release of energy actively transports  $H^+$  ions from the matrix to the intermembrane space, thus making the matrix negatively charged and the intermembrane space positively charged. This distribution of ions across the inner membrane is called the mitochondrial transmembrane potential ( $\Delta\psi_m$ ). The opening of megachannels or permeability transition (PT) pores which span the inner to the outer mitochondrial membrane are necessary for the equilibrium of essential ions between the cytosol and the mitochondrial matrix. These PT pores open irreversibly during apoptosis and it is believed that this disruption in PT is the cause of the collapse in the  $\Delta\psi_m$  (*Mignotte and Vayssiere (1998) and Susin et al 1996*). This collapse consequently leads to a reduction in the production of ATP. ATP is essential for all cells to carry out their specific activities including programmed cell death, as it serves as the primary donor of free energy. Apoptosis is an energy driven process that requires ATP to carry out its specialised functions. Reports have indicated the requirement for ATP during Fas mediated apoptosis for active nuclear exchange of large molecules across the membrane (*Yasuhara et al (1997)*). It has also been suggested that whilst programmed cell death requires ATP it is not necessary during necrosis (*Tsujimoto (1997)*). Depletion in cellular ATP levels are therefore an accurate indicator of the viability of a cell, as all cells have an absolute requirement for ATP (*Crouch et al (1993)*).

The acknowledgement in 1947 by McElroy that the luciferase reaction in the Firefly (*Photinus pyralis*) required ATP led to an extensive investigation into the use of bioluminescence as a measure of ATP within cells. It was not until the 1980's however that bioluminescence became more widely used within laboratories. Up until this time only crude luciferase / luciferin reagents were available to the researcher, this combined with the poor methods of extraction of ATP and the lack of commercially available luminometers, led to extensive analytical problems (Lundin (1990)) and halted progress within this field. The development of a purified luciferase with a stable light emission in the late 1970's however led to bioluminescence becoming the most widely used method of measuring ATP due to its ease, reproducibility and sensitivity over other assays. Experiments performed by Crouch et al, showed how bioluminescence correlated well with the traditional methods for determining cell proliferation by tritiated thymidine and cytotoxicity by crystal violet (Crouch et al (1993)).

Initial aims of this chapter will be to establish the sensitivity of this ATP bioluminescence method (ViaLight HS), firstly by the use of ATP standards and then dilutions of cells, whereby extrapolating a value of ATP per cell. Another of the aims of this chapter will be to continue the use ViaLight HS as a measure of cytotoxicity and to investigate the possibility of its use as a mitochondrial stress indicator by comparisons with mitochondrial transmembrane potential dyes such as 5,5',6,6'-tetrachloro-1,1',3,3'-tetraethylbenzimidazolcarbocyanine iodide (JC-1).

The ATP/ADP translocase can be found spanning the inner mitochondrial membrane and closely monitors the flow of ATP from the mitochondria to the cytoplasm, which is closely coupled to the influx of ADP from the cytoplasm to the mitochondria. The rate at which oxidative phosphorylation proceeds within the mitochondria is dependent upon the levels of ADP (Alberts et al 1989)). During a cells normal activities ATP is consumed and ADP is produced as a result. This increase in ADP in normal healthy cells leads to the synthesis of ATP to maintain the

ATP/ADP balance. Disruption of the electron transport chain will eventually lead to a build up of ADP as the cells ATP stores are depleted (*Bradbury et al (2000)*). The observation that these biochemical changes occur during cell death led to the development of a bioluminescent method of detecting the levels of ATP and ADP within cell populations in order to determine and distinguish between programmed cell death and the more violent form of cell death necrosis, within one assay (ApoGlow™). As it has already been reported ATP levels are maintained to carry out the specialised functions of apoptosis thereby cells dying by this method maintain a relatively high ATP level for some time. Cells dying by necrosis however show a dramatic decrease in ATP stores coupled to an increase in cellular ADP almost instantly. The ApoGlow™ assay allows the detection of small quantities of ADP in the presence of high levels of ATP, which is sensitive enough to distinguish between necrotic cell death and apoptosis. The sensitivity of this assay will be investigated firstly by the use of ADP standards and later used to measure necrosis within heat treated cells. This chapter will then go on to establish whether the ApoGlow™ assay can be used to distinguish between cells undergoing apoptosis and secondary necrosis assessed by their ability to exclude cell viability dyes such as propidium iodide (PI).

## **3.2 Results**

### **3.2.1 Measuring ATP using the ViaLight HS protocol**

Initial experiments carried out for this thesis were to determine the reliability of the bioluminescent assay ViaLight HS. This assay was developed for the detection of ATP within viable cells by utilising the Luciferin / Luciferase reaction outlined in chapter 1 (figure 1.11).

If all factors in the reaction mechanism are saturated it can be deduced that the light emission is linearly related to the concentration of ATP present. This light is then detected by a luminometer and expressed as the relative light units or RLUs.

### **3.2.2 ATP standards**

It is well established that the Luciferase reaction is quenched by intensely coloured mediums. RPMI 1640 media containing phenol red and foetal bovine serum was used in the culture of the suspension cell lines used within this study, so therefore ATP standards were carried out diluted in both RPMI complete media (CM) and TAB to observe the quenching effect created by the mediums.

The linearity of the ViaLight HS assay was verified by performing ATP standard curves using ATP diluted 1:10 in TAB or CM. From a starting concentration of  $1\mu\text{mol ml}^{-1}$ , samples of the dilutions were then plated into a 96 well white luminometer plate in 100 $\mu\text{l}$  aliquots. The plate was measured using ViaLight HS on a Berthold MPL3 luminometer; see Figure 3.01.

Figure 3.01

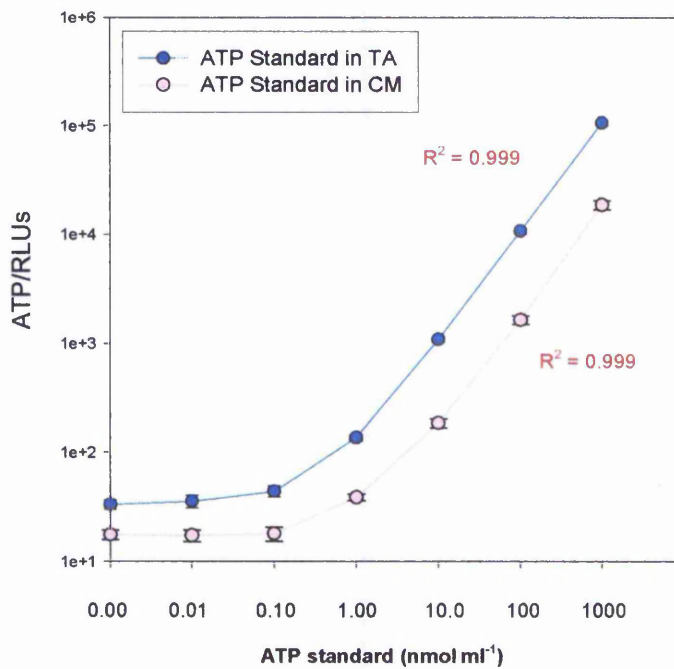


**Figure 3.01.** Measurement of ATP standards diluted 1:10 in either TAB or CM, ATP was detected using ViaLight HS and measured on a MPL3 luminometer (Berthold). The results are expressed as n = 8 separate experiments +/- SEM.

Figure 3.01 compares the ATP standards made up in TAB and CM showing a linear response to the measurement of ATP with  $R^2$  values of 0.999. The ViaLight HS kit showed sensitivity down to  $1\text{nmol ml}^{-1}$  ATP with a percentage CV of less than 10% over the  $1\text{nmol ml}^{-1}$  to  $1000\text{nmol ml}^{-1}$  concentration range for ATP standards diluted in both TAB or CM.

It can be observed that the RLUs have decreased by a factor of 10 for the ATP standards diluted in CM. A concentration of  $1000\text{nmol ml}^{-1}$  ATP in TAB gave RLUs of approximately 110,000 whereas ATP diluted in CM gave 18,000 RLUs for the same concentration of ATP. Despite this quenching effect the sensitivity of the ViaLight HS assay is unchanged as standards diluted in CM show comparable sensitivity with standards diluted in TAB.

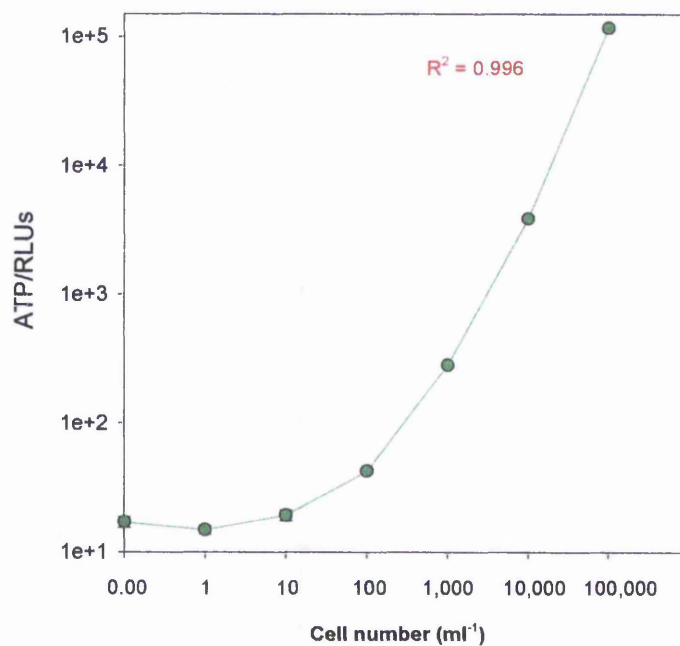


### 3.2.3 Measuring ATP within cells

The experimental procedure was extended to investigate the measurement of ATP within cells. The ViaLight HS kit contains Nucleotide Releasing Reagent (NRR). NRR contains a non ionic detergent that punches holes into the cell membrane and allows for the release of the nucleotides within the cells. Following the incubation with NRR, ATP can be measured as in the previously mentioned Luciferin / Luciferase reaction. The cells used in this investigation were a human leukaemia cell line K562 diluted 1:10 from a seeding density of  $1 \times 10^5$  cells  $\text{ml}^{-1}$  in CM shown in figure 3.02. The ViaLight HS kit for this particular cell line showed sensitivity down to 50 cells per well giving an  $R^2$  value of 0.996 and a percentage CV of less than 10% over the 100,000 cells  $\text{ml}^{-1}$  to 10 cells  $\text{ml}^{-1}$  range.

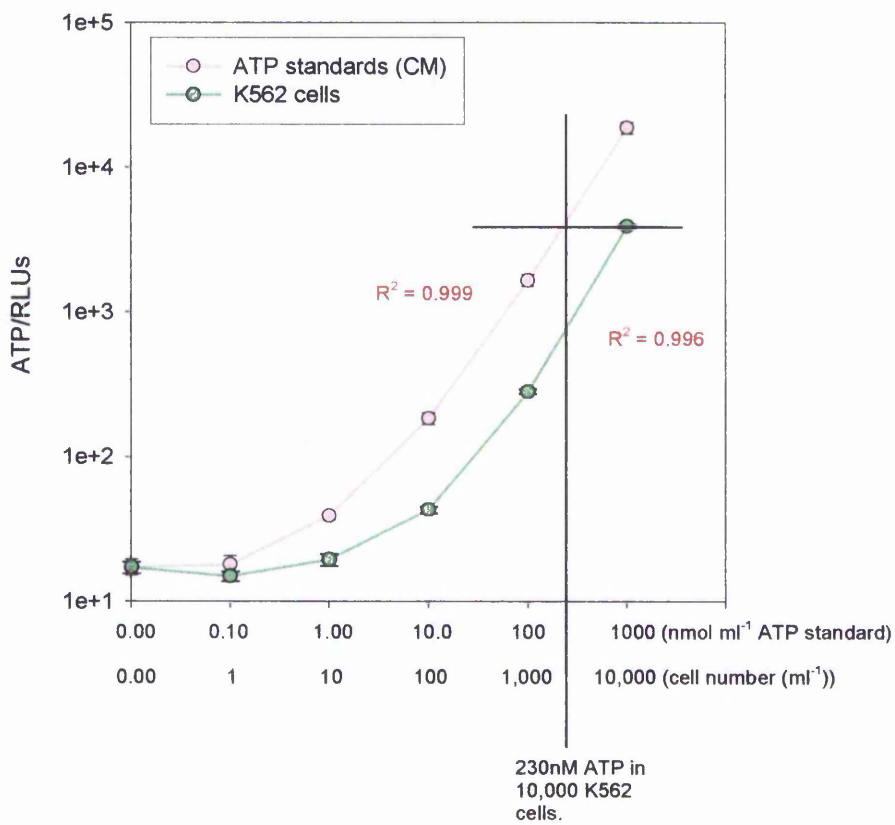
The 1:10 dilutions of K562 cells and ATP standards diluted 1:10 in CM were placed on the same graph, figure 3.03, so that a value of ATP within a population of 10,000 K562 cells could be calculated. In this particular case a value of 230nM ATP could be detected in 10,000 K562 cells.

Figure 3.02



**Figure 3.02.** Measurement of K562 cells diluted 1:10 in CM, ATP detected using ViaLight HS and measured on a MPL3 luminometer (Berthold). The results are expressed as n = 8 separate experiments +/- SEM.

**Figure 3.03**

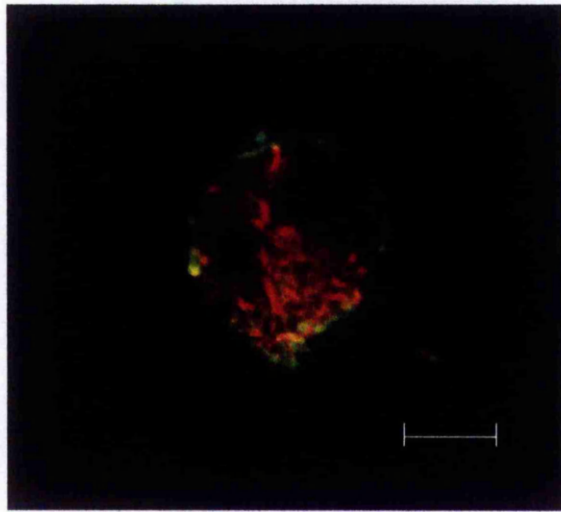


**Figure 3.03.** Measurement of ATP standards diluted 1:10 in CM and K562 cells diluted 1:10 in CM, measured on a MPL3 luminometer (Berthold) where ATP was detected using ViaLight HS. The results are expressed as n = 8 separate experiments +/- SEM.

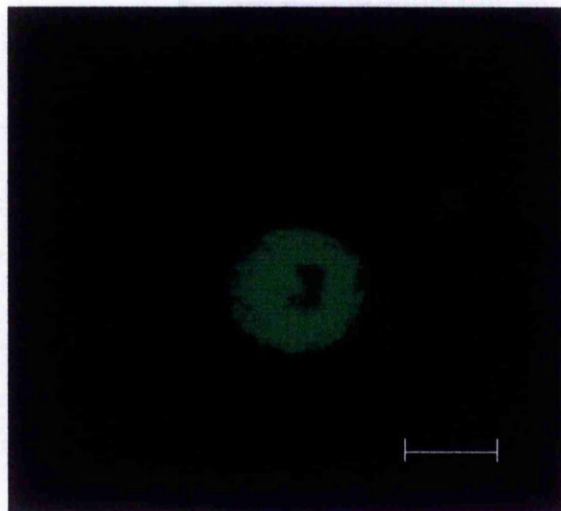
### 3.2.4 Measuring the mitochondrial transmembrane potential ( $\Delta\psi_m$ )

As already mentioned the irreversible opening of PT pores during apoptotic cell death is believed to be the cause of the collapse of the  $\Delta\psi_m$ . The loss of  $\Delta\psi_m$  can be detected by the use of fluorescent probes such as 5,5',6,6'-tetrachloro-1,1',3,3'-tetraethylbenzimidazolcarbocyanine iodide (JC-1), 3,3'-dihexyloxacarboxyanine iodide (DiOC<sub>6</sub>) and Rhodamine123 (Rh123) through fluorescent microscopy and flow cytometric analysis. Functioning mitochondria in viable cells have a high  $\Delta\psi_m$  and as a consequence actively uptake the dye. The dual emission potential sensitive probe JC-1 used in this study exists as green monomers until concentrated above 1 $\mu$ M inside the mitochondria where it will fluoresce red. Figure 3.04 shows Jurkat cells incubated for 48 hours with and without 10 $\mu$ M Ara-C, it can be seen that the healthy untreated cell has functioning mitochondria as it has accumulated the JC-1 to a concentration above 1 $\mu$ M where red J-Aggregates have formed, whereas the 10 $\mu$ M Ara-C treated cell fluoresces green as the JC-1 remains as green monomers.

**Figure 3.04**



**A**



**B**

**Figure 3.04.** The apoptotic model Jurkat and Ara-C incubated with the dual emission potential sensitive probe JC-1. 3mls of cell suspension ( $5 \times 10^5$  cells  $\text{ml}^{-1}$ ) were placed in each well of a 12 well tissue culture plate and dosed with either 0 (control) or  $10 \mu\text{M}$  Ara-C and incubated at  $37^\circ \text{C}$  in a humidified atmosphere in 5% (v/v)  $\text{CO}_2$ , 95% (v/v) air for 48 hours. The JC-1 was filtered prior to use and added to the cell suspension and incubated for 30 minutes at  $37^\circ \text{C}$ . Slide A shows an untreated cell with red fluorescing, functioning mitochondria, where slide B shows a cell treated with  $10 \mu\text{M}$  Ara-C showing green monomers only. Scale bar:  $10 \mu\text{m}$ .

One of the benefits of JC-1 staining is that it has been found to be unaffected by agents that depolarise the plasma membrane, whilst it is strongly affected by drugs that dissipate the  $\Delta\psi_m$  such as the drug Valinomycin (*Salvioli et al (2000)*). The cytotoxicity model Jurkat and Ara-C was incubated for 48hours and tested with ViaLight HS and the  $\Delta\psi_m$  dye JC-1. Both the ATP/RLUs and the % J-Aggregates (Figure 3.05) showed a drug dependent decrease where the ATP/RLUs went from 5026.57 in the control to 492.85 in the 10 $\mu$ M Ara-C concentration and the % J-Aggregates reduced from 94% in the control to 14% in the 10 $\mu$ M Ara-C concentration, showing significant correlation ( $p < 0.02$ ) when assessed with Spearman's Rho. From the Wilcoxon matched pairs test that was carried out both the ATP/RLUs and the % J-Aggregates showed significant difference to the control ( $p < 0.05$ ).

Figure 3.05

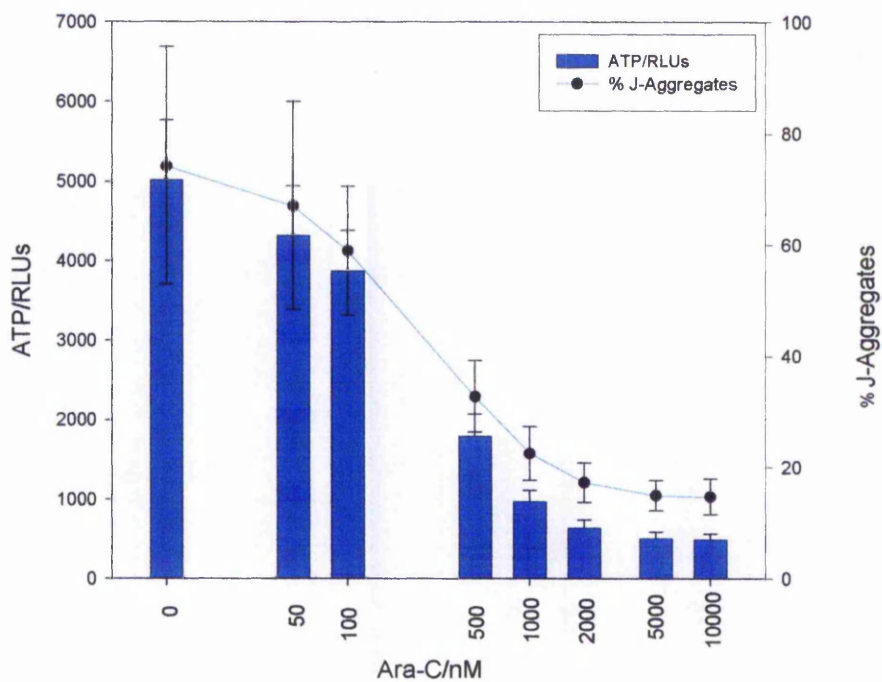


**Figure 3.05.** Comparison between the decrease in ATP/RLUs measured using ViaLight HS and the loss of the  $\Delta\psi_m$  measured using JC-1. The results are expressed as the means of  $n = 7$  separate Jurkat + Ara-C experiments incubated for 48 hours (+/- SEM (ATP/RLUs) and SD (% J-Aggregates)).

Table 3.01 shows data obtained from a Jurkat and Ara-C time course experiment over 4, 24 and 48 hours measuring ATP/RLUs, loss of  $\Delta\Psi_m$  measured using JC-1 and ATP per cell. This data was obtained by extrapolating the cell number as determined with Trypan Blue with an ATP standard curve diluted in CM. After 4 hours incubation there is no evidence of the effect of the drug in either the ATP/RLUs, % J-Aggregates, cell number or ATP per cell, all compare to the control showing healthy cells. Ara-C is a potent inhibitor of DNA replication in mammalian cells and as the cell enters S phase cell cycle arrest is induced (*Wills et al (1996) and Decker et al (2003)*) and eventual entry into apoptosis. Cell cycle arrest is evident in the 24 hour and 48 hour data where the drug treated samples remained at the seeding density of  $5 \times 10^5$  cells  $\text{ml}^{-1}$  throughout the 48 hour period whereas the cell count was seen to increase from the seeding density of  $5 \times 10^5$  cells  $\text{ml}^{-1}$  to  $1 \times 10^6$  cells  $\text{ml}^{-1}$  at 24 hours to  $2 \times 10^6$  cells  $\text{ml}^{-1}$  after 48 hours in the control sample. When visualised microscopically the drug treated samples appeared twice the size of the drug treated samples suggesting that these cells had doubled up their cellular content but had not been able to enter  $G_2/M$  phase of the cell cycle and divide.

The ATP/RLUs were also seen to increase at each time point in the control sample reflecting the proliferation of the cells. ATP per cell in the control cells however were seen to decrease over this period which maybe due to the cells becoming overcrowded and competing for remaining nutrients as the Jurkat cells are maintained below  $1 \times 10^6$  cells  $\text{ml}^{-1}$  in culture. ATP per cell was maintained in all of the drug treated samples over the 4 hours and 24 hours period where the ATP/RLUs and ATP per cell were only seen to drastically drop at the 1000nM Ara-C concentration after 48 hours incubation. The % J-Aggregates were maintained until 1000nM Ara-C in the 24 hours incubation decreasing from 82.30% in the control to 68.47% in the 1000nM concentration down to 52.44% in the 10,000nM concentration of the drug showing that half of the mitochondria remained viable. The % J-Aggregates after 48 hours



incubation however showed significant difference from the control at 50nM Ara-C dropping from 83.7% in the control to 72.71% in the 50nM concentration down to 12.47% in the 10,000nM sample. When the samples were observed down a light microscope, the drug treated samples at 48 hours were seen to have increased in their overall size, suggesting that these cells had replicated their DNA but had not been able to divide. If therefore these cells had completed their cell division the ATP per cell obtained would be halved in the 48 hours samples giving a dramatic loss of ATP at 500nM Ara-C. In the absence of functioning mitochondria cells would eventually cease to function once intracellular ATP stores had been depleted (*Tsujimoto (1997)*).

	ATP/RLUs			% J-Aggregates			ATP per single cell		
	4 hours	24 hours	48 hours	4 hours	24 hours	48 hours	4 hours	24 hours	48 hours
Ara-C/1M	2065.79 +/-412.93	2889.22 +/-882.68	4533.08 +/-1281.07	83.78 +/-9.04	82.30 +/-7.79	83.70 +/-3.11	16pM	12pM	11pM
0	2202.11 +/-523.38	3268.77 +/-947.50	3819.08 * +/-1157.57	84.52 +/-9.85	81.26 +/-7.17	72.71 * +/-6.44	20pM	32pM	21pM
50	2306.46 +/-706.84	3488.53 +/-1001.41	3503.04 * +/-937.69	83.21 +/-10.6	80.72 +/-7.42	60.52 * +/-4.61	16pM	30pM	29pM
100	2016.19 +/-627.00	2990.54 +/-813.63	1520.27 * +/-366.36	82.78 +/-10.22	76.02 +/-7.43	32.17 * +/-3.11	17pM	26pM	14pM
500	2375.97 +/-725.32	2481.26 +/-845.31	967.79 * +/-211.17	84.35 +/-10.06	68.47 * +/-7.24	23.54 * +/-2.95	20pM	24pM	9pM
1000	2122.76 +/-569.87	2200.15 * +/-496.27	558.61 * +/-170.43	84.60 +/-10.77	59.63 * +/-6.42	16.98 * +/-1.76	20pM	24pM	6pM
5000	2275.17 +/-528.91	2037.19 * +/-546.26	442.47 * +/-143.16	83.95 +/-8.44	54.54 * +/-7.23	13.57 * +/-2.28	21pM	20pM	5pM
10,000	2208.66 +/-518.10	2117.29 * +/-541.43	429.59 * +/-148.97	84.97 +/-8.98	52.44 * +/-7.31	12.47 * +/-1.10	22pM	22pM	4pM

**Table 3.01.** Comparison between the decrease in ATP/RLUs measured using Vialight HS on a 1450 Microbeta Jet (Wallac) and the loss of the  $\Delta v_m$  measured using JC-1. The JC-1 was filtered prior to use and added in twice the volume of cell suspension and incubated for 30 minutes at 37°C before measuring on a FACScan (Becton Dickinson) flow cytometer. The results are expressed as the means of 5 separate Jurkat and Ara-C experiments incubated for 4, 24 and 48 hours (+/- SEM (ATP/RLUs) and SD (% J-Aggregates)), where \* represents a significant difference from the time point control with a p value of < 0.05 assessed with the Wilcoxon matched pairs test. Cell counts were also carried out at each time point on each sample with trypan blue where all samples compared to the seeding density of  $5 \times 10^5$  cells  $ml^{-1}$  apart from the two controls at 24 hours which had doubled to that of the 4 hour control and again after 48 hours, these cell counts were used along with a ATP standard curve diluted in CM measured on a 1450 Microbeta Jet (Wallac) to obtain a ATP value per cell.

Table 3.02 shows K562 cells incubated with a range of the topoisomerase II inhibitor Etoposide. The control cells were observed to proliferate from the seeding density of  $2.5 \times 10^5$  cells  $\text{ml}^{-1}$  to  $1.31 \times 10^6$  cells  $\text{ml}^{-1}$  over a 72 hours incubation compared to an average total cell number of  $3.7 \times 10^5$  cells  $\text{ml}^{-1}$  for the drug treated samples. When the cell counts were placed alongside ATP standard curves an amount of ATP per cell was extrapolated and it was found that the drug treated samples contained approximately four times the amount of ATP as the control in the  $0.5 \mu\text{g ml}^{-1}$  concentration and twice the amount in the  $2 \mu\text{g ml}^{-1}$  and  $4 \mu\text{g ml}^{-1}$  drug concentrations. When cytopsin slides were observed microscopically these drug treated samples contained cells that had increased in size dramatically over that of the control showing trinuclear cells, suggesting that these cells were perhaps able to replicate their DNA but unable to divide.

Etoposide $\mu\text{g ml}^{-1}$	ATP/RLUs	Total cell number Seeding density = $2.5 \times 10^5$ cells $\text{ml}^{-1}$	ATP per single cell
0	14913.43 +/- 1386.44	$1.31 \times 10^6$	26pM
0.5	16465.57 +/- 1606.02	$3.00 \times 10^5$	117pM
2	13498.15 +/- 1638.73	$3.90 \times 10^5$	79pM
4	12134.39 +/- 156432	$4.30 \times 10^5$	67pM

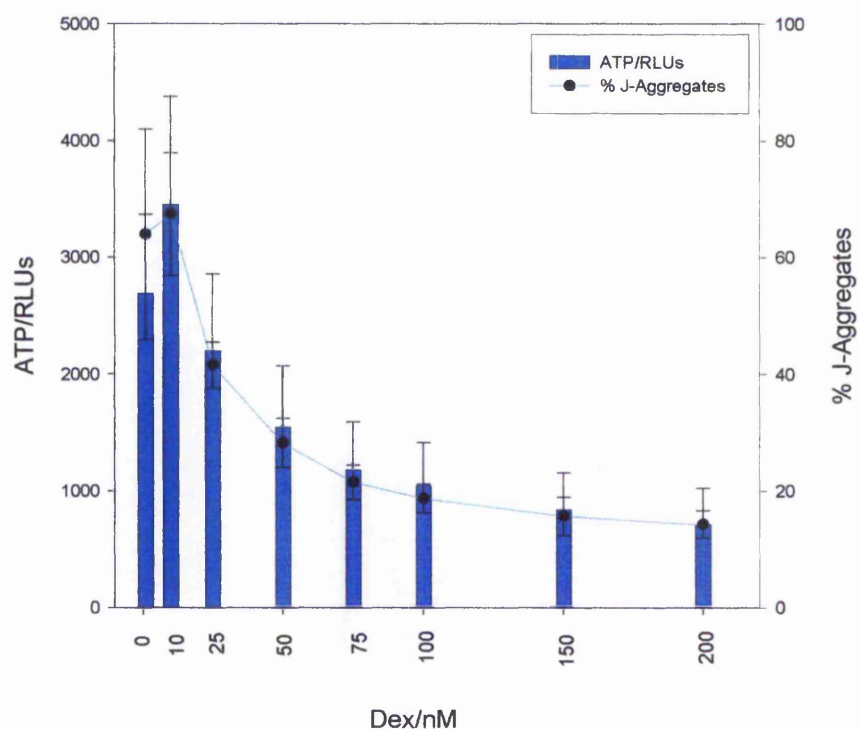
**Table 3.02.** ATP/RLUs measured using ViaLight HS on a Berthold MPL3 luminometer. Cell counts were also carried out on each sample with trypan blue where they were used along with a ATP standard curve diluted in CM measured on a Berthold MPL3 luminometer to obtain a ATP value per cell. The results are expressed as the means of 4 separate K562 and Etoposide experiments incubated for 72 hours (+/- SEM).

The correlation of the loss of ATP measured by bioluminescence using the ViaLight HS kit and the loss of the  $\Delta\psi_m$  was investigated. Figure 3.06 shows the correlation between ATP/RLUs and loss of the  $\Delta\psi_m$  measured by the decrease in red fluorescence using the probe JC-1 in the cytotoxicity model CEM-7 and Dexamethasone. The ATP/RLUs and % J-Aggregates show a significant correlation when assessed using

Spearman's Rho (2 tailed) ( $p < 0.02$ ). The ATP/RLUs reduce significantly from 2692.51 in the control to 308.64 in the 200nM concentration of Dexamethasone and there is a corresponding reduction in % J-Aggregates from 63.93% in the control to 14.23% in the 200nM concentration of Dexamethasone. Both showed an initial increase in both ATP/RLUs and red fluorescence for the 10nM concentration of Dexamethasone. This suggests that the mitochondria were either proliferating or were producing more ATP as the cell counts carried out on these samples showed no proliferation in the 10nM sample over the control. The evidence would support the proliferation of the mitochondria due to the measurable increase in red fluorescence detected where both ATP/RLUs and % J-Aggregates showed a significant difference from the control when measured using a Wilcoxon matched pairs test ( $p < 0.05$ ).

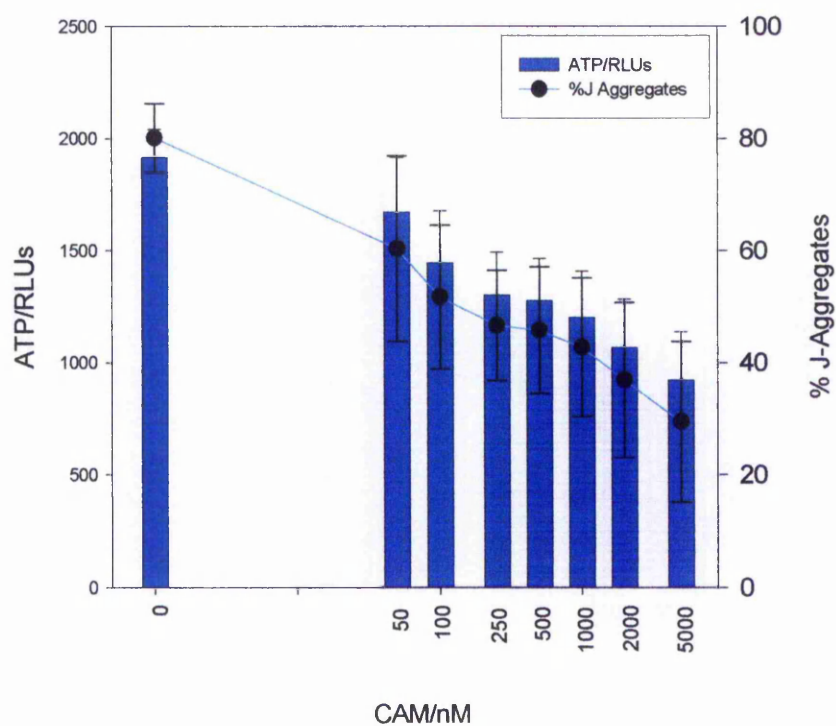
The CEM-7 and Dexamethasone model incubated for 72 hours is a model that is in the later stages of apoptosis and is entering into secondary necrosis at the time of measurement assessed by PI, therefore a comparison was made between the ATP/RLUs and the measurement of the  $\Delta\psi_m$  with JC-1 with the HL60 and camptothecin model, which was shown to be in the early stages of apoptosis (figure 3.07).

Figure 3.06



**Figure 3.06.** Comparison between the decrease in ATP/RLUs measured using ViaLight HS and the loss of the  $\Delta\psi_m$  measured using JC-1. The results are expressed as the means of  $n = 5$  separate CEM-7 and Dexamethasone experiments incubated for 72 hours (+/- SEM (ATP/RLUs) and SD (% J-Aggregates)).

Figure 3.07



**Figure 3.07.** Comparison between the decrease in ATP/RLUs measured using ViaLight HS and the loss of the  $\Delta\psi_m$  measured using JC-1. The results are expressed as the means of  $n = 5$  separate HL60 and Camptothecin experiments incubated for 4 hours ( $\pm$  SEM (ATP/RLUs) and SD (% J-Aggregates)).

The ATP/RLUs and % J-Aggregates both showed a drug dependent effect and showed significant correlation when analysed using Spearman's Rho (2 tailed) ( $p < 0.02$ ). Again the ATP/RLUs reduced from 1914.93 in the control to 924.19 in the 5000nM concentration of Camptothecin and there was a corresponding reduction in the % J-Aggregates decreasing from 80.12% in the control to 29.44% in the 5000nM concentration of Camptothecin. Both assays illustrated a significant difference from drug treated samples to the control when assessed using the Wilcoxon matched pairs test ( $p < 0.05$ ).

### 3.2.5 Development of the ApoGlow™ bioassay

The recognition of the changes in the relative levels of ATP to ADP during cell death led to the development of the bioluminescent ApoGlow™ assay which is capable of converting and detecting small amounts of ADP to ATP using the reactions and calculation outlined in Chapter 1, figures 1.11, 1.12 and 1.13.

Figure 3.08 shows the ATP/RLUs detected after 5 minutes of ADP conversion of ADP standard to ATP. ADP standards were diluted 1:10 in TAB from a starting concentration of  $1000\text{nmol ml}^{-1}$  and plated out in  $100\mu\text{l}$  aliquots in triplicate into a 96 well white luminometer plate and measured using the ApoGlow™ protocol on the Berthold MPL3 luminometer. Figure 3.08 shows a linear response to the measurement of ADP with a  $R^2$  value of 0.999. The ApoGlow™ assay shows sensitivity down to  $1\text{nmol ml}^{-1}$  ADP with a percentage CV of less than 10% over the  $1\text{nmol ml}^{-1}$  to  $1000\text{nmol ml}^{-1}$  concentration range.



**Figure 3.08**

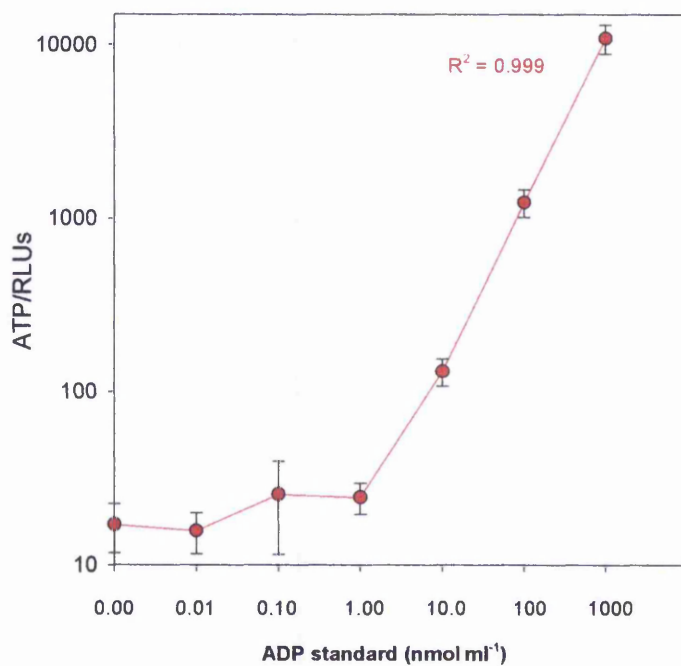


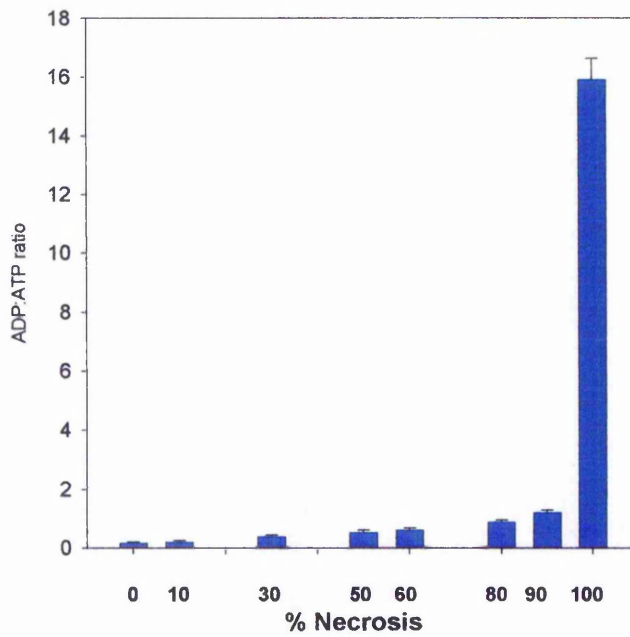
**Figure 3.08.** Measurement of ADP standards detected using ApoGlow<sup>TM</sup> and measured on a MPL3 luminometer (Berthold). Measurements were taken after 5 minutes of ADP conversion to ATP. The results are expressed as 8 separate experiments +/- SEM.

### 3.2.6 Measuring apoptosis and necrosis

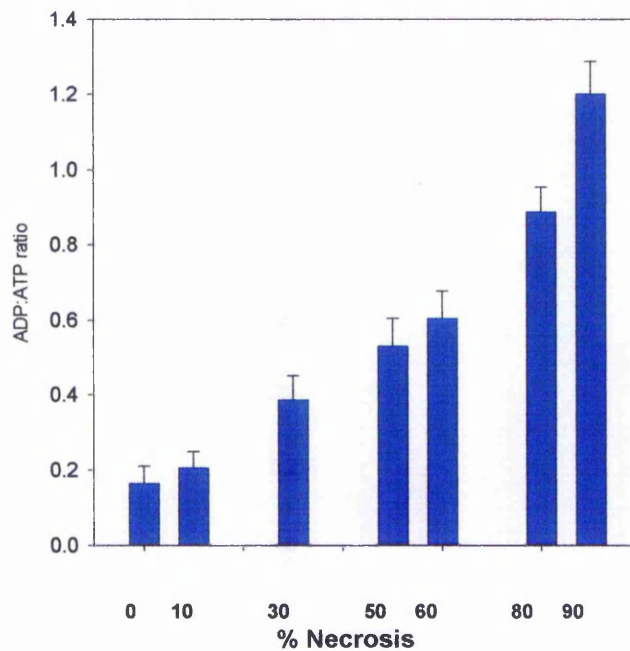
Cells dying by necrosis and apoptosis not only appear different but have very different biochemistry. K562 cells at  $1 \times 10^6 \text{ ml}^{-1}$  were induced to necrose by heating at  $56^\circ\text{C}$  for 1 hour. These were mixed with healthy (control) cells at  $1 \times 10^6 \text{ cells ml}^{-1}$  as follows 0, 10, 30, 50, 60, 80, 90 and 100% necrotic as outlined in Chapter 2, section 2.6, and measured using ApoGlow™ as outlined in Chapter 2, section 2.10.3.2. Figure 3.09 shows the necrotic and healthy mixture data with and without the 100% necrotic sample.

It can be observed from the heat treated data that an addition of only 10% healthy cells to a necrotic population will lower the ADP:ATP ratio dramatically from a ratio of 15.91 in the 100% necrotic sample to 1.20 in the 90% necrotic sample. This difference can be apportioned to the initial ATP readings taken which in 100% necrotic cells is negligible therefore when the readings are calculated the ratio is proportionally high.

Figure 3.09



A



B

**Figure 3.09.** Measurement of the ADP:ATP ratio measured using ApoGlow™ with necrotic and healthy mixtures of K562 cells at  $1 \times 10^6$  cells  $\text{ml}^{-1}$  where the cells were heat treated at  $56^\circ\text{C}$  for 1 hour and plated out in  $100\mu\text{l}$  volumes in 96 well white luminometer plates (Porvair). Figure A includes 100% necrosis and figure B shows the same data without 100% necrosis. The results are expressed as  $n = 11$  separate experiments  $\pm$  SEM.

Primary necrosis is generally a quicker process than that of apoptosis although timings will vary depending upon the method of induction. This means that necrotic cells do not have the time to die in an orderly fashion but will react and die with leakage of toxins from their burst membranes causing inflammation in the surrounding area. This explains the very different ADP:ATP ratios observed in cells that have undergone primary necrosis, secondary necrosis and cells that are in the earlier stages of apoptosis with their cell membranes still intact. Figure 3.10 shows typical kinetics of cells that are healthy, growth arrested, apoptotic and necrotic. The kinetics of healthy and growth arrested cells are quite similar to one another showing the initial A reading to be the highest, B the lowest and C to be slightly higher than the B reading due to the tiny amount of ADP present in healthy and growth arrested cells. The apoptotic kinetics shows a similar profile to the healthy cells in that A is still the highest reading, although the ATP RLUs are greatly reduced to that of the control and B is the lowest reading but reading C this time comes back up to the initial ATP reading showing increased amounts of ADP in these apoptotic cells. 100% Necrotic kinetics however are different in that reading A is the lowest with an immediate increase in ATP with the addition of the ADP converting reagent due to the large amounts of ADP present in necrotic cells which is shown to steadily increase over the next 10 minutes of measurement.

Figure 3.11 shows a Jurkat and IgM CD95 experiment over a time course of 4 and 24 hours incubation and demonstrates the difference in the ADP:ATP ratios obtained in cells that are apoptotic and secondarily necrotic. Cell membrane integrity was assessed with the DNA binding probe propidium iodide (PI). The ADP:ATP ratios taken at 4 hours were seen to increase from 0.14 in the control to 0.21 in the 250ng ml<sup>-1</sup> concentration which was found to be significant from 100ng ml<sup>-1</sup> when analysed with the Wilcoxon matched pairs test ( $p < 0.05$ ).

Figure 3.10

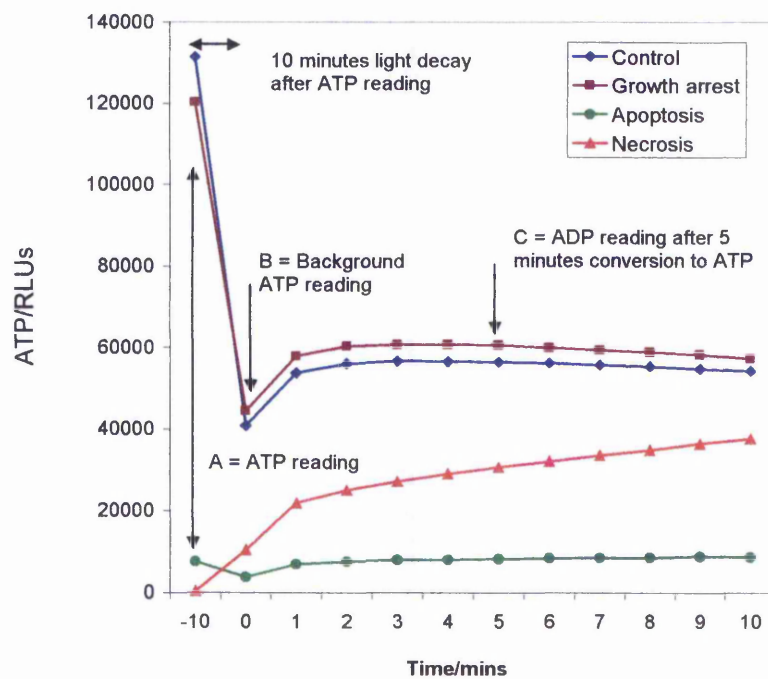
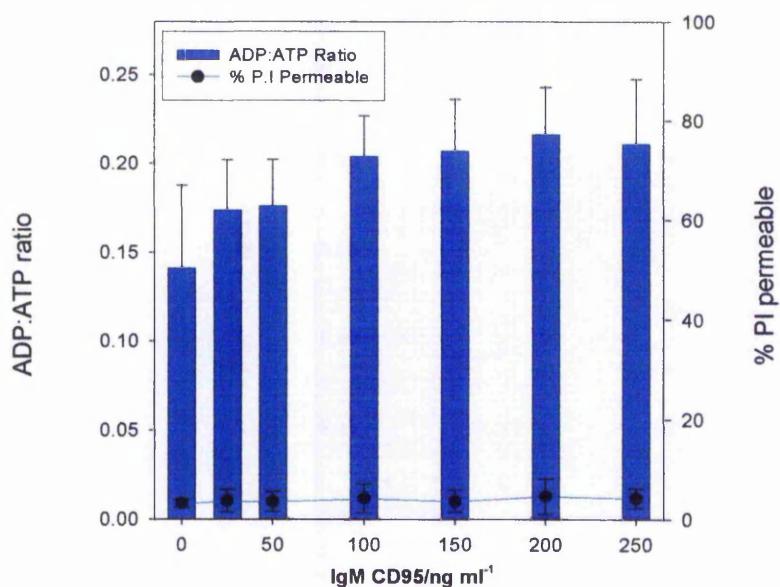
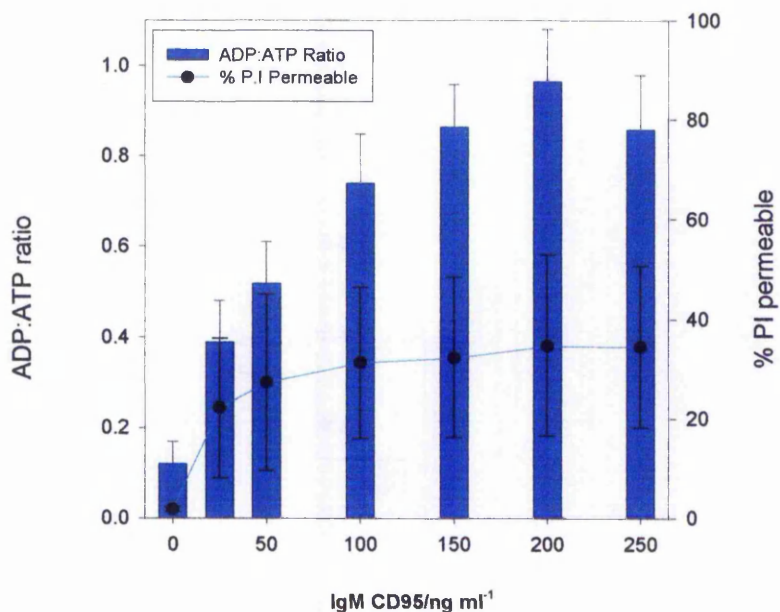


Figure 3.10. Kinetics of the ApoGlow™ assay. Schematic representation of the typical ATP/RLUs obtained for healthy control cells, growth arrested cells, apoptotic cells and necrotic cells.

**Figure 3.11**



**A**



**B**

**Figure 3.11.** Comparison between the increase in ADP:ATP ratios detected using ApoGlow™ measured on a MPL3 luminometer (Berthold) and the maintenance of the cell membrane measured using PI. The samples were analysed immediately after a 5 minute incubation at room temperature on a Becton Dickinson FACscan Flow Cytometer. The results are expressed as the means of 4 separate Jurkat + IgM CD95 experiments incubated for 4 hours (A) and 24 hours (B) (+/- SEM (ADP:ATP Ratios) and SD (% PI Permeable)).

After 24 hours incubation the ADP:ATP ratios can be seen to go from 0.12 in the control to 0.86 in the 250ng ml<sup>-1</sup> concentration of IgM CD95 showing significant difference from the control when assessed with Wilcoxon matched pairs test ( $p < 0.05$ ). This ADP:ATP ratio of 0.86 in the 250ng ml<sup>-1</sup> concentration when the cells have entered secondary necrosis was compared to the ADP:ATP ratio of 0.21 for the same concentration of IgM CD95 but where the cells are apoptotic. When cells lose their cell membrane integrity they enter what is termed as secondary necrosis and they become permeable to dyes such as PI. After 24 hours incubation with IgM CD95, Jurkat cells uptake PI and go from 1.81% in the control to 27.11% in the 250ng ml<sup>-1</sup> concentration, a significant difference between control and death receptor treated sample was found when assessed using the Wilcoxon matched pairs test ( $p < 0.05$ ).

### 3.3 Discussion

The use of bioluminescence as a measurement of ATP has been around since the mid 1980's due to its sensitivity, reliability and speed over alternative methods such as tritiated thymidine uptake that requires the use of radioisotopes. The bioluminescent ATP kit ViaLight HS was able to measure a 96 well white plate in 5 minutes showing sensitivity and reliability down to 50 cells per well and over the ATP standard range.

The running of ATP concentration curves to obtain an ATP standard curve along side cells demonstrated how a value of ATP within a cell population could be attained by extrapolating the cell number against the ATP standard curve. The amount of detectable ATP depends upon the quantity of mitochondria, which varies between the cell types. The positioning of the mitochondria within the cell is unique to each particular cell type and appears to be associated with microtubules which seem to determine the orientation and distribution of the mitochondria becoming localised to sites of high ATP consumption such as packed between adjacent myofibrils in a cardiac muscle cell (*Alberts et al (1989)*). The differences in measurable ATP are also reflected in the size of the cell.

The study carried out on CEM -7 and Dexamethasone showed increased ATP/RLUs, which correlated with an increase in JC-1 uptake showing evidence of mitochondrial proliferation during apoptosis. The cell counts carried out on these samples showed no proliferation over that of the control, this suggested therefore that it was either increased ATP production or mitochondrial proliferation. The data presented supported the proliferation of the mitochondria over increased production of ATP due to the measurable increase in red fluorescence. It has been suggested that the proliferation of mitochondria during programmed cell death is an integral part of the apoptotic cascade (*Eliseev et al (2003)*). Their work however showed that the proliferating cells found in the apoptotic model HL60 and Etoposide were impaired in that they showed a decrease in the mitochondrial transmembrane potential ( $\Delta\psi_m$ ) and ATP



content. Mitochondrial proliferation in their study was assessed by mitochondrial DNA content which was found to correlate with the elevated expression of mtSSB one of the regulators of mitochondrial DNA replication (*Eliseev et al (2003)*).

As apoptosis is an energy driven process it follows that the ATP levels within the cell would remain constant to carry out the specialised functions of programmed cell death. In the Jurkat and Ara-C cytotoxicity model there was evidence of mitochondrial stress but the ATP present per cell remained comparable to that of the control over the same concentration range, suggesting that although the mitochondria were starting to show signs of stress they were still able to produce the ATP required to drive the apoptotic processes. There is evidence to suggest that some malignant cells and some IL-3-dependent cell lines are able to shift their energy production to glycolysis when the  $\Delta\psi_m$  has become compromised (*Chen (1988) and Garland and Halestrap (1997)*). Maybe therefore during apoptotic cell death there is a shift to glycolysis that enables the continuation of the apoptotic processes. This concentration range showed other signs of the affects of the drug through increased cell size over that of the control. Ara-C is a potent inhibitor of DNA replication in mammalian cells and as the cell enters S phase cell cycle arrest is induced (*Wills et al (1996) and Decker et al (2003)*). This is evident after 24 hours incubation where the cell size is seen to be double that of the control cell. This increase in size suggests that the cells have replicated their cellular content but have not been able to divide, which is seen in the total cell number counts where the control cells have doubled in number in 24 hours, whereas the drug treated cells remain at the seeding density. Morphological signs of apoptosis seemed to appear with the decrease in the ATP/RLUs and ATP present per cell (data not shown). In the absence of functioning mitochondria, cells would eventually cease to function once intracellular ATP stores had been depleted (*Tsujimoto (1997)*).

Bioluminescence has been found to be an excellent alternative method for cell proliferation assays. It has been shown that the luciferin-luciferase reaction is a suitable substitute for tritiated thymidine uptake in the cell lines MOLT-4, HL60, TF-1 and NFS-60 (*Crouch et al (1993)*). The luciferin-luciferase assay has also been shown to give increased sensitivity over other cell proliferation assays such as the MTT assay on Daudi and CCRF-CEM cell lines (*Petty et al (1995)*).

The measurement of ATP has also been shown to successfully compare with traditional cytotoxicity assays such as crystal violet. Tumour necrosis factor  $\alpha$  (TNF $\alpha$ ) was shown to induce cytotoxicity in the mouse fibroblast cell line L-929 (*Crouch et al (1993)*). A drug dependent effect was detected in the cytotoxicity assays Jurkat and Ara-C, CEM-7 and Dexamethasone and HL60 and Camptothecin. The loss of the  $\Delta\psi_m$  measured by JC-1 correlated with the decrease in ATP/RLUs. Mitochondrial stress was reflected in the loss of red fluorescence and increase in green fluorescence measured and the loss of ATP detected. This would suggest that the use of bioluminescence as a measure of ATP was a good indicator of mitochondrial state.

ViaLight HS offers many benefits over conventional assays by avoiding the use of radioisotopes and showing greater sensitivity and reproducibility over traditional methods. Due to the speed and ease of use of this method it lends itself particularly well to high throughput assays and drug screening.

An initial study carried out using ApoGlow<sup>TM</sup> demonstrated the ability and sensitivity of the assay to convert and detect ADP. The ApoGlow assay showed sensitivity across the ADP standard concentration range. By measuring and comparing the relative amounts of ADP to ATP it was found that by the use of the bioluminescent ApoGlow<sup>TM</sup> assay it was possible to screen for all outcomes in a cell viability study. The human leukaemia cell lines K562 and Jurkat gave healthy ADP:ATP ratios that

were reflected in the initial ATP readings taken. The kinetics of the ApoGlow™ reaction (see figure 3.10) for a healthy population of cells is one where the A value is highest and C is slightly higher than B although it is not uncommon in a healthy population of cells to obtain a negative ADP:ATP ratio due to extremely low levels of ADP. Proliferation over a 24 hour period was evident in the Jurkat control cells where the ATP/RLUs had nearly doubled in 24 hours. The ApoGlow™ kinetics during proliferation show elevated ATP RLU's over the control but the converted ADP values remain low, thereby giving comparable ADP:ATP ratios to the control. The kinetics of the ApoGlow™ reaction during primary necrosis are different in that the C and B readings were both higher than reading A. There is so much ADP present during primary necrosis that conversion and detection of ADP to ATP occurs immediately as the ADP Converting Reagent is added to the sample and the ATP/RLUs are seen to continue to rise over a 10 minute period. This continued rise in converted ADP to ATP is not seen to happen with only 10% addition of healthy cells to the necrotic population where the ADP:ATP ratios drop dramatically. It is the extremely low ATP readings initially in 100% necrosis that leads to the proportionally high ADP:ATP ratio.

The Jurkat and IgM CD95 treated data showed an increase in ADP:ATP ratios indicative of cells passing from apoptosis at 4 hours incubation to secondary necrosis after 24 hours incubation. The increase in ADP:ATP ratios were reflected in the maintenance of the plasma membrane at 4 hours incubation becoming permeable to the DNA binding probe propidium iodide (PI) after 24 hours exposure. The ApoGlow kinetics for the 250ng ml<sup>-1</sup> CD95 activating antibody treated sample at 4 and 24 hours incubation showed the A reading to have higher ATP/RLUs at 4 hours than 24 hours. These measurements demonstrated how the cells were becoming more susceptible to the death receptor IgM CD95 antibody after 24 hours incubation compared to 4 hours incubation. The initial ATP readings for the 250ng ml<sup>-1</sup> sample for both 4 and 24 hours were considerably lower than that of the control but gave increased levels of ADP over the control.

The kinetics of growth arrest show ATP/RLUs that are comparable or slightly higher than that of the control population and ADP levels that also compare to the control. These comparable RLUs therefore, when calculated give ADP:ATP ratios similar to that of the control. The Jurkat and Ara-C time course experiment showed evidence of growth arrest in the 50nM to 2000nM drug concentrations at 24 hours incubation. These growth arrested cells gave comparable ATP/RLUs and ADP:ATP ratios to that of the control but showed no increase in cell counts over the seeding density, where the control population had doubled in cell number during the 24 hours incubation. This study demonstrated how it is important not only to evaluate the ADP:ATP ratios of the samples whilst using the ApoGlow™ assay, but also to study and compare the ATP and ADP measurements obtained to create a clearer picture of the viability of the cells being analysed.

The data presented in this study suggests that ApoGlow™ can distinguish between late and earlier events in apoptosis. The ADP:ATP ratio was shown to increase regardless of cell membrane integrity measured by PI uptake. Loss of cell membrane integrity is indicative of secondary necrosis whereas maintenance of the plasma membrane implies a cell in the earlier stages of apoptosis. The next stage of this study therefore will be to investigate the comparability of the ApoGlow™ assay to earlier stages of apoptosis than that of loss of cell membrane integrity such as DNA fragmentation and also events believed to occur prior to this such as phosphatidyl serine flip from the inner cell membrane to the outer cell membrane, loss of the mitochondrial transmembrane potential and cytochrome c release.

## **Chapter 4 – The comparison of bioluminescence with conventional methods of detecting apoptosis and necrosis**

### **4.1 Introduction**

In the previous chapter the bioluminescent assay ApoGlow™ was used successfully to distinguish between necrotic cell death and cells during pre and post plasma membrane permeability as assessed by propidium iodide (PI) exclusion. The Jurkat and CD95 death receptor model shown in section 3.2.6 showed increasing ADP:ATP ratios as the cells passed through into secondary necrosis indicated by their permeability to PI. The ADP:ATP ratio was also shown to correlate with apoptosis that had occurred with and without the loss of the integrity of the plasma membrane in the cytotoxic model CEM-7 and Dexamethasone (*Bradbury et al (2000)*). Examination of both ATP and ADP levels within cell populations proved useful in screening for the various outcomes in a cytotoxic model and when used in conjunction with other methods was able to confirm viable, proliferating, growth arrested, apoptotic and necrotic cell populations.

One of the earliest events during apoptosis is believed to be the externalisation of the protein phosphatidyl serine (PS) from the inner cell membrane to the outer cell membrane, where it is believed to act as an apoptotic marker for the cells removal during phagocytosis (*Verhoven et al (1995)*). Early apoptotic cells expose PS without cell leakage allowing the differentiation between apoptotic and necrotic cells by dual staining with a combination of PI and (FITC)-conjugated Annexin V and analysis on a flow cytometer. Apoptotic cells will fluoresce green as the PS binds to the (FITC)-conjugated Annexin V. Secondly necrotic and necrotic cells will fluoresce both red and green as the cells become permeable to PI.

Megachannels or permeability transition (PT) pores span the inner to the outer mitochondrial membrane and are thought to open irreversibly at an early stage in the apoptotic cascade (*Susin et al (1996)*). The opening of these PT pores is believed to lead to the loss of the mitochondrial transmembrane potential ( $\Delta\Psi_m$ ) as the flow of ions across the membrane becomes disrupted. The loss of the  $\Delta\Psi_m$  can be measured by flow cytometry with the dual emission potential sensitive probe 5,5',6,6'-tetrachloro-1,1',3,3'-tetraethylbenzimidazolcarbocyanine iodide (JC-1). It is not quite clear whether this loss of  $\Delta\Psi_m$  is the cause or the consequence of the release of cytochrome c from the inner mitochondrial membrane to the cytosol. During normal cellular conditions cytochrome c behaves as an electron carrier between the complexes III and IV where it is active in the synthesis of ATP. Upon its release into the cytosol cytochrome c binds with Apaf-1 and ATP, to produce the apoptosome and the recruitment of procaspase 9, see Chapter 1, figure 1.05. The release of cytochrome c into the cytosol is an excellent early indicator of the onset of apoptosis and for the purposes of this study was analysed by fluorescent microscopy.

Other apoptotic markers include those that show the later stages of apoptosis, including DNA fragmentation which gives rise to the characteristic 'ladder' appearance on DNA electrophoresis gels (*Kerr et al (1972)* and *Wyllie et al (1984)*) and the sub  $G_0$  peak observed with flow cytometry using the DNA binding probe PI (*Nicoletti et al (1991)*). The maintenance of the plasma membrane during apoptosis is one of the characteristic cell morphology indicators that allow us to distinguish this form of cell death from other more violent forms such as necrosis by the ability of the cell to exclude various dyes such as trypan blue and propidium iodide (PI) and will be used in this Chapter to confirm the that the apoptotic models used in this study were in the early or later stages of apoptosis. With the loss of plasma membrane integrity comes the release of enzymes such as adenylate kinase (AK) and lactate dehydrogenase (LDH) from the cell. As these proteins normally reside within the cell their

release indicates a leaky cell membrane and as such can be used to determine cell death by the use of bioluminescence and fluorimetry. PI (flow cytometry) and LDH (plate reading fluorescence) are traditional methods of measuring necrosis and will be used to evaluate the bioluminescent method of measuring necrosis by the detection of AK. Other classic morphology markers include nuclei shrinkage, cell blebbing and apoptotic bodies. A common method of analysing cell morphology is through Romanovsky stained cytospin preparations which were carried out on all of the apoptotic models used in this study to first confirm apoptosis along with further verification of apoptosis and necrosis through the use of traditional flow cytometric methods.

The apoptotic models were chosen within this study to observe the different death pathways drugs work to induce apoptosis and the speed at which the cells progress through apoptosis into secondary necrosis.

The problems that can be attributed to some of the conventional methods of measuring apoptosis is the subjectivity associated with the analysis and the necessity for the combination of dyes to differentiate between viable, apoptotic and necrotic cell populations. For this reason the bioluminescent ApoGlow™ assay will be compared to the traditional methods through analysis of the following apoptotic models and assays. In this chapter the ApoGlow™ assay will be compared to JC-1, PI permeability, % hypodiploid and Annexin V. Cytochrome c release will be carried out on the models Jurkat and Ara-C and Jurkat and CD95L. Apoptosis will be confirmed by visualisation of the cell morphology using cytospin preparations. It is anticipated from previous observations that the bioluminescent ApoGlow™ kit would be sensitive enough to detect early signs of apoptosis and allow the user in one assay to monitor the early signs of apoptosis through to secondary necrosis.

## 4.2 Results

### 4.2.1 Changes in apoptotic and necrotic cell morphology

Cytospin preparations were carried out on the six cytotoxic models HL60 and Camptothecin (CAM), K562 and Etoposide, CEM-7 and Dexamethasone (DEX), U937 and CAM, Jurkat and IgM CD95 and Jurkat and 1- $\beta$ -D-Arabinofuranosylcytosine (Ara-C), to observe for the morphological characteristics of apoptosis and necrosis. Figure 4.01 shows the differences observed in the morphology between healthy and apoptotic cells in HL60 cells dosed with 0.05 $\mu$ M CAM for an incubation of 4 hours. This slide indicates how after 4 hours incubation with 0.05 $\mu$ M CAM there is a population of cells that have not yet been affected by the drug and also cells with nuclei shrinkage convoluted cell membrane and cell blebbing showing apoptotic morphology.

**Figure 4.01**

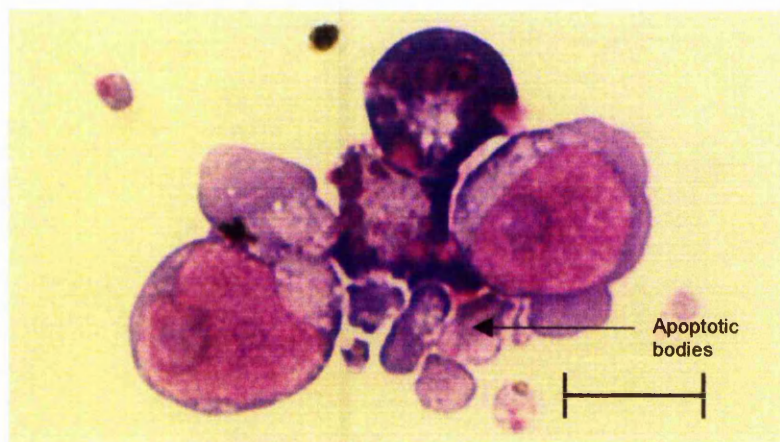


**Figure 4.01.** Cytospin preparations of the cytotoxicity model HL60 and Camptothecin, incubated for 4 hours. The cytospins were kindly stained by the Haematology department at the Nottingham City Hospital. The cytospin slides were prepared using a Shandon cytospin 3 centrifuge, where 100 $\mu$ l of sample ( $5 \times 10^5$  cells  $\text{ml}^{-1}$ ) were added to the chamber. Scale bar: 10 $\mu$ m.



## **4.2.2 Measuring apoptosis**

The apoptotic models as outlined in Chapter 2, table 2.03 were set up and analysed for all of the apoptotic outcomes including phosphatidyl serine (PS) exposure, loss of the mitochondrial transmembrane potential ( $\Delta\Psi_m$ ), cytochrome c release, DNA fragmentation and PI permeability. For the purposes of this chapter of results however the model Jurkat and IgM CD95 was taken as representative data and compared with one other model of interest for that particular assay. All samples were compared to the bioluminescent ADP:ATP ratio assay ApoGlow utilising the reaction outlined in section 2.10.3.2.

## **4.2.3 Early indicators of apoptosis**

### **4.2.3.1 Phosphatidyl serine 'flip' from the inner to the outer cell membrane**

Figure 4.02 shows dot plot analysis of Jurkat cells incubated for 4 hours with IgM CD95 and analysed on a Becton Dickinson FACScan flow cytometer for PS exposure and loss of cell membrane integrity using dual staining with (FITC)-conjugated Annexin V and PI. The samples are analysed using both green and red fluorescence. The FL-1/FL-2 dot plot indicates green and red fluorescence and the FSC-H/SSC-H dot plot represents the size and granularity of the cell.

**Figure 4.02**

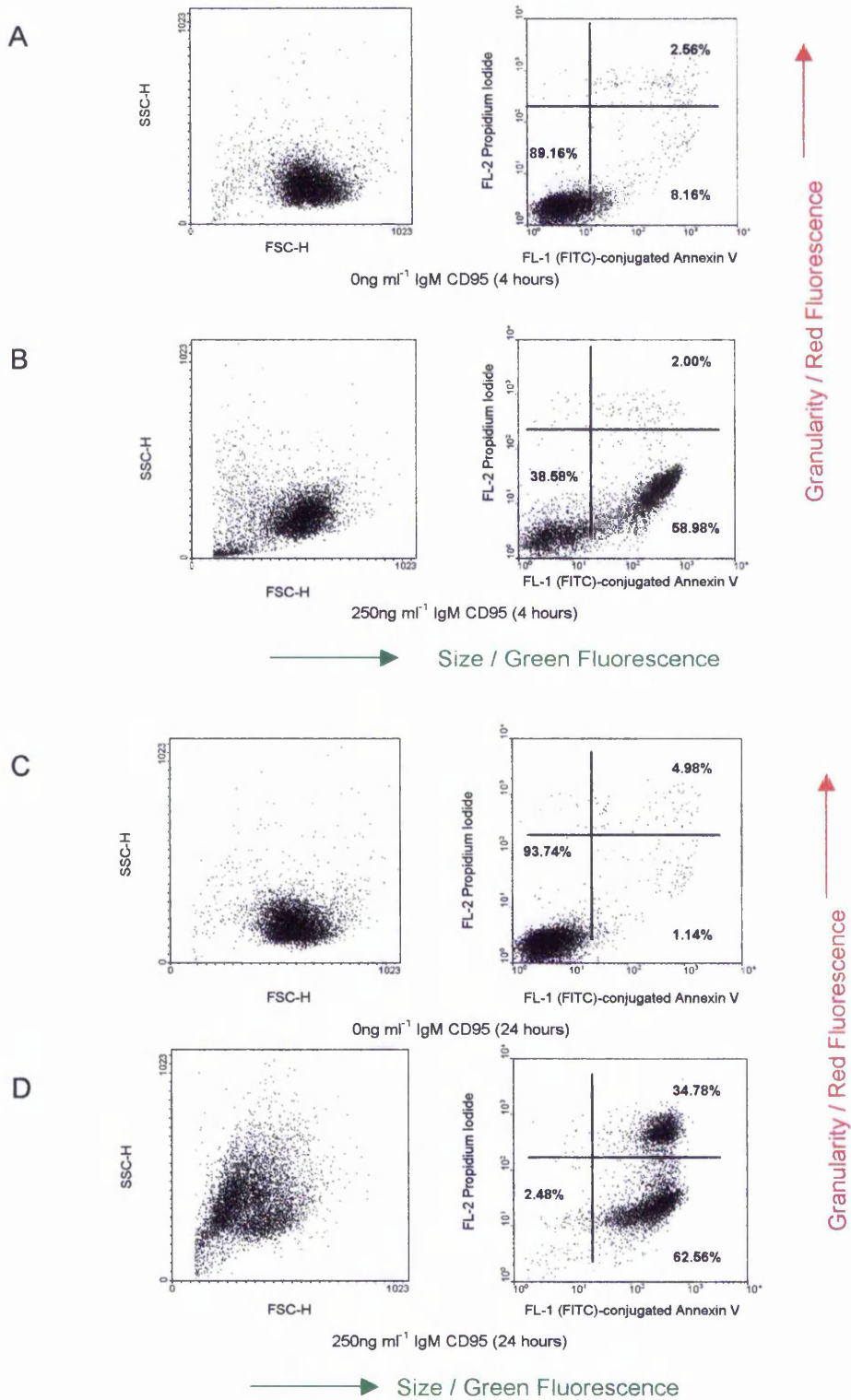
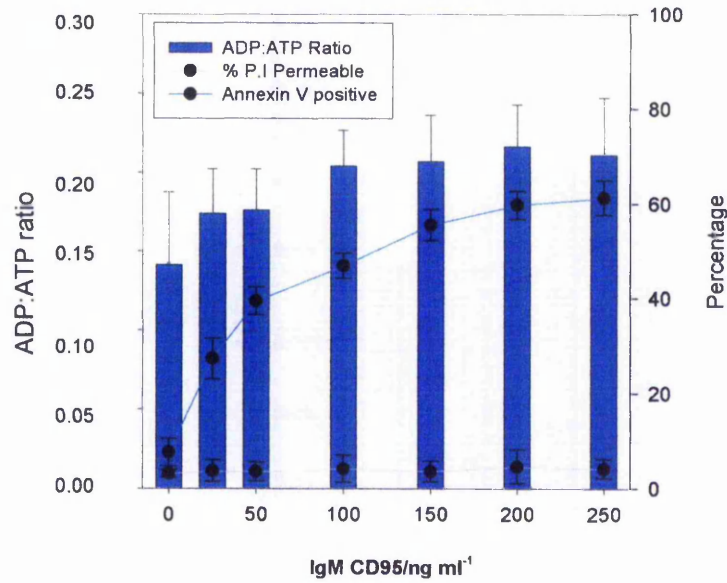


**Figure 4.02.** Flow cytometry dot plots showing Jurkat and IgM CD95 stained with Annexin V and PI as outlined in Chapter 2, 2.10.3.1. Samples were subsequently analysed on a Becton Dickinson FACscan flow cytometer. A shows 0ng ml<sup>-1</sup> IgM CD95 and B shows 250ng ml<sup>-1</sup> IgM CD95 after 4 hours incubation and C shows 0ng ml<sup>-1</sup> IgM CD95 and D shows 250ng ml<sup>-1</sup> IgM CD95 after 24 hours incubation.

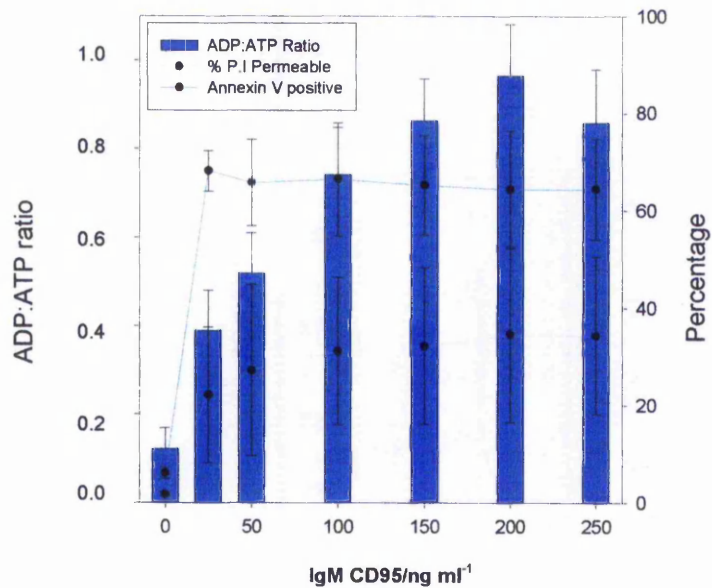
The Jurkat cells incubated with IgM CD95 for 4 hours show an increase in green fluorescent cells going from 8.16% in the control to 58.98% in the 250ng ml<sup>-1</sup> IgM CD95 treated sample but no significant difference in red fluorescence. After 24 hours incubation in the 250ng ml<sup>-1</sup> IgM CD95 treated sample the amount of green fluorescing cells also increases from 1.14% in the control to 62.56% and there is a rise from 4.98% in the control to 34.78% in red fluorescence indicating membrane permeability and the cells entry into secondary necrosis. Apoptotic cell morphology was presumed to become more granular and the cells to reduce in size. Here both reduction in cell size and granularity does not become apparent until 24 hours incubation with the loss of the cell membrane integrity, suggesting these phenomena to be associated with a later stage of apoptosis.

Figure 4.03 shows the correlation between the ADP:ATP ratio and Annexin V positive cells. ApoGlow™ ADP:ATP ratios were found to correlate with early apoptosis measured using Annexin V when assessed with Spearman's Rho (2 tailed) ( $p < 0.02$ ). The ADP:ATP ratios and Annexin V positive cells were found to be significantly different when drug treated samples were compared to the control with the Wilcoxon matched pairs test ( $p < 0.05$ ). At 4 hours incubation it can be observed how the cell membrane integrity is maintained by the cells ability to exclude PI. After an incubation of 24 hours all concentrations of IgM CD95 samples are apoptotic they are just in different stages of secondary necrosis, indicated by the fact that the percentage of Annexin V positive cells increases from 1.14% in the control to around 62% in all of the IgM CD95 treated samples. There is no significant correlation between Annexin V positive cells and ADP:ATP ratios when assessed with Spearman's Rho (2 tailed) but there is a significant correlation between the ADP:ATP ratios and percentage of PI permeable cells when assessed with Spearman's Rho (2 tailed) ( $p < 0.02$ ).

Figure 4.03



A (4 hours)



B (24 hours)

Figure 4.03. Comparison between the increase in ADP:ATP ratios detected using ApoGlow™ measured on a MPL3 luminometer (Berthold). The maintenance of the cell membrane was measured using PI and detection of PS with Annexin V. The samples were analysed on a Becton Dickinson FACscan Flow Cytometer. The results are expressed as the means of n= 4 separate Jurkat + IgM CD95 experiments incubated for 4 hours (A) and 24 hours (B) (+/- SEM ( ADP:ATP ratios) and SD (% PI Permeable and % Annexin V positive)).

This data suggests that ApoGlow™ is capable of distinguishing in one assay between apoptotic and necrotic cells within a cell population proven by the steady increase in ADP:ATP ratios observed when the cells are apoptotic increasing from 0.14 in the control to 0.21 in the 250ng ml<sup>-1</sup> concentration after 4 hours incubation to the ADP:ATP ratio of 0.86 for the same concentration of IgM CD95 after 24 hours when the cells have entered secondary necrosis. The continued rise in ADP:ATP ratios correlates with the steady increase in PI permeable cells demonstrating the ability of ApoGlow™ to differentiate between early and late apoptotic events.

Table 4.01 shows a comparison between the human leukaemia cell line Jurkat induced to apoptose with the DNA synthesis inhibitor Ara-C at a concentration of 5µM over an incubation period of 4 hours, 24 hours and 48 hours and the activating antibody IgM CD95 at a concentration of 250ng ml<sup>-1</sup> incubated for 4 hours and 24 hours compared to a control. The differences between the two methods of inducing apoptosis are shown in the time scale of detection of PS flip from the inner to the outer cell membrane. The Jurkat and IgM CD95 data showed a system in which cells seemed to pass through the stages of apoptosis in an orderly fashion. PS becomes externalised at 4 hours showing a rise in Annexin V binding from 7.57% +/- 2.84 in the control to 61.24% +/- 3.67 in the 250ng ml<sup>-1</sup> treated sample with no detectable PI uptake. The Jurkat and Ara-C model however shows no PS externalisation until 24 hours incubation increasing from 5.00% +/- 4.26 in the control to 29.10% +/- 14.56 in the 5µM concentration accompanied by a rise in cells with compromised plasma membranes increasing from 4.25% +/- 1.33 to 19.29% +/- 8.42. The ability of the Jurkat cells to maintain their plasma membrane after 4 hours incubation with IgM CD95 is also reflected in the ADP:ATP ratios which rose from 0.14 +/- 0.05 in the control to 0.21 +/- 0.04 in the 250ng ml<sup>-1</sup> concentration compared to an increase from 0.12 +/- 0.05 in the control to 0.86 +/- 0.12 in the 250ng ml<sup>-1</sup> concentration after 24 hours incubation with 31.33% +/- 10.16 PI permeable cells. This data showed how ApoGlow™ was sensitive enough to detect this increase in a

population of cells that had passed into secondary necrosis within a mixed population of apoptotic and viable cells. The capability of ApoGlow™ to detect secondarily necrotic cells within apoptotic and viable cell populations was also evident in the Jurkat and Ara-C model where the ratio was seen to increase in the 5µM concentration of Ara-C from 0.17 +/- 0.07 after 4 hours incubation to 0.30 +/- 0.09 at 24 hours and 0.63 +/- 0.06 after 48 hours incubation. This compared to the rise in PI permeable cells which increased from 5.62% +/- 2.69 after 4 hours incubation to 19.29% +/- 8.42 at 24 hours to 45.71% +/- 15.49 after 48 hours incubation with 5µM of drug.

Model	ADP:ATP Ratio		Annexin V positive		Annexin V + PI positive	
<b>Jurkat + Ara-C</b>	<b>Control</b>	<b>5µM</b>	<b>Control</b>	<b>5µM</b>	<b>Control</b>	<b>5µM</b>
<b>4 hours incubation</b>	<b>0.16</b> +/- 0.07	<b>0.17</b> +/- 0.07	<b>6.42%</b> +/- 4.26	<b>9.78%</b> +/- 4.54	<b>7.76%</b> +/- 3.80	<b>5.62%</b> +/- 2.69
<b>24 hours incubation</b>	<b>0.17</b> +/- 0.05	<b>0.30</b> +/- 0.09	<b>5.00%</b> +/- 4.26	<b>29.10%</b> +/- 14.56	<b>4.25%</b> +/- 1.33	<b>19.29%</b> +/- 8.42
<b>48 hours incubation</b>	<b>0.14</b> +/- 0.02	<b>0.63</b> +/- 0.06	<b>4.14%</b> +/- 3.31	<b>32.51%</b> +/- 22.86	<b>2.89%</b> +/- 1.10	<b>45.71%</b> +/- 15.49
<b>Jurkat + IgM CD95</b>	<b>Control</b>	<b>250ng ml<sup>-1</sup></b>	<b>Control</b>	<b>250ng ml<sup>-1</sup></b>	<b>Control</b>	<b>250ng ml<sup>-1</sup></b>
<b>4 hours incubation</b>	<b>0.14</b> +/- 0.05	<b>0.21</b> +/- 0.04	<b>7.57%</b> +/- 2.84	<b>61.24%</b> +/- 3.67	<b>4.33%</b> +/- 1.37	<b>4.47%</b> +/- 2.92
<b>24 hours incubation</b>	<b>0.12</b> +/- 0.05	<b>0.86</b> +/- 0.12	<b>6.01%</b> +/- 1.19	<b>64.40%</b> +/- 10.24	<b>2.24%</b> +/- 0.71	<b>31.33%</b> +/- 10.16

**Table 4.01.** Comparisons between the two apoptotic models Jurkat and Ara-C incubated for a time course of 4 hours, 24 hours and 48 hours and Jurkat and CD95 activating antibody incubated for a time course of 4 hours and 24 hours. Both models were analysed using ApoGlow measured on a MPL3 luminometer (Berthold) and (FITC)-conjugated Annexin V and PI, where the data is shown as the mean of n = 4 experiments for each model +/- SEM for the ADP:ATP ratio and SD for the Annexin V positive and Annexin V + PI positive data.

#### **4.2.3.2 Detecting changes in the mitochondrial transmembrane potential ( $\Delta\psi_m$ ) with the dual emission potential sensitive probe 5,5',6,6'-tetrachloro-1,1',3,3'-tetraethylbenzimidazolcarbocyanine iodide (JC-1)**

The loss of the mitochondrial transmembrane potential ( $\Delta\psi_m$ ) is also believed to be an early event in apoptosis preceding DNA fragmentation. The  $\Delta\psi_m$  was measured by the dual emission potential sensitive probe JC-1 and was either analysed by fluorescent microscopy or flow cytometry, see Chapter 3, section 3.2.4. Figure 4.04 shows Jurkat cells incubated for 4 hours and 24 hours with IgM CD95 and analysed on a Becton Dickinson FACScan flow cytometer with JC-1. The samples were analysed for both green and red fluorescence and size and granularity of the cell. The FL-1/FL-2 dot plot indicates green and red fluorescence and the FSC-H/SSC-H dot plot represents the size and granularity of the cell. Healthy functioning mitochondria actively uptake JC-1, and accumulation of the dye above  $0.1\mu\text{M}$  results in the formation of red fluorescing J-Aggregates. Therefore green fluorescence is indicative of non-functioning mitochondria and a loss of the  $\Delta\psi_m$  signifying a breakdown in the electron transport chain and disruption in the synthesis of ATP leading to an increase in ADP.

Jurkat cells incubated with IgM CD95 for 4 hours show a loss of red J-Aggregates from 93.72% in the control to 65.88% in the  $250\text{ng ml}^{-1}$  IgM CD95 treated sample compared to 24 hours incubation where the loss of J-Aggregates decreased dramatically from 89.22% in the control to 7.86% in the  $250\text{ng ml}^{-1}$  IgM CD95 treated sample. The loss in J-Aggregates is mirrored by the change in green monomers which increased from 4.56% in the control to 31.70% in the  $250\text{ng ml}^{-1}$  IgM CD95 treated sample at 4 hours incubation with an increase from 10.88% in the control to 91.74% in the  $250\text{ng ml}^{-1}$  IgM CD95 treated sample after 24 hours incubation. The change in both size and granularity of the cells again does not become apparent until 24 hours incubation.

**Figure 4.04**

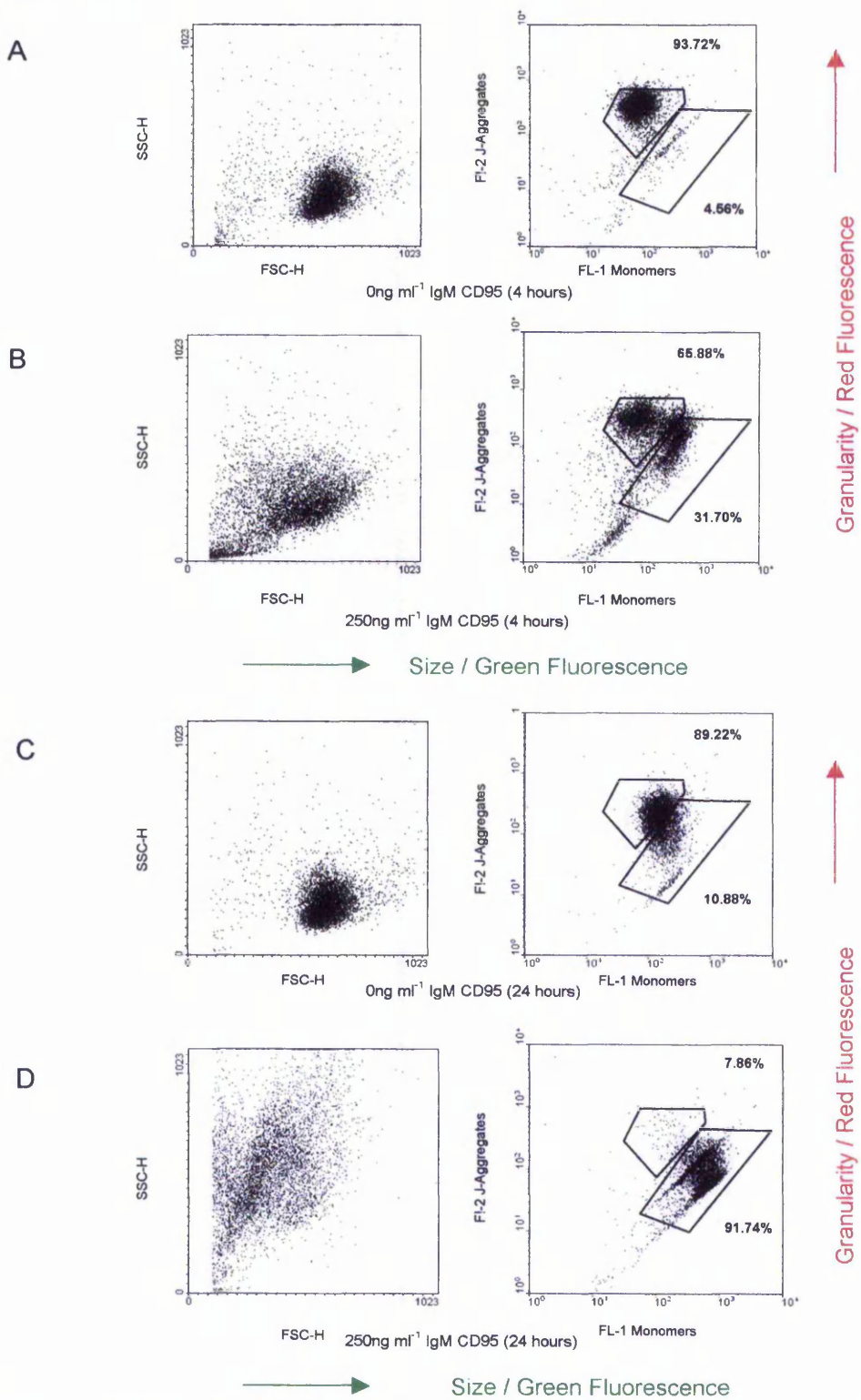


**Figure 4.04.** Flow cytometry dot plots showing Jurkat and CD95 activating antibody stained with JC-1 as outlined in Chapter 2, 2.10.5. Samples were subsequently analysed on a Becton Dickinson FACscan flow cytometer. A shows 0ng ml<sup>-1</sup> IgM CD95 and B shows 250ng ml<sup>-1</sup> IgM CD95 after 4 hours incubation and C shows 0ng ml<sup>-1</sup> IgM CD95 and D shows 250ng ml<sup>-1</sup> IgM CD95 after 24 hours incubation.



Figure 4.05 shows how ADP:ATP ratios correlate significantly with the increase in green monomers indicative of the loss of the  $\Delta\psi_m$  when assessed with Spearman's Rho (2 tailed) ( $p < 0.02$ ) for both 4 hours and 24 hours incubation. The two different assays gave significant differences when the drug treated sample was compared to the control when assessed with the Wilcoxon matched pairs test ( $p < 0.05$ ). After 4 hours incubation the loss of the  $\Delta\psi_m$  was only small where the green monomers increased from 4.56% in the control to 31.70% in the IgM CD95 treated sample, compared to 24 hours incubation where there was an increase from 10.88% in the control to 91.74% in the 250ng ml<sup>-1</sup> concentration. This was reflected in the change in ADP:ATP ratios where there was an increase from 0.14 in the control to 0.21 for the 250ng ml<sup>-1</sup> concentration of IgM CD95 when incubated for 4 hours compared to the rise from 0.12 in the control to 0.86 in the death receptor treated sample again showing significant correlation when assessed with Spearman's Rho (2 tailed) ( $p < 0.02$ ) and ( $p < 0.05$ ) when the drug treated samples were compared to the control using the Wilcoxon matched pairs test in both assays.

**Figure 4.05**

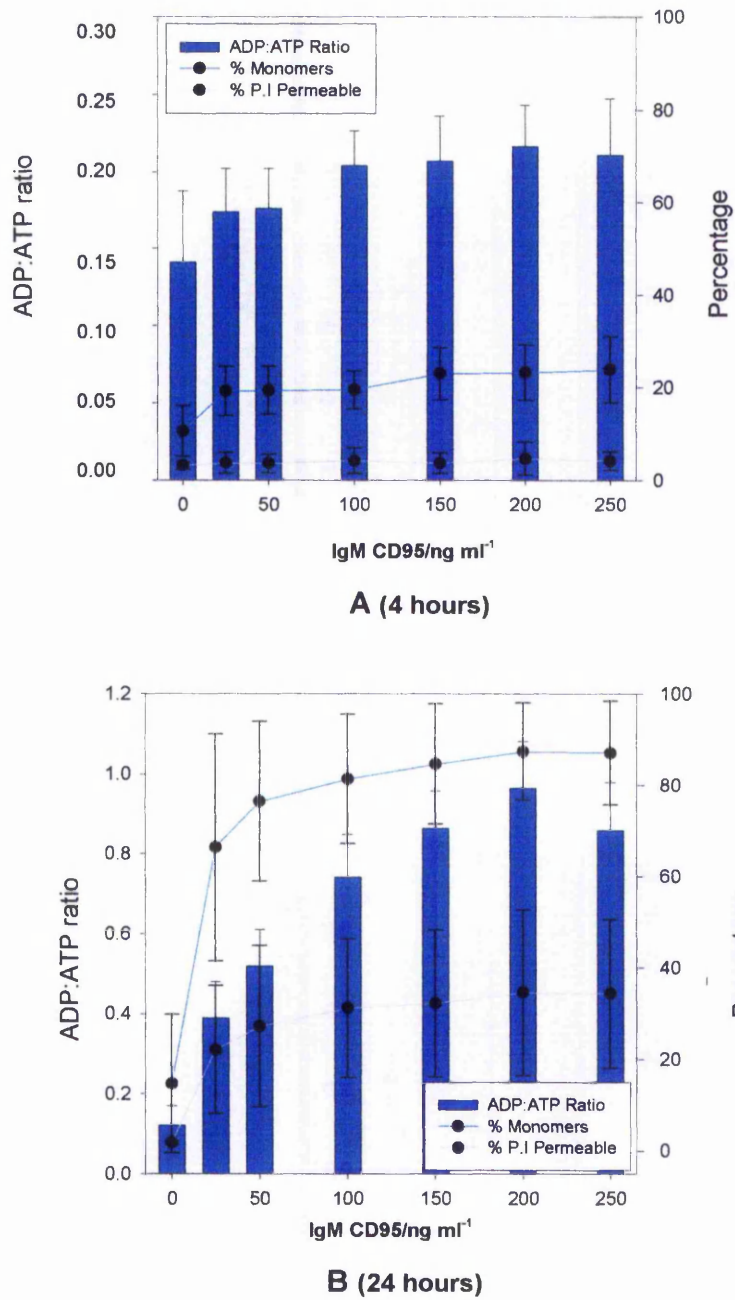


**Figure 4.05.** Comparison between the increase in ADP:ATP ratios detected using ApoGlow™ measured on a MPL3 luminometer (Berthold). The maintenance of the cell membrane was measured using PI and measurement of  $\Delta\psi_m$  with JC-1. The samples were analysed on a Becton Dickinson FACscan Flow Cytometer. The results are expressed as the means of  $n = 4$  separate Jurkat + IgM CD95 experiments incubated for 4 hours (A) and 24 hours (B) (+/- SEM (ADP:ATP ratios) and SD (% PI Permeable and % Monomers)).

As the loss of the  $\Delta\psi_m$  is a reflection of the health of the mitochondria and the function of the electron transport chain this correlation between the ADP:ATP ratios and JC-1 suggests that ApoGlow™ can be used as a reliable indicator of mitochondrial stress. As the loss of the  $\Delta\psi_m$  occurred after 4 hours incubation this would suggest that it was an early event in the apoptotic cascade shown by the ability of the cells to exclude PI at 4 hours. The considerable increase in ADP:ATP ratios after 24 hours incubation increasing from 0.12 in the control to 0.86 in the 250ng ml<sup>-1</sup> sample indicated the changes observed in secondarily necrotic cells from cells during apoptosis. The ADP:ATP ratios correlated significantly with the loss of the plasma membrane when assessed with the Spearman's Rho (2 tailed) ( $p < 0.02$ ), where both assays showed a significant difference from the drug treated samples to the control when analysed using the Wilcoxon matched pairs test ( $p < 0.05$ ).

Figure 4.06 shows the correlation between ADP:ATP ratios and loss of  $\Delta\psi_m$  measured with JC-1 for the two cytotoxicity assays HL60 and Camptothecin (CAM) and Jurkat and 1- $\beta$ -D-Arabinofuranosylcytosine (Ara-C). The HL60 and CAM model was incubated for 4 hours and is an example of a model with early signs of apoptosis but where the cells have maintained their cell membrane integrity. The Jurkat and Ara-C assay was incubated for 48 hours and illustrates a model where cell membrane integrity has become compromised indicating secondarily necrotic cells.

Figure 4.06

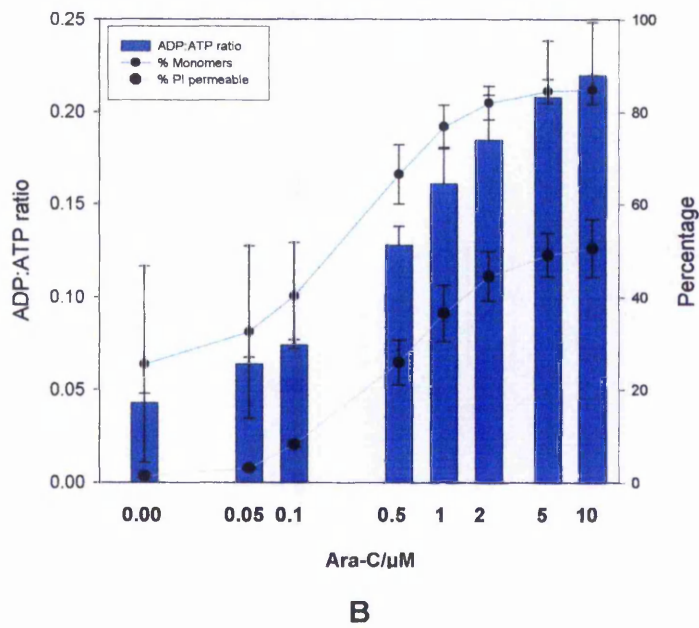
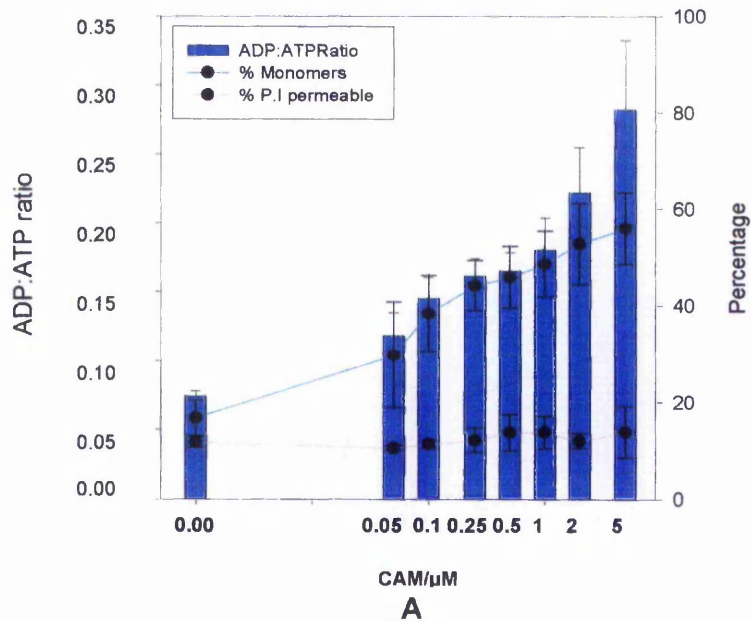


**Figure 4.06.** Comparison between the increase in ADP:ATP ratios detected using ApoGlow™ measured on a Microbeta Jet (Wallac). The maintenance of the cell membrane was measured using PI and measurement of  $\Delta\psi_m$  with JC-1. The samples were analysed on a Becton Dickinson FACscan Flow Cytometer. The results are expressed as the means of  $n = 5$  separate HL60 + CAM experiments incubated for 4 hours (A) and  $n = 7$  Jurkat + Ara-C experiments incubated for 48 hours (B) (+/- SEM (ADP:ATP ratios) and SD (% PI Permeable and % Monomers)).

The HL60 and CAM model incubated for 4 hours showed significant correlation when comparing the ADP:ATP ratios and the increase in green monomers analysed with JC-1 ( $p < 0.02$ ) when assessed with Spearman's Rho (2 tailed). This model showed a more rapid loss of the  $\Delta\psi_m$  during the 4 hours of incubation increasing from 16.66% in the control to 56.01% in the 5 $\mu$ M drug concentration compared to the Jurkat and IgM CD95 model where the green monomers were shown to rise more gradually at 4 hours incubation from 4.56% in the control to 31.70% in the 250ng ml<sup>-1</sup> concentration. This maintenance of the  $\Delta\psi_m$  was also reflected in the ADP:ATP ratios where the ratios were seen to escalate from 0.07 in the control to 0.28 in the drug treated sample compared to the smaller increase in ADP:ATP ratios detected in the Jurkat and IgM CD95 model which increased from 0.14 in the control to 0.21 in the 250ng ml<sup>-1</sup> concentration. Both models reflected the maintenance of the plasma membrane with ADP:ATP ratios of between 0.20 and 0.30.

The Jurkat and Ara-C model shows a gradual increase in green monomers over the drug concentration range increasing from 16.07% in the control to 86.86% in the 10 $\mu$ M drug concentration with correlating ADP:ATP ratios increasing from 0.04 in the control to 0.35 in the highest concentration of the drug, showing significant correlation with Spearman's Rho ( $p < 0.02$ ). The Jurkat and IgM CD95 model at 24 hours incubation however appeared to lose the  $\Delta\psi_m$  at the lower drug concentrations which were reflected in the considerable increase in ADP:ATP ratios detected rising from 0.12 in the control to 0.86 in the 250ng ml<sup>-1</sup> concentration of the CD95 activating antibody. The two models showed uptake of PI which is indicative of the loss of the plasma membrane and cells becoming secondarily necrotic. Both models showed a similar percentage of cells undergoing secondary necrosis and loss of  $\Delta\psi_m$  but differing ADP:ATP ratios, as this was the same cell line but induced to apoptose with different agents it would suggest that the induction of apoptosis affects the metabolism of the cells in different ways.

#### **4.2.3.3 Measuring cytochrome c release from the inner mitochondrial membrane to the cytosol**

Cytochrome c was one of the first mitochondrial membrane proteins found to be linked with the apoptotic cascade, its release into the cytosol is believed to be an early event during apoptosis. This event was first measured by producing cytosolic and mitochondrial fractions to be probed using antibody to cytochrome c on western blots. This method proved difficult however in obtaining pure fractions due to the fragility of the cells used. Instead cytochrome c release was measured by fluorescent microscopy. This technique was carried out on the two apoptotic models, Jurkat and Ara-C and Jurkat and CD95 activating antibody. The two models were set up at the same time so both sets of drug treated samples share the same control.

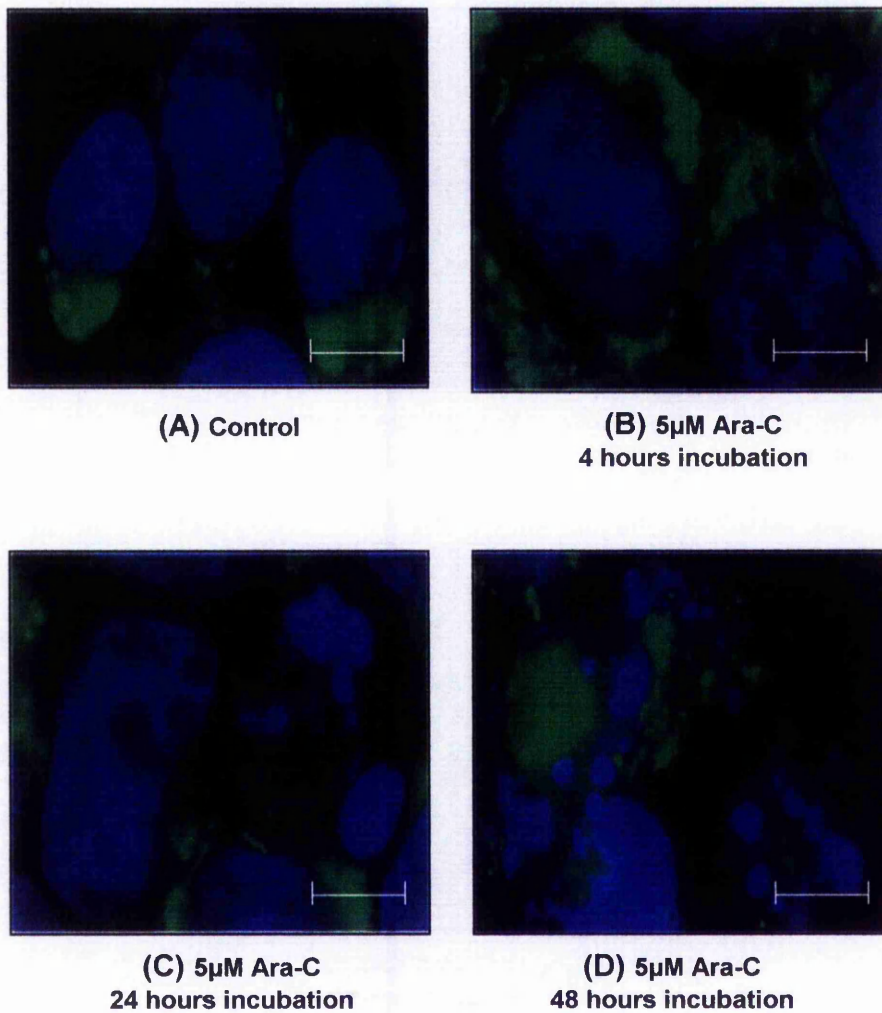
The data found in this study suggested that cytochrome c release preceeded loss of the  $\Delta\psi_m$ , PS externalisation and increase in the ADP:ATP ratio in the Jurkat and Ara-C model. Table 4.02 shows the increases in ADP:ATP ratios, Annexin V positive cells and % monomers measured by JC-1 over a time course of 4 hours, 24 hours and 48 hours for Jurkat cells induced to undergo apoptosis with 5 $\mu$ M of Ara-C. The data shows no significant difference from the control until 24 hours incubation.

Ara-C/5 $\mu$ M	ADP:ATP Ratio	Annexin V positive	% monomers
<b>4 hours incubation</b>	<b>0.17</b> +/- 0.07	<b>9.78%</b> +/- 4.54	<b>15.00%</b> +/- 8.21
<b>24 hours incubation</b>	<b>0.30</b> +/- 0.09	<b>29.10%</b> +/- 14.56	<b>44.64%</b> +/- 7.10
<b>48 hours incubation</b>	<b>0.63</b> +/- 0.06	<b>32.51%</b> +/- 22.86	<b>85.42%</b> +/- 2.53
<b>Average control</b>	<b>0.16</b> +/- 0.02	<b>4.97%</b> +/- 2.51	<b>16.03%</b> +/- 0.94
Ara-C/5 $\mu$ M	ADP:ATP Ratio	Annexin V positive	% monomers
<b>4 hours incubation</b>	<b>0.17</b> +/- 0.07	<b>9.78%</b> +/- 4.54	<b>15.00%</b> +/- 8.21
<b>24 hours incubation</b>	<b>0.30</b> +/- 0.09	<b>29.10%</b> +/- 14.56	<b>44.64%</b> +/- 7.10
<b>48 hours incubation</b>	<b>0.63</b> +/- 0.06	<b>32.51%</b> +/- 22.86	<b>85.42%</b> +/- 2.53
<b>Average control</b>	<b>0.16</b> +/- 0.02	<b>4.97%</b> +/- 2.51	<b>16.03%</b> +/- 0.94

**Table 4.02.** Comparison between the increase in ADP:ATP ratios detected using ApoGlow<sup>TM</sup> measured on a MPL3 (Berthold). PS externalisation was measured with Annexin V and measurement of  $\Delta\psi_m$  with JC-1. The samples were analysed on a Becton Dickinson FACscan Flow Cytometer. The results are expressed as the means of  $n = 4$  separate Jurkat + Ara-C experiments incubated for 4, 24 and 48 hours (+/- SEM (ADP:ATP ratios) and SD (% Annexin V positive and % Monomers)).

From the above data it would suggest that the cells commitment to die does not occur until after 24 hours incubation in the Jurkat and Ara-C model, however figure 4.07 suggests there may be some cytochrome c release after 4 hours incubation. Figure 4.07 shows the human leukaemia cell line Jurkat treated with 5 $\mu$ M of the DNA synthesis inhibitor Ara-C analysed over a time course of 4 hours, 24 hours and 48 hours incubation. At each time point cytopsin slides were prepared as outlined in Chapter 2, section 2.10.7. The slides were viewed under a fluorescence microscope observing for blue fluorescing nuclei, showing intact round nuclei in healthy cells and nuclear blebbing in apoptotic cells. Cytochrome c fluoresces green, which in healthy cells gives distinct tight green groups, this becomes dispersed when cytochrome c has been released from the mitochondria.

**Figure 4.07**



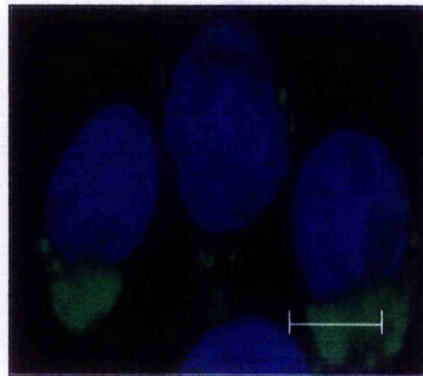
**Figure 4.07.** Jurkat cells treated with Ara-C – Used to measure cytochrome c release and nuclei blebbing with fluorescent imaging. A = control cells, B = 5µM Ara-C treated for 4 hours, C = 5µM Ara-C treated for 24 hours and D = 5µM Ara-C treated for 48 hours. Scale bar: 10µm.



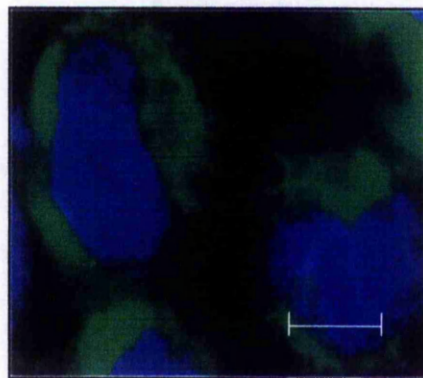
Figure 4.07 (A) shows control cells with round intact nuclei fluorescing blue with discrete groups of green fluorescing cytochrome c. After 4 hours incubation (B) the nuclei still appear intact but there is some suggestion of the green fluorescence becoming dispersed indicating cytochrome c has been released from the mitochondria into the cytosol. As cytochrome c is an essential protein during oxidative phosphorylation shuttling electrons between the complexes III and IV it could be assumed that the synthesis of ATP would decrease as the electron transport chain is broken. The 5 $\mu$ M drug treated sample however gave ATP/RLUs of 7492.36  $\pm$  1187.32 compared to 7607.01  $\pm$  129.44 in the control after 4 hours incubation. There was also evidence of the maintenance of the  $\Delta\psi_m$  where the % J-Aggregates stayed constant at 83.95%  $\pm$  8.44 in the 5 $\mu$ M concentration compared to 83.78%  $\pm$  9.04 in the control. After 24 hours incubation with 5 $\mu$ M of the drug there is evidence of nuclei blebbing, and this becomes even more prominent after 48 hours incubation. The appearance of nuclei blebbing seems to coincide with the loss of the plasma membrane, which is considered to be a marker of the cell entering into secondary necrosis. This transfer into late apoptosis corresponds with the elevated ADP:ATP ratios detected which increase from 0.17  $\pm$  0.07 after 4 hours to 0.30  $\pm$  0.06 at 24 hours to 0.63  $\pm$  0.06 following 48 hours incubation.

Figure 4.08 shows Jurkat cells incubated for a time course of 4 hours and 24 hours with 250ng ml<sup>-1</sup> of the CD95 activating antibody and again stained for cytochrome c and the condition of the nucleus. The control slide (A) shows intact, round nuclei fluorescing blue with distinct groups of green fluorescing cytochrome c. Slide (B) again suggests evidence of cytochrome c release with the green fluorescence becoming diffuse, although the nucleus remains round and intact.

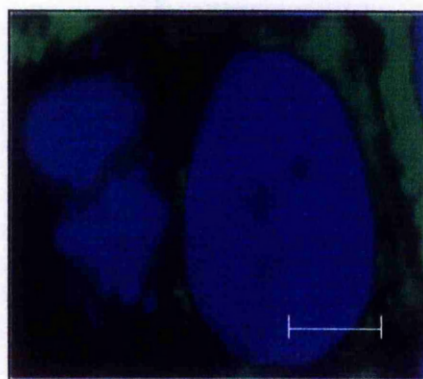
**Figure 4.08**



**(A) Control**



**(B) 250ng ml<sup>-1</sup>  
4 hours incubation**



**(C) 250ng ml<sup>-1</sup>  
24 hours incubation**

**Figure 4.08.** Jurkat cells treated with IgM CD95, used to measure cytochrome c release and nuclei blebbing with fluorescent imaging. A = Control cells, B = 250ng ml<sup>-1</sup> IgM CD95 treated for 4 hours and C = 250ng ml<sup>-1</sup> IgM CD95 treated for 24 hours. Scale bar: 10µm.

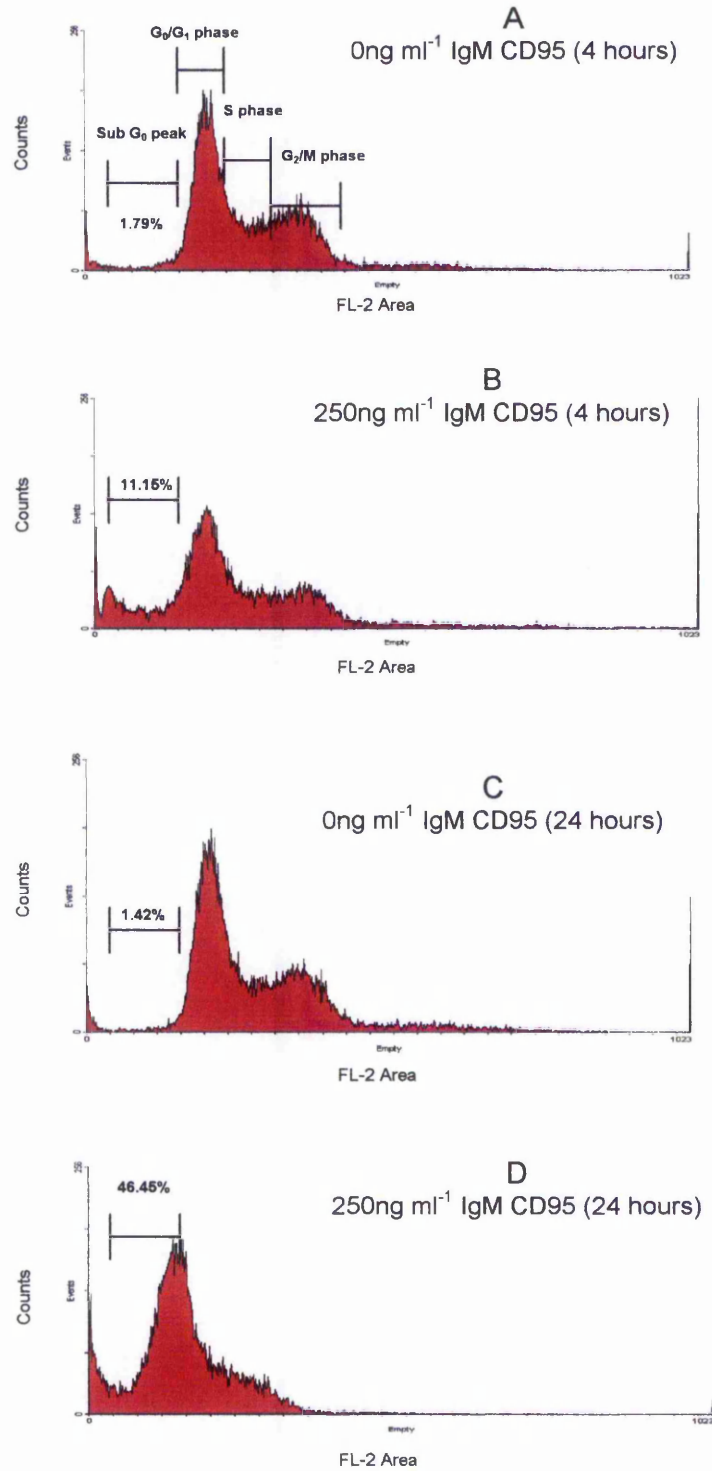
After 24 hours of incubation the cell is now showing evidence of nuclear blebbing (C), this late apoptotic event again corresponds with the loss of plasma membrane integrity as PI is taken up. This model however differs from the previous model in that cytochrome c release seems to coincide with the detection of the other early apoptosis indicators. PS externalisation occurs with an increase from 6.79% +/- 1.10 in the averaged control to 61.24% +/- 3.67 after 4 hours to 64.40% +/- 10.24 following 24 hours incubation. The loss of the  $\Delta\psi_m$  also occurs with a rise from 12.60% +/- 2.91 in the control to 23.81% +/- 7.15 after 4 hours to 87.14% +/- 11.33 following 24 hours incubation. With the loss of the  $\Delta\psi_m$  comes the disruption of ATP synthesis and consequently elevated levels of cellular ADP as indicated by the increase in the ADP:ATP ratios rising from 0.13 +/- 0.01 in the control to 0.21 +/- 0.04 following 4 hours to 0.86 +/- 0.12 after 24 hours incubation.

## **4.2.4 Measuring later indicators of apoptosis**

### **4.2.4.1 Detection of DNA fragmentation by the sub G<sub>0</sub> peak with the DNA binding probe propidium iodide**

Propidium iodide (PI) is a probe that binds proportionally to DNA so therefore the amount of fluorescence detected is proportional to the amount of DNA present hence PI can be used to assess the cell cycle using flow cytometry after fixation with 70% ethanol (4°C). The four consecutive phases of a typical cell cycle begins with the G<sub>1</sub> phase where the cell contains a full compliment of DNA, followed by S phase (DNA synthesis) then culminating in G<sub>2</sub>/M where cells divide. Figure 4.09 (A) shows untreated Jurkat cells stained with PI and analysed on a Becton Dickinson FACScan Flow Cytometer. The G<sub>1</sub> phase is shown here to contain the highest proportion of cells suggesting that this phase is the longest phase that the cells pass through. Nicoletti et al (1991) demonstrated how from cell cycle studies the amount of apoptotic cells within a population could be analysed by the study of the sub G<sub>0</sub> peak giving a percentage of hypodiploid cells. This peak was shown to increase with apoptosis from 1.79% in the control to 11.15% in the 250ng ml<sup>-1</sup> IgM CD95 treated sample at 4 hours rising to 46.45% after 24 hours incubation.

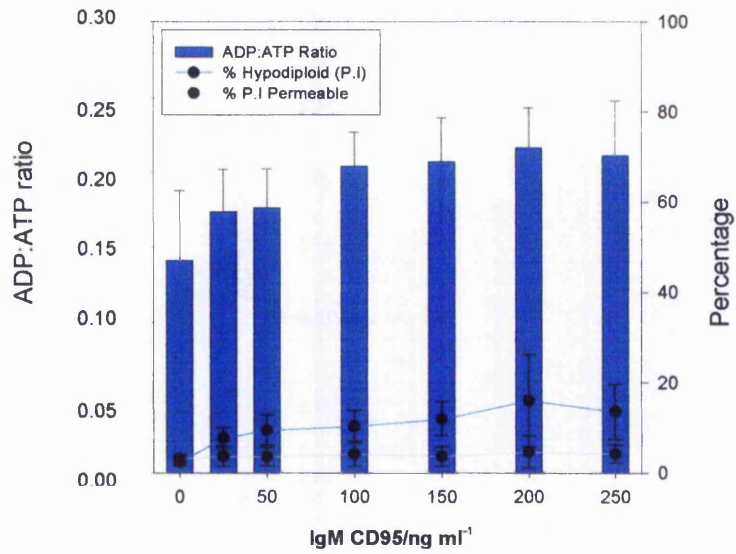
**Figure 4.09**



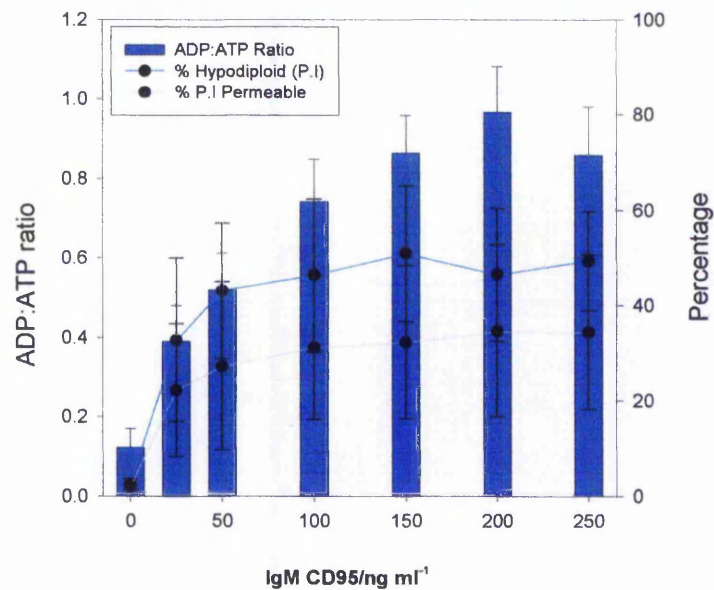
**Figure 4.09.** Flow cytometry histogram plots showing Jurkat and IgM CD95 stained with PI as outlined in Chapter 2, 2.10.4. Samples were subsequently analysed on a Becton Dickinson FACScan flow cytometer. A shows 0ng ml<sup>-1</sup> IgM CD95, B shows 250ng ml<sup>-1</sup> IgM CD95 after 4 hours incubation, C shows 0ng ml<sup>-1</sup> IgM CD95 and D shows 250ng ml<sup>-1</sup> IgM CD95 after 24 hours incubation.

Figure 4.10 (A) shows Jurkat cells treated with the CD95 activating antibody for an incubation period of 4 hours. The ADP:ATP ratios are seen to increase from 0.14 in the control to 0.21 in the 250ng ml<sup>-1</sup> treated sample. The population of cells showing fragmented DNA at 4 hours incubation rises slightly from 1.79% in the control to 11.15% in the 250ng ml<sup>-1</sup> concentration. This population increases dramatically following 24 hours incubation to 46.45% showing DNA fragmentation in this model to be a late event. The percentage of hypodiploid cells at 4 hours incubation correlates significantly with the ADP:ATP ratios ( $p < 0.02$ ) when assessed with Spearman's Rho (2 tailed). After 24 hours incubation the percentage of cells with fragmented DNA also correlates with the increase in ADP:ATP ratios at 24 hours ( $p < 0.02$ ) when assessed with Spearman's Rho (2 tailed) where the ADP:ATP ratios are seen to increase from 0.12 in the control to 0.86 in the 250ng ml<sup>-1</sup> sample. When assessed with the Wilcoxon matched pairs test, a significant difference between the control and the treated samples was found ( $p < 0.05$ ) for ADP:ATP ratios and % hypodiploid at both 4 hours and 24 hours.

**Figure 4.10**



**A (4 hours)**



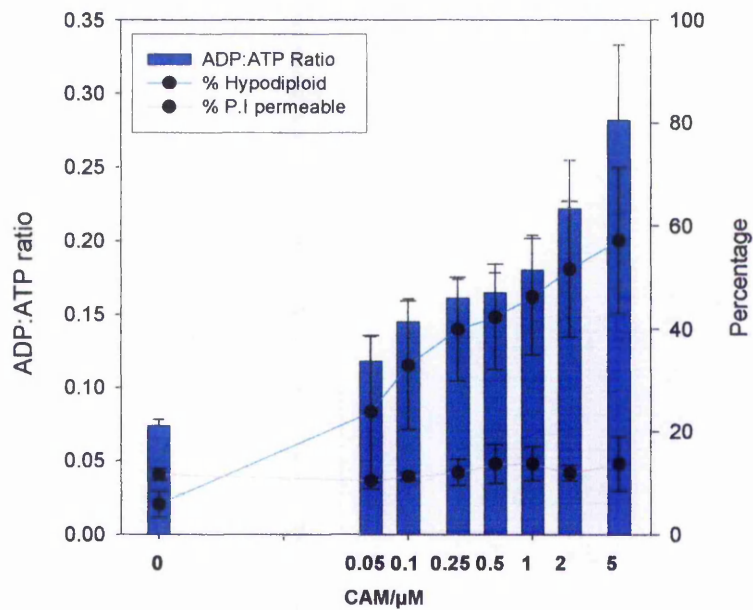
**B (24 hours)**

**Figure 4.10.** Comparison between the increase in ADP:ATP ratios detected using ApoGlow™ measured on a MPL3 luminometer (Berthold). The maintenance of the cell membrane was measured using PI and analysis of the sub G<sub>0</sub> peak was measured using PI on fixed cells. The samples were analysed on a Becton Dickinson FACscan Flow Cytometer. The results are expressed as the means of n = 4 separate Jurkat + IgM CD95 experiments incubated for 4 hours (A) and 24 hours (B) (+/- SEM (ADP:ATP ratios) and SD (% PI Permeable and % hypodiploid)).

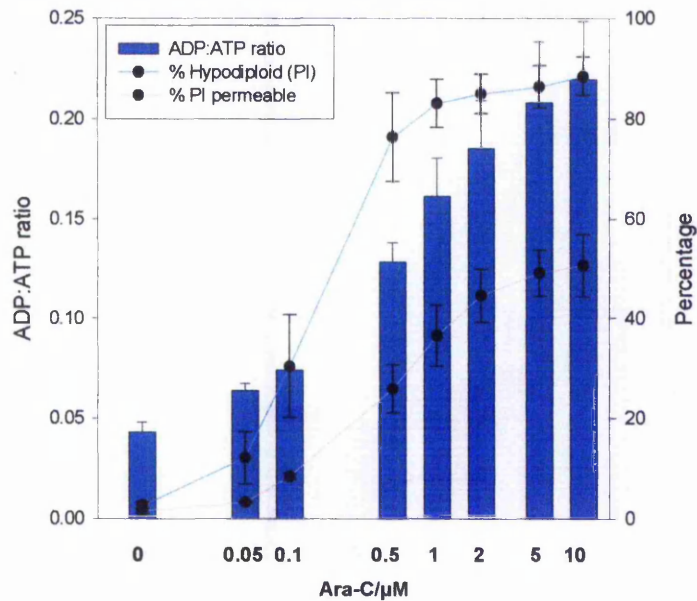
The data presented here shows an apoptotic model where DNA fragmentation occurs at a later stage compared to cytochrome c release, PS externalisation, and the loss of the  $\Delta\psi_m$  leading to a decrease in ATP synthesis and corresponding increase in ADP levels. The appearance of cells with fragmented DNA coincides with the loss of the plasma membrane integrity as measured with PI increasing from 1.73% in the control to 34.35% in the 250ng ml<sup>-1</sup> sample, confirming DNA fragmentation to be a late event in this model. The HL60 and Camptothecin model, Figure 4.11 (A) showed an example of a model where DNA fragmentation occurs much earlier in the apoptotic cascade. The percentage of hypodiploid cells increases from 5.87% in the control to 57.21% in the 5 $\mu$ M drug concentration after 4 hours incubation but the plasma membrane remains intact. The rise in the number of cells with fragmented DNA correlated with the ADP:ATP ratio ( $p < 0.02$ ) when analysed with Spearman's Rho. Both % hypodiploid and ADP:ATP ratios showed significant difference from the control when assessed with the Wilcoxon matched pairs test ( $p < 0.05$ ).



**Figure 4.11**



**A**



**B**

**Figure 4.11.** Comparison between the increase in ADP:ATP ratios detected using ApoGlow™ measured on a Microbeta Jet (Wallac). The maintenance of the cell membrane was measured using PI and the measurement of the % hypodiploid population was measured using PI on fixed cells, the samples were analysed on a Becton Dickinson FACscan Flow Cytometer. The results are expressed as the means of  $n = 5$  separate HL60 + CAM experiments incubated for 4 hours (A) and  $n = 7$  Jurkat + Ara-C experiments incubated for 48 hours (B) (+/- SEM (ADP:ATP ratios) and SD (% PI permeable and % hypodiploid)).

Figure 4.11 (B) shows Jurkat cells incubated for 48 hours with the drug Ara-C. The ADP:ATP ratios were seen to increase from 0.04 in the control to 0.22 in the 10 $\mu$ M drug concentration, correlating with the percentage of hypodiploid cells rising from 2.5% in the control to 88.46% in the 10 $\mu$ M sample ( $p < 0.02$ ) when assessed with Spearman's Rho (2 tailed). A significant correlation when analysed with Spearman's Rho (2 tailed) was also observed when the ADP:ATP ratios were compared to the loss of the plasma membrane measured with PI ( $p < 0.02$ ). Both ADP:ATP ratios, % hypodiploid and PI permeable cells gave significant differences ( $p < 0.05$ ) when the drug treated samples were compared to the control with the Wilcoxon matched pairs test.

Figure 4.12

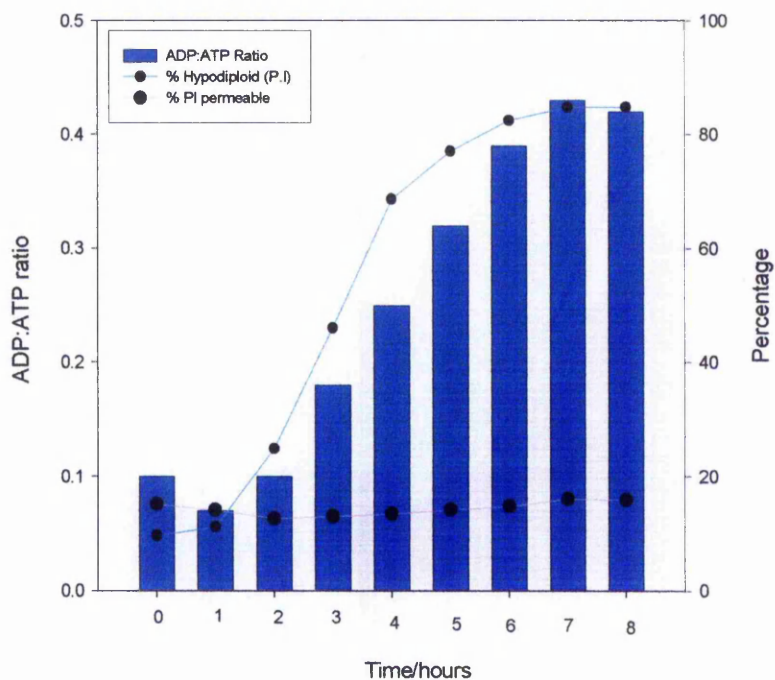


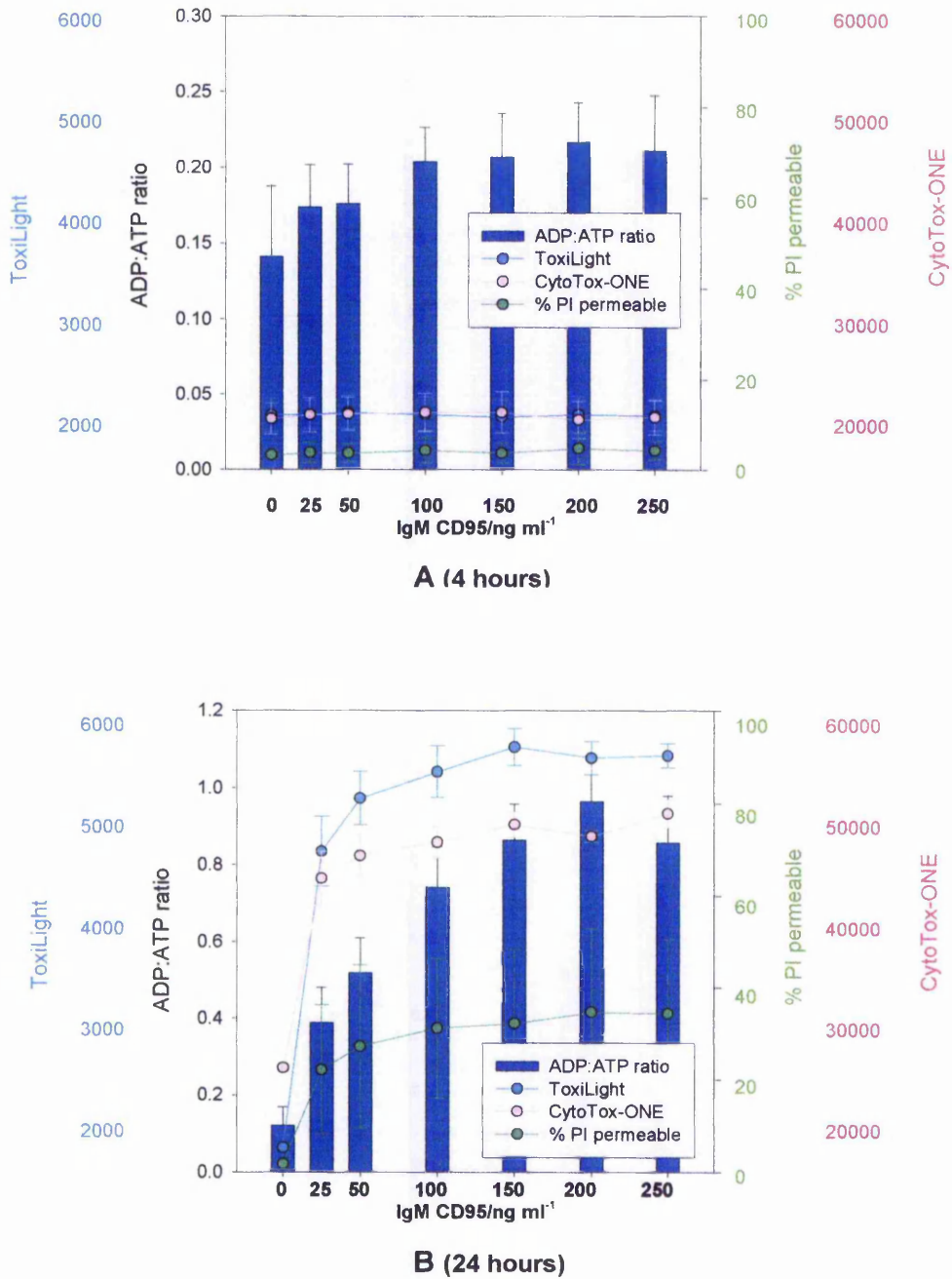
**Figure 4.12.** Comparison between the increase in ADP:ATP ratios detected using ApoGlow™ measured on a MPL3 luminometer (Berthold) and the analysis of the sub G<sub>0</sub> peak measured using PI on fixed cells, the maintenance of the plasma membrane was assessed with PI and analysed on a Becton Dickinson FACscan Flow Cytometer. The results are expressed as the representative data of HL60 and 5µM Camptothecin incubated for a time course of 0 hours to 8 hours.

The changes observed during Ara-C induced apoptosis on Jurkat cells shows apoptosis to occur gradually somewhere between 4 hours and 24 hours after the detectable release of cytochrome c. For this reason the HL60 and Camptothecin model was used to try to monitor the changes from a healthy population of cells through to apoptosis analysed using ApoGlow and PI on fixed cells. Figure 4.12 shows HL60 cells induced to undergo apoptosis with 5 $\mu$ M of Camptothecin, measured every hour over a period of 8 hours. The ADP:ATP ratios increase over the 8 hours period from 0.10 at time = 0 hours to 0.42 after time = 8 hours incubation with the drug. It can be seen that there was no real difference observed in the ADP:ATP ratios until after at least 3 hours incubation. The increase in the population of cells with fragmented DNA increased from 9.60% at 0 hours incubation to 84.78% after 8 hours. The detection of hypodiploid cells occurred after only 2 hours incubation with 5 $\mu$ M Camptothecin. The cells were observed to maintain their plasma membrane over this 8 hours incubation period.

#### 4.2.4.2 Detection of Cytolysis

The morphological differences observed between apoptosis and necrosis, are evident from the early stages of the cells death. Necrotic cells are seen to increase in size as the organelles become disorganised and the mitochondrial inner membrane shrinks away from the outer membrane during accumulation of lipid rich particles inside the mitochondria causing the organelle to swell. Initially there is little change observed in the chromatin, which disperses and becomes flocculent after cell structure has been lost and proteases, nucleases and lysosomal contents have been released. Eventually the cell membrane ruptures causing an inflammatory response as toxins are released into the surrounding area *in-vivo*. The permeability of the cell membrane allows for the entry of cell viability dyes such as propidium iodide (PI), which binds to DNA. The rupture of the cell membrane also allows for the release of enzymes such as adenylate kinase (AK) and lactate dehydrogenase (LDH) where both enzymes can be used as cytotoxicity markers. The release of AK into the supernatant was measured using ToxiLight which is a non-destructive bioluminescent cytotoxicity assay which detects AK in two stages following the reactions outlined in Chapter 2, figure 2.08, whereas LDH was measured by CytoTox-ONE. CytoTox-ONE is a homogeneous membrane integrity assay that uses fluorescence to measure the release of LDH into the supernatant from dead cells as outlined in Chapter 2, figure 2.09.

**Figure 4.13**

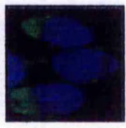
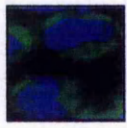



**Figure 4.13.** Comparison between the increase in ADP:ATP ratios detected using ApoGlow™ measured on a MPL3 luminometer (Berthold). The maintenance of the cell membrane was either measured using PI where the samples were analysed on a Becton Dickinson FACscan Flow Cytometer, bioluminescence using ToxiLight on a MPL3 luminometer or fluorescence using CytoTox-ONE on a Victor II fluorimeter (Wallac). The results are expressed as the means of n = 4 separate Jurkat + IgM CD95 experiments incubated for 4 hours (A) and 24 hours (B) (+/- SEM (ADP:ATP ratios, ToxiLight and CytoTox-ONE)) and +/- SD for PI.

Figure 4.13 shows Jurkat cells induced to undergo apoptosis with the CD95 activating antibody at 4 hours and 24 hours incubation. It can be observed from the data that there is no significant correlation between the ADP:ATP ratios and percentage of permeable cells measured with either PI, ToxiLight or CytoTox-ONE until 24 hours incubation when analysed with Spearman's Rho (2 tailed) where all three methods gave significant correlation ( $p < 0.02$ ). When the control was compared to the drug treated samples with the Wilcoxon matched pairs test a significant difference from the control sample to the treated sample was found in the ADP:ATP ratios for both 4 and 24 hours ( $p < 0.05$ ), whereas percentage PI permeable cells, ToxiLight or CytoTox-ONE did not show significant difference from the control until 24 hours incubation ( $p < 0.05$ ) for all methods.

#### **4.2.5 Summary of results**

Table 4.03 shows the summary of the results found within this Chapter for the apoptotic model Jurkat and IgM CD95.

Jurkat and IgM CD95	ATP/RLUs	ADP:ATP ratios	% J-Aggregates	% Monomers	% Annexin V Positive	% hypodiploid	% PI permeable	Cytochrome c release
<b>Control</b>	(4hrs) 40950 +/- 6217.19 (24hrs) 92746 +/- 5070.60	<b>0.13</b> +/- 0.01	<b>86.78%</b> +/- 2.40	<b>12.60%</b> +/- 2.91	<b>6.79%</b> +/- 1.10	<b>2.34%</b> +/- 0.05	<b>3.29%</b> +/- 1.48	
<b>4 hours</b>	<b>16268</b> +/- 4148.37	<b>0.21</b> +/- 0.04	<b>73.39%</b> +/- 7.55	<b>23.81%</b> +/- 7.15	<b>61.24%</b> +/- 3.57	<b>13.56%</b> +/- 6.05	<b>4.47%</b> +/- 2.92	
<b>24 hours</b>	<b>904</b> +/- 115.62	<b>0.86</b> +/- 0.12	<b>12.93%</b> +/- 11.01	<b>87.14%</b> +/- 11.33	<b>64.40%</b> +/- 10.24	<b>49.30%</b> +/- 10.42	<b>31.33%</b> +/- 10.16	

**Table 4.03.** Summary of the appearance of apoptotic events during CD95 activating antibody induced apoptosis in Jurkat cells, incubated for 4 hours and 24 hours (n = 4 separate experiments). The ADP:ATP ratios and ATP/RLUs were measured using ApoGlow™ and detected on a MPL3 luminometer (Berthold). Cytochrome c release was detected using fluorescent imaging and all other data was measured on a Becton Dickinson FACScan flow cytometer using the dyes, JC-1, Annexin V in conjunction with PI and PI alone on fixed and unfixed cells.



### 4.3 Discussion

The human leukaemia cell line Jurkat expresses the cell surface antigen CD95 and undergoes apoptosis when incubated with the CD95 activating antibody (IgM CD95). The interaction between the receptor and the CD95 activating antibody induces apoptosis in the same way as the CD95 Ligand by trimerisation of the receptor. Apoptosis is induced via the mitochondrial route leading to the release of cytochrome c, loss of the  $\Delta\psi_m$  and PS exposure on the cell surface, which are all classic early indicators of apoptosis (Zörnig *et al* (2001), Susin *et al* (1996), Verhoven (1995)). Fragmentation of the DNA is considered to be a later event in the apoptotic cascade, but the appearance of fragmented DNA has been found within this study to be either an early or late event depending upon the cell line and the apoptotic agent employed. The loss of plasma membrane integrity signifies the passage of the cells from apoptosis to secondary necrosis.

When (FITC)-conjugated Annexin V and PI was used to identify PS flip in Jurkat cells that had been induced to undergo apoptosis with the IgM CD95, the ADP:ATP ratios were shown to correlate with samples measured after 4 hours incubation. After 24 hours incubation with the activating antibody however no correlation between the ADP:ATP ratios and the percentage of Annexin V positive cells was found. The Annexin V data was shown to have plateaued at 24 hours, where all samples with the IgM CD95 gave around 60% Annexin V positive cell populations. These samples however exhibited cells in varying stages of secondary necrosis indicated by their inability to exclude the dye PI. The ADP:ATP ratios continued to increase over the 24 hours period and when compared to the uptake of PI there was found to be a significant correlation, thus demonstrating the capability of ApoGlow™ to detect the biochemical changes that are observed with the cells passage from apoptosis to necrosis.

The results obtained seemed to signify in the case of the Jurkat and IgM CD95 model that a ADP:ATP ratio of between 0.20 and 0.30 was indicative of a cell population during the early stages of apoptosis and above 0.30 cells entering into secondary necrosis, as the cells became increasingly leaky the ratios reflected this by continuing to rise.

The ADP:ATP ratios for viable, apoptotic and secondarily necrotic cell populations seem to depend upon the cell line and treatment undertaken. A change in the ratios was not detected until 24 hours incubation for the cytotoxic model Jurkat and Ara-C, coinciding with a significant change in the Annexin V positive population, decrease in the  $\Delta\psi_m$ , DNA fragmentation and evidence of the cells becoming permeable to PI. The HL60 and Camptothecin model gives an example of a model where DNA fragmentation occurs much earlier in the apoptotic cascade occurring after only 4 hours incubation with the drug compared to the Jurkat and Ara-C model where significant DNA fragmentation does not occur until 48 hours incubation with the drug, this was demonstrated by the ability of the HL60 cells to exclude the dye PI. This has also been observed in the two cytotoxic models CEM-7 and dexamethasone and U937 and camptothecin (*Bradbury et al (2000)*). The loss of plasma membrane integrity was reflected in the higher ADP:ATP ratios that were observed after 24 hours incubation, compared to the 4 hours treatment with the IgM CD95 when plasma membrane integrity was maintained. These changes detected in the ratios indicated the capability of ApoGlow™ to monitor the transfer of cell populations from apoptosis to secondary necrosis.

When the Jurkat cells were incubated with Ara-C for 48 hours and IgM CD95 for 24 hours both models showed a similar percentage of cells undergoing secondary necrosis and loss of  $\Delta\psi_m$ . These two models however illustrated differing ADP:ATP ratios which would suggest that as it was the same cell line but induced to apoptose with different agents, that this affects the metabolism of the cells in different ways. Evidence seems to suggest that ATP levels are critical during the onset of

apoptosis and may even act as an apoptotic mediator during some forms of apoptosis induction (*Stefanelli et al (1997)*).

Cytochrome c release was found to precede PS externalisation and disruption of the  $\Delta\psi_m$  in the Jurkat and Ara-C model. There have been many theories put forward as to the mechanism of externalisation of cytochrome c to the cytosol, one such theory being mitochondrial swelling. The rupture of the mitochondrial membrane could arise through either formation of the permeability transition pores, allowing for the entry of water and solutes into the matrix, or closure of the voltage dependent anion channel (VDAC), (*Zörnig et al (2001)*). Closure of the VDAC would result in disruption of the exchange of ATP and ADP across the mitochondrial membrane, leading to hyperpolarisation and subsequent matrix swelling. With the loss of the  $\Delta\psi_m$  and release of cytochrome c it would follow that ATP synthesis would cease, but as neither  $\Delta\psi_m$  or ATP synthesis were affected, this would suggest that either enough cytochrome c remained within the inner mitochondrial membrane to allow for the electron transport chain to continue, or the cell switches to another method for the production of ATP (*Chen (1988) and Garland and Halestrap (1997)*). In cells containing high levels of cytochrome c there will be enough of the protein available to be released to activate the caspases and remain docked to the inner mitochondrial membrane to maintain the electron transport chain (*Green and Reed (1998)*).

As the detection of cytochrome c within the cytosol, loss of ATP and increase in ADP:ATP ratios coincided with the other early apoptotic events in the Jurkat and IgM CD95 model, it would suggest that in death receptor induced killing that this switch between the mechanisms of ATP production can not occur. The differences in the sequence of apoptotic events detected between these two models may reflect the mechanism of externalisation of cytochrome c from the inner mitochondrial membrane. Maintenance of the  $\Delta\psi_m$  during Jurkat treatment with Ara-C would not support the theory of mitochondrial swelling and eventual membrane

rupture as described previously, but rather the formation of pores. Bax is a prime candidate for the formation of such pores either alone or cooperating with the VDAC to form cytochrome c conducting channels (Zörnig et al (2001)).

The release of cytochrome c at 4 hours incubation in the Jurkat and Ara-C model indicates early signs of the cells commitment to apoptosis, although this data could only suggest cytochrome c release at this time as mitochondrial and cytosol fractions could not be obtained due to the fragility of the cells used to perform corroborating western blots. Signs of apoptosis were not reflected in the other markers of early apoptosis including PS externalisation. Other indicators of early apoptosis could not be detected until 24 hours incubation along with the increase in ADP:ATP ratios. The HL60 and Camptothecin model was shown to have increasing ratios after only 4 hours incubation, which was proven to correlate with the increase in green monomers, but the cell membrane remained intact. This again reflects the ability of ApoGlow™ to detect the earlier signs of apoptosis, although it does expose the need to assess apoptotic models on an individual basis when using ApoGlow™ to assess apoptosis and necrosis, due to the varying ADP:ATP ratios obtained on different models. This becomes obvious when comparing the HL60 and Camptothecin ratio of 0.28 in the 5µM concentration with an intact plasma membrane with the Jurkat and Ara-C ratio of 0.22 in the 10µM drug concentration where plasma membrane integrity is lost.

The ApoGlow™ assay is unique in that it combines in one assay the ability to assess a cell population for the different forms of cell death, which can be identified by the very different changes in the amount of measurable ATP and ADP within the population. ApoGlow™ can analyse 96 samples in 25 minutes, whereas flow cytometry samples would take over 3 hours to measure the same number. The loss of ATP is quite noticeable at 4 hours incubation in the Jurkat and IgM CD95 model, as is the loss of the  $\Delta\psi_m$  and PS flip. Detectable ADP and DNA fragmentation

are not quite so noticeable until 24 hours later, which would support the theory that DNA fragmentation is a later marker of apoptosis and that ATP levels are maintained by the cell to drive the active processes involved in programmed cell death. Once ATP levels have dropped significantly the cell enters necrosis, it has been observed that renal tubular cells will undergo necrosis when their ATP stores are severely depleted, apoptosis can only occur in these cells if enough energy is available to drive the active processes during apoptotic cell death (*Lieberthal et al (1998)*). DNA fragmentation was also found to be a later event in the Jurkat and Ara-C model, correlating with both the increase in ADP:ATP ratios and percentage of PI permeable cells. There was almost a five times increase in the amount of measurable DNA fragmentation from 4 to 24 hours incubation but an almost ten fold increment in ADP:ATP ratios. The considerable increase in the ADP:ATP ratios again signifies the capability of ApoGlow™ to follow the death process through from the early to the later stages of apoptosis to secondarily necrotic cells.

The avoidance of an inflammatory response during apoptosis by the maintenance of the cell membrane is the main distinguishing feature of apoptosis from necrosis. ApoGlow™ was seen to correlate significantly with three methods of measuring the loss of plasma membrane integrity including uptake of PI, adenylate kinase (AK) release and loss of lactate dehydrogenase (LDH) from the cell during IgM CD95 induced cell death in Jurkat cells after 24 hours incubation. The bioluminescent method of measuring cytolysis compared well with the conventional methods and may prove useful in combination with ApoGlow™ to give a clearer picture of apoptotic and necrotic cells whereby cells with a loss of ATP and increase in ADP:ATP ratios but no detectable AK would indicate apoptosis, where cells with detectable AK would indicate cells in necrosis.

The sequence in which the events of apoptosis can be detected have been shown to vary between the different apoptotic models. The point at which cytochrome c is released into the cytosol seems to have a

profound effect on the appearance of other apoptotic marker and may signify the cells commitment to apoptosis. The following chapter aims to investigate the sequence of events during apoptosis and at which stage marks the point of no return when the cell has committed itself to die. It will examine the role of the caspases and the involvement of the apoptotic regulators.

## **Chapter 5 – The cells commitment to programmed cell death**

### **5.1 Introduction**

Cells undergoing apoptosis are believed to go through a distinct series of stages. The first stage of apoptosis is the initiation phase which can be the removal of essential growth factors such as granulocyte macrophage colony stimulating factor (GM-CSF) from TF1 cells, or addition of cytotoxic agents such as the topoisomerase I inhibitor Camptothecin to U937 cells. The initiation phase is thought to be reversible until the cell enters the commitment phase and the decision for the cell to die is made. As the apoptotic cascade proceeds the caspases are activated which in turn activate nucleases responsible for the cleavage of DNA (*Clarke (2002)*). Fragmented DNA and other morphological characteristics such as nuclei shrinkage, cell blebbing, and apoptotic bodies can also be detected at this time. The appearance of these visually apoptotic cells marks the executioner phase of programmed cell death (*McCarthy (2002)*).

The commitment phase of apoptosis appears controversial and seems to depend upon the cell itself, and the stimulus to which it was induced to undergo apoptosis. A prime candidate for the cells entrance into the commitment phase is the release of apoptogenic stimuli from the mitochondria, such as cytochrome c, Second mitochondrion derived activator of caspases direct IAP binding protein with low pI (Smac/Diablo) and apoptosis inducing factor (AIF) (*McCarthy et al (2002)*). It is debateable however as to whether it is the release of the apoptotic factors, or the mechanism by which they are released which commits the cell to die. One theory envisages mitochondrial swelling and eventual rupture as the cause of cytochrome c release. Closure of the voltage dependent anion channel (VDAC) would result in disruption of the exchange of ATP and ADP across the mitochondrial membrane, leading to hyperpolarisation and subsequent matrix swelling. The formation of the permeability transition (PT) pores by the irreversible opening of the adenine nucleotide

translocator (ANT) and the VDAC across the mitochondrial membrane would allow for the entry of water and solutes into the matrix and eventual swelling of the mitochondria (*Zörnig et al 2001*). The opening of these pores would eventually lead to the disruption of the  $\Delta\Psi_m$ , oxidative phosphorylation and synthesis of ATP. Investigations have shown that it is the loss of the  $\Delta\Psi_m$  that marks the point of no return for the cell (*Susin et al (1996)*). Other data supports the theory that the mitochondrial membrane remains intact and that it is the creation of cytochrome c conducting channels that allows for its release (*Martinou et al (2000)*). A member of the Bcl-2 family of proteins Bax, appears to be a prime candidate for the formation of these channels, whether it is acting alone or in conjunction with the VDAC. Studies have shown that the addition of pro-apoptotic Bcl-2 family members to isolated mitochondria induces cytochrome c release (*Zörnig et al 2001*). Research has revealed however that microinjection of cytochrome c into the cell does not always induce apoptosis (*Garland and Rudin (1998) and Deshmukh and Johnson (1998)*), which would suggest that other factors are required in addition to cytochrome c for the cells commitment to die.

Apoptosis occurs in all multicellular organisms and is essential in maintaining tissue homeostasis, in eliminating damaged or abnormal cells, for the regulation of cell numbers and in the fight against infections. However it is vitally important that this process is regulated, as abnormalities are evident in several human diseases such as cancer, neurodegenerative disorders and AIDS. Regulation is finely balanced by pro and anti apoptotic members of the Bcl-2 family of proteins, where Bcl-2, Bcl-X<sub>L</sub> are anti apoptotic and Bcl-X<sub>S</sub>, Bax and Bid are pro apoptotic. These proteins support the theory that the mitochondria play an important role in the cells commitment to cell death as Bcl-2 is active in blocking the release of cytochrome c, whilst Bax and Bid play critical roles in its release from the mitochondria. Upon its release into the cytosol cytochrome c binds with Apaf-1 and ATP, to produce the apoptosome and the recruitment of procaspase 9, see Chapter 1, figure 1.05. Oligomerisation



of pro-caspase 9 leads to autoproteolysis and activation of the downstream caspases, the main one being caspase 3. Active caspase 3 is believed to be involved in the proteolysis of other important molecules during apoptosis such as the cleavage of Poly (ADP-ribose) Polymerase (PARP) (*Nicholson et al (1995)*) and ICAD (*Clarke (2002)*).

Synthetic caspase inhibitors are developed based upon the substrate cleavage site of the caspase and as such are competitive inhibitors of this region. Z-VAD-FMK is an irreversible, general caspase inhibitor, containing three aspartate residues and has been proven in many studies to inhibit the effects of apoptosis (*Nicholson (1999)*). Through the use of caspase inhibition and drug removal from apoptotic models already proven in this study, the sequence of events during the cells progression from the early to the later stages of apoptosis will be explored together with the triggers and mechanisms by which the cell becomes committed to die.

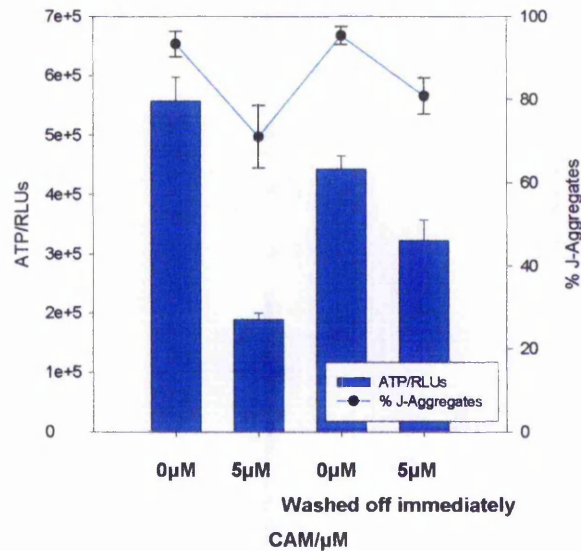
## 5.2 Results

### 5.2.1 The apoptotic cascade and the cells commitment to apoptosis

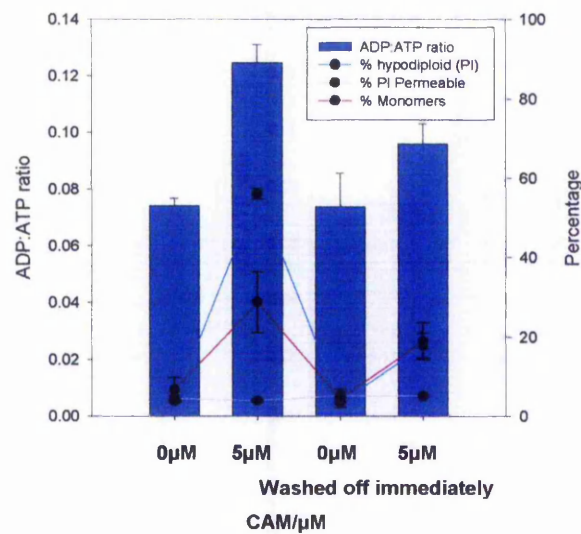
Historically apoptosis was identified morphologically by the appearance of chromatin condensation, convolution of the cell membrane and apoptotic bodies. Cellular blebbing occurs early during apoptosis and it is believed that cells are phagocytosed *in vivo* at this time by the exposure of phosphatidyl serine (PS) on the outer cell membrane (Zörnig *et al* (2001)). Over recent years apoptosis has become identified by the release of cytochrome c from the inner mitochondrial membrane to the cytosol, PS externalisation, loss of the mitochondrial transmembrane potential ( $\Delta\Psi_m$ ) and activation of the caspases. It is believed that the changes to the mitochondria during the early stages of apoptosis mark the point of no return and the cells commitment to die.

In order to try to identify the point of no return and the cells commitment to apoptosis washing experiments were carried out on the following cytotoxicity models, HL60 and camptothecin, U937 and camptothecin and Jurkat and Ara-C. Initially camptothecin was washed from the U937 cells after 30 minutes and 60 minutes incubation with 5 $\mu$ M of the drug (data not shown), these results however highlighted no significant change from those samples where the drug was removed and those where the drug remained throughout the experiment. Therefore the drug was removed immediately after exposure to the cells and after 4 hours incubation they were analysed for signs of apoptosis. Figure 5.01 shows U937 cells incubated with 5 $\mu$ M camptothecin for 4 hours with and without immediate removal of the drug.

**Figure 5.01**



**A**



**B**

**Figure 5.01.** Comparison between the ATP/RLUs measured using ViaLight HS on a Micro Beta Jet luminometer (Wallac) and the loss of the  $\Delta\Psi_m$  analysed using JC-1 on a Becton Dickinson FACscan Flow Cytometer (A). The ADP:ATP ratios were measured using ApoGlow<sup>TM</sup> on the Micro Beta Jet and were compared with the loss of the  $\Delta\Psi_m$  by the increase in % green monomers. The maintenance of the cell membrane was measured using PI and analysis of the sub G<sub>0</sub> peak was measured using PI on fixed cells, the samples were analysed on a FACscan Flow Cytometer (B). The results are expressed as the means of n = 6 separate U937 and CAM experiments incubated for 4 hours following the protocol outlined in Chapter 2, section 2.5.2 (+/- SEM (ATP/RLUs and ADP:ATP ratios) and SD (% PI permeable, % J-Aggregates, % Monomers and % hypodiploid)).

The data obtained shows how in the model U937 and camptothecin, the cells are committed to apoptose immediately after exposure to the drug, although drug removal does seem to decrease the signs of apoptosis by half. When analysed with the Wilcoxon matched pairs test a significant difference was found ( $p < 0.05$ ) between the control and both the drug treated samples with and without the immediate removal of the drug for all tests carried out, but there was no significant difference between the control and the washed control. Significant correlations were found between the loss in ATP/RLUs and percentage loss of red fluorescing J-Aggregates ( $p < 0.02$ ) and ADP:ATP ratios compared to either the percentage increase in cells with fragmented DNA and percentage increase in green fluorescing monomers, when assessed with Spearman's Rho (2 tailed) ( $p < 0.02$ ).

Figure 5.02 shows HL60 cells incubated with  $5\mu\text{M}$  camptothecin for 4 hours with and without immediate removal of the drug. This time there does seem to be a protective affect with immediate removal of the drug, where there was no significant change between the control and both of the washed samples with and without the drug camptothecin when assessed with the Wilcoxon matched pairs test. When the drug remained on the cells for the 4 hours incubation there was a significant difference from drug treated sample to the control with the Wilcoxon matched pairs test ( $p < 0.05$ ). Significant correlations were found between the loss in ATP/RLUs and percentage loss of red fluorescing J-Aggregates and ADP:ATP ratios compared to either the percentage increase in cells with fragmented DNA and percentage increase in green fluorescing monomers when assessed with Spearman's Rho (2 tailed) ( $p < 0.02$ ).

**Figure 5.02**

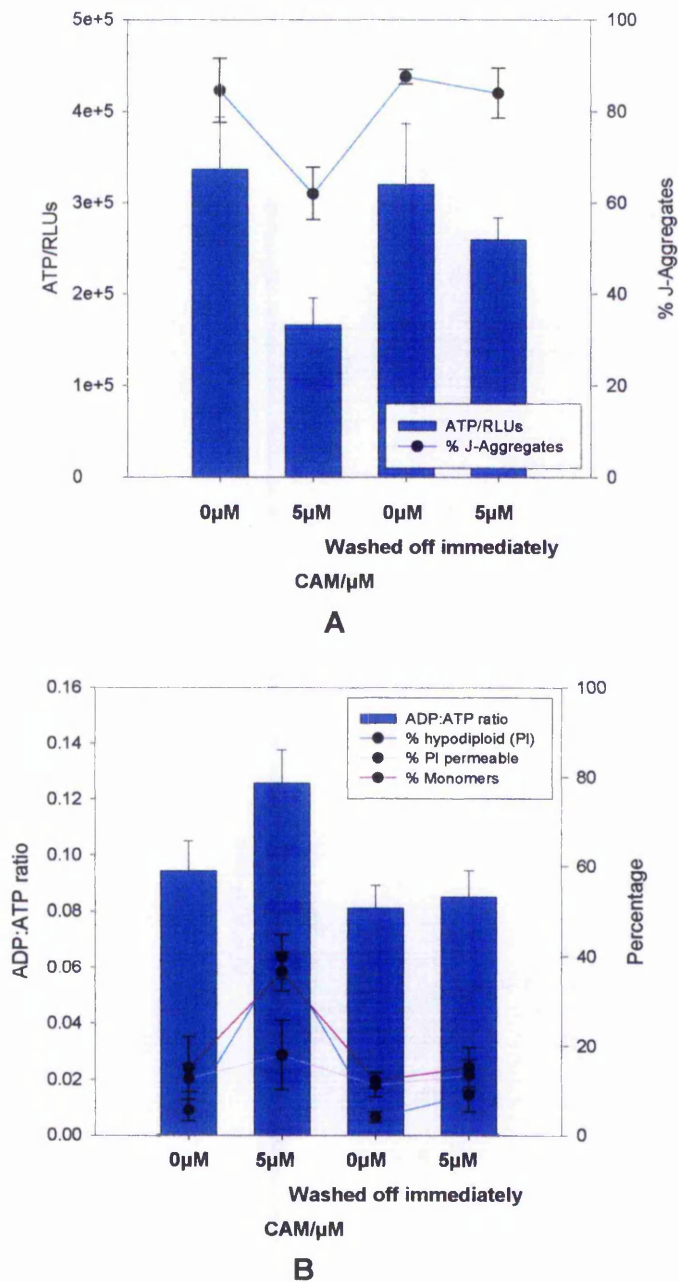
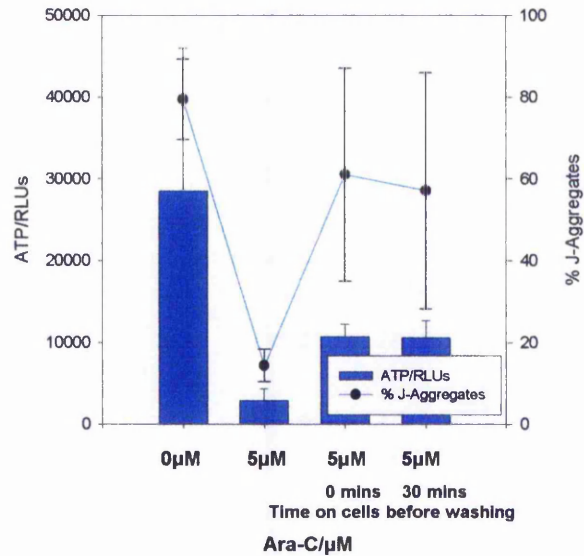


**Figure 5.02.** Comparison between the ATP/RLUs measured using ViaLight HS on a Micro Beta Jet luminometer (Wallac) and the loss of the  $\Delta\Psi_m$  analysed using JC-1 on a Becton Dickinson FACscan Flow Cytometer (A). The ADP:ATP/ratios were measured using ApoGlow<sup>TM</sup> on the Micro Beta Jet and were compared with the loss of the  $\Delta\Psi_m$  by the increase in % green monomers. The maintenance of the cell membrane was measured using PI and analysis of the sub  $G_0$  peak was measured using PI on fixed cells, the samples were analysed on a FACscan Flow Cytometer (B). The results are expressed as the means of  $n = 5$  separate HL60 and CAM experiments incubated for 4 hours following the protocol outlined in Chapter 2, section 2.5.2 (+/- SEM (ATP/RLUs and ADP:ATP ratios) and SD (% PI permeable, % J-Aggregates, % Monomers and % Hypodiploid)).

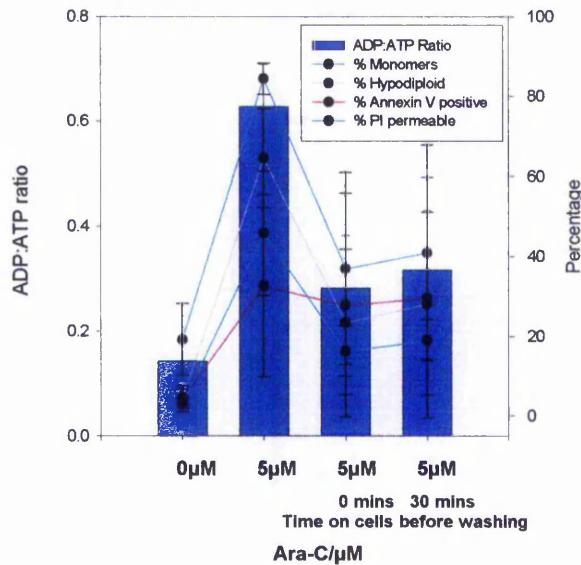
As the Jurkat and Ara-C model is incubated for 48 hours the drug was washed off immediately and after 30 minutes incubation. Figure 5.03 shows Jurkat cells incubated with 5 $\mu$ M Ara-C for 48 hours with and without immediate removal of the drug and removal after exposure to the drug for 30 minutes. The Jurkat and Ara-C model shows the cells are committed to apoptose immediately after exposure to the drug, although drug removal does seem to decrease the signs of apoptosis by half. There appears to be a slight difference between the sample where the drug was removed immediately and where the cells were exposed to the drug for 30 minutes throughout all of the tests where p was found to be less than 0.05 when analysed with the Wilcoxon matched pairs test, apart from the ATP/RLUs and ADP:ATP ratios which showed no significant difference between the two exposure times.

Significant correlations were found between the loss in ATP/RLUs and percentage loss of red fluorescing J-Aggregates and ADP:ATP ratios compared to either the percentage increase in cells with fragmented DNA, externalised PS, loss of plasma membrane and increase in green fluorescing monomers, when assessed with Spearman's Rho (2 tailed) ( $p < 0.02$ ).

**Figure 5.03**



**A**



**B**

**Figure 5.03.** Comparison between the ATP/RLUs measured using ViaLight HS on a MPL3 luminometer (Berthold) and the loss of the  $\Delta\Psi_m$  analysed using JC-1 on a Becton Dickinson FACscan Flow Cytometer (A). The ADP:ATP ratios were measured using ApoGlow™ on the MPL3 luminometer (Berthold) and were compared with the loss of the  $\Delta\Psi_m$  by the increase in % green monomers. Phosphatidyl serine was detected using Annexin V and the maintenance of the cell membrane was measured using PI, analysis of the sub  $G_0$  peak was measured using PI on fixed cells, the samples were analysed on a FACscan Flow Cytometer (B). The results are expressed as the means of  $n = 4$  separate Jurkat and Ara-C experiments incubated for 48 hours following the protocol outlined in Chapter 2, section 2.5.2 (+/- SEM (ATP/RLUs and ADP:ATP ratios) and SD (% PI Permeable, % J-Aggregates, % Monomers, % Annexin V positive and % hypodiploid)).

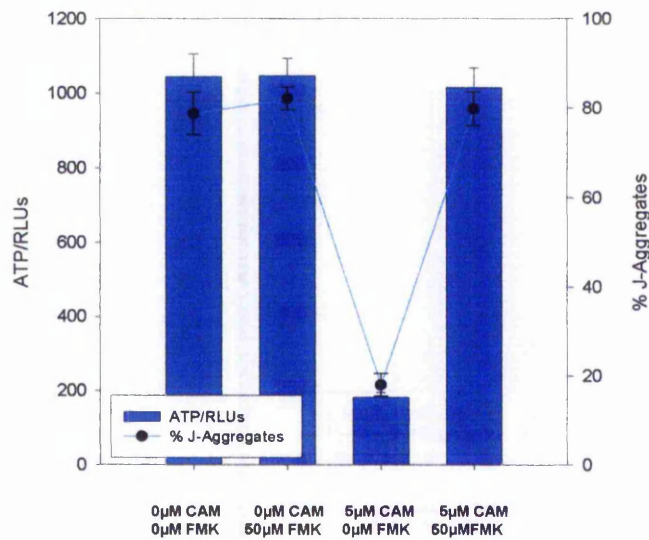
### 5.2.2 The involvement of the caspases

Caspases are cysteine proteases that cleave at sites of aspartic acid residues. All caspases share a common requirement for aspartic acid in their P1 site and as such has led to the development of a range of caspase inhibitors that utilise this requirement. The fluoromethyl ketone Z-VAD-FMK is a general caspase inhibitor and was used within this study to monitor the involvement of the caspases during apoptosis. Figures 5.04 and 5.05 show HL60 and U937 cells incubated for 4 hours with 5 $\mu$ M of the topoisomerase inhibitor camptothecin (CAM), with and without 50 $\mu$ M of the caspase inhibitor Z-VAD-FMK.

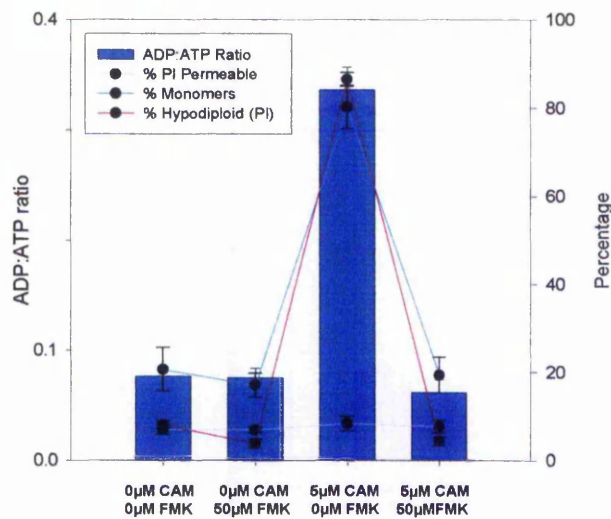
Significant correlations were found between the loss in ATP/RLUs and percentage loss of red fluorescing J-Aggregates and ADP:ATP ratios compared to either the percentage increase in cells with fragmented DNA, externalised PS and increase in green fluorescing monomers when assessed with Spearman's Rho (2 tailed) for both HL60 and U937 data ( $p < 0.02$ ). Both sets of data showed how Z-VAD-FMK inhibited the signs of apoptosis after 4 hours incubation with CAM. The samples with both 5 $\mu$ M CAM and 50 $\mu$ M Z-VAD-FMK showed no significant difference from the control sample when assessed with the Wilcoxon matched pairs test compared to the control and the 5 $\mu$ M CAM sample ( $p < 0.05$ ).



**Figure 5.04**



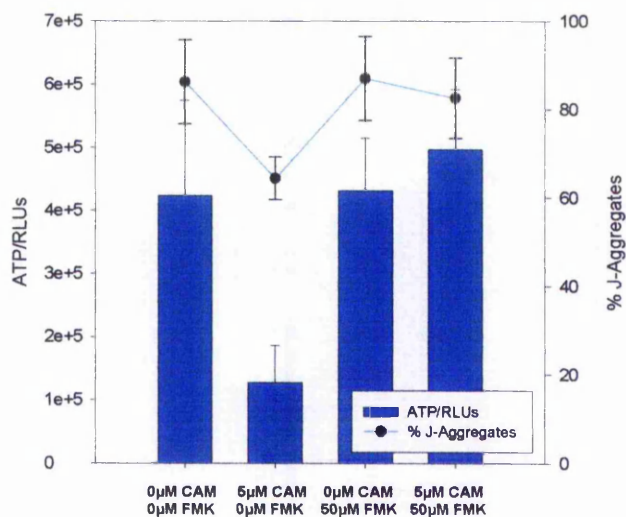
**A**



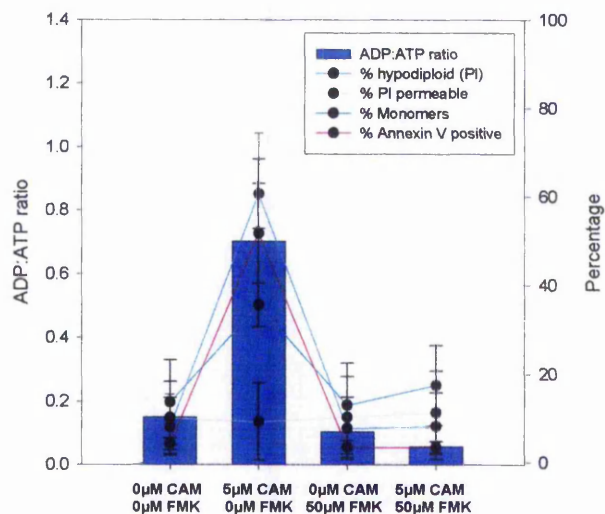
**B**

**Figure 5.04.** Comparison between the ATP/RLUs measured using ViaLight HS on a Micro Beta Jet luminometer (Wallac) and the loss of the  $\Delta\Psi_m$  analysed using JC-1 on a Becton Dickinson FACscan Flow Cytometer (A). The ADP:ATP ratios were measured using ApoGlow™ on the Micro Beta Jet and were compared with the loss of the  $\Delta\Psi_m$  by the increase in % green monomers. The maintenance of the cell membrane was measured using PI and analysis of the sub  $G_0$  peak was measured using PI on fixed cells, the samples were analysed on a FACscan Flow Cytometer (B). The results are expressed as the means of  $n = 4$  separate HL60 and CAM experiments incubated for 4 hours following the protocol outlined in Chapter 2, section 2.5.3 (+/- SEM (ATP/RLUs and ADP:ATP ratios) and SD (% PI Permeable, % J-Aggregates, % Monomers and % hypodiploid)).

**Figure 5.05**



**A**



**B**

**Figure 5.05.** Comparison between the ATP/RLUs measured using ViaLight HS on a Micro Beta Jet luminometer (Wallac) and the loss of the  $\Delta\Psi_m$  analysed using JC-1 on a Becton Dickinson FACscan Flow Cytometer (A). The ADP:ATP ratios were measured using ApoGlow™ on the Micro Beta Jet and were compared with the loss of the  $\Delta\Psi_m$  by the increase in % green monomers. The maintenance of the cell membrane was measured using PI and analysis of the sub G<sub>0</sub> peak was measured using PI on fixed cells, PS externalisation was measured using Annexin V where the samples were analysed on a FACscan Flow Cytometer (B). The results are expressed as the means of n = 4 separate U937 and CAM experiments incubated for 4 hours following the protocol outlined in Chapter 2, section 2.5.3 (+/- SEM (ATP/RLUs and ADP:ATP ratios) and SD (% PI Permeable, % J-Aggregates, % Monomers, % Annexin V positive and % hypodiploid)).

The data shown in figure 5.05 (B) was used to compare the activation of caspases 3, 8 and 9 and the cleavage of PARP. All of the western blots were run alongside rainbow markers and a control of the apoptotic model B-JABS and IgM CD95 known to activate the proteins of interest to give a positive control, this data is not shown.

Caspase 3 exists in its inactive form as a 32kDa proenzyme and is cleaved into its active subunits of 17kDa and 11kDa early during apoptosis. Figure 5.06 shows how after 4 hours incubation with 5 $\mu$ M CAM, the cell line U937 is expressing the active form of caspase 3 where both the 17kDa and 11kDa bands are clearly seen. These bands are missing from non-drug treated samples and also with the addition of 50 $\mu$ M of the general caspase inhibitor Z-VAD-FMK. The loss of the active caspase 3 in the Z-VAD-FMK treated sample coincides with the loss of cells showing PS externalisation, fragmented DNA, loss of the  $\Delta\Psi_m$  and increase in ADP:ATP ratios which suggests that activation of caspase 3 precedes these events during CAM induced apoptosis in U937 cells. Active caspase 3 is believed to be involved in the proteolysis of other important molecules during apoptosis such as the cleavage of Poly (ADP-ribose) Polymerase (PARP). Figure 5.06 shows PARP cleavage in U937 cells incubated for 4 hours with 5 $\mu$ M CAM.

PARP is an 116kDa enzyme involved in DNA repair and is cleaved during apoptosis into 85kDa and 25kDa fragments which results in the loss of the enzymes normal function. After 4 hours incubation with 5 $\mu$ M CAM, the cell line U937 is expressing the 85kDa fragment. This band is missing from non-drug treated samples and also with the addition of 50 $\mu$ M of the general caspase inhibitor Z-VAD-FMK. The loss of the active caspase 3 in the Z-VAD-FMK treated sample again coincides with the loss of cells showing PS externalisation, fragmented DNA, loss of the  $\Delta\Psi_m$  and increase in ADP:ATP ratios. The loss of PARP cleavage with the addition of 50 $\mu$ M Z-VAD-FMK would support the idea that PARP is cleaved by caspase 3.

**Figure 5.06**

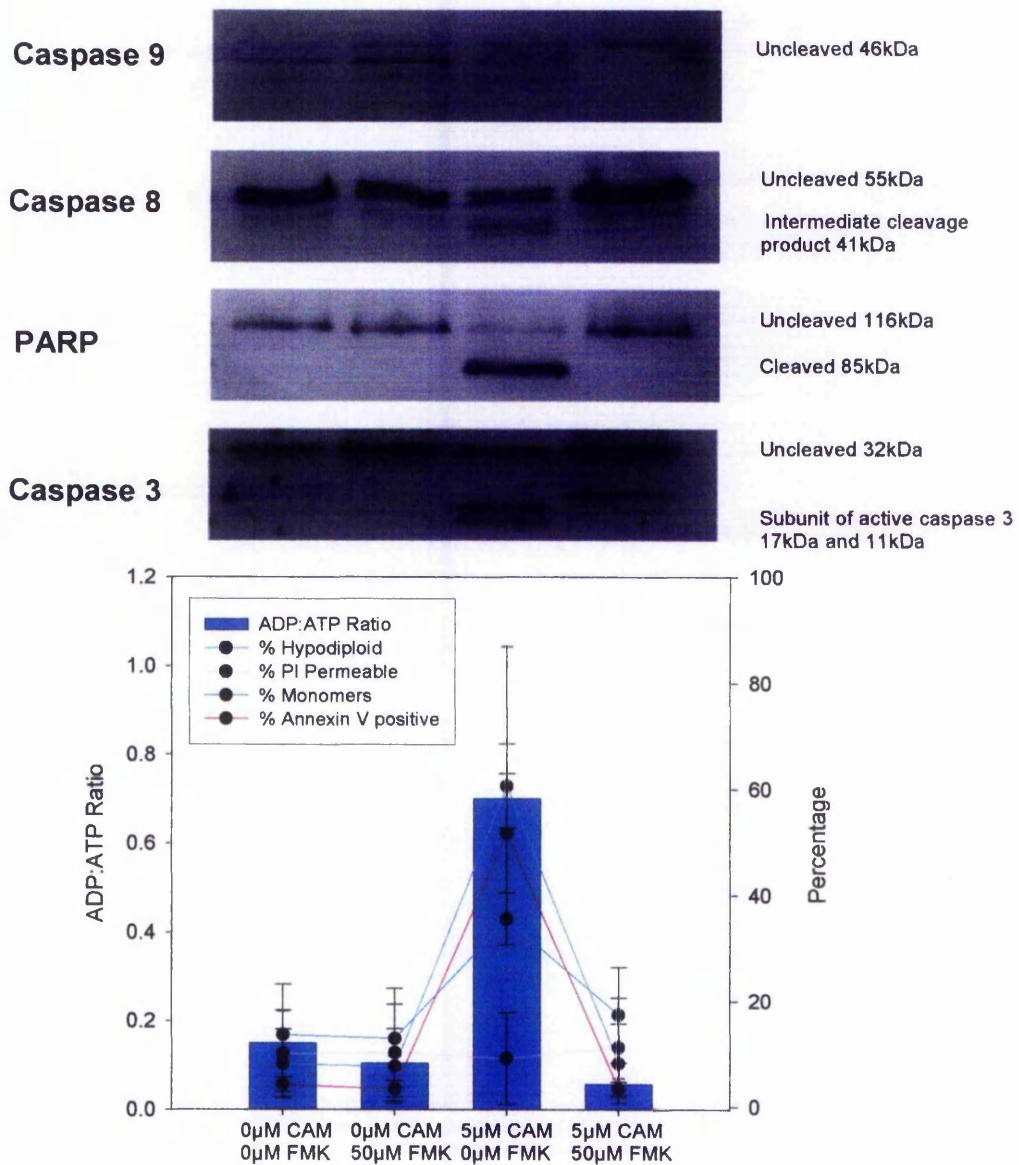


**Figure 5.06.** Comparison between the ADP:ATP ratios measured using ApoGlow™ on the Micro Beta Jet and the loss of the  $\Delta\Psi_m$  by the increase in % green monomers. The maintenance of the cell membrane was measured using PI and analysis of the sub G<sub>0</sub> peak was measured using PI on fixed cells, PS externalisation was measured using Annexin V where the samples were analysed on a FACscan Flow Cytometer. The western blot images show samples probed for caspase 9, caspase 8, PARP and caspase 3. The results are expressed as the means of n = 4 separate U937 and camptothecin (CAM) experiments incubated for 4 hours following the protocol outlined in Chapter 2, section 2.5.3 (+/- SEM (ADP:ATP ratios) and SD (% PI Permeable, % Monomers, % Annexin V positive and % hypodiploid)).

Procaspase 8 is recruited to the activated death receptor CD95 via DED interactions between itself and FADD. It exists as a 55kDa zymogen and during apoptosis is first cleaved into an intermediate cleavage product of 41kDa and subsequently processed to the 18kDa active form. Figure 5.06 shows that after 4 hours incubation with 5 $\mu$ M CAM, the cell line U937 is expressing the 41kDa intermediate cleavage product and not the active form of the caspase. This intermediary band is missing from non-drug treated samples and also with the addition of 50 $\mu$ M of the general caspase inhibitor Z-VAD-FMK. The loss of this band in the Z-VAD-FMK treated sample again coincides with the loss of cells showing PS externalisation, fragmented DNA, loss of the  $\Delta\Psi_m$  and increase in ADP:ATP ratios.

The 41kDa intermediate cleavage product and the 18kDa active form of the caspase was detected in the control sample where B-JABS were induced to undergo apoptosis with the IgM CD95 (data not shown). This data suggests that caspase 8 is not a critical caspase during CAM induced apoptosis and is possibly cleaved to its intermediary product during the caspase cascade. As caspase 8 is not the initiator caspase during this model of apoptosis another candidate for this position is caspase 9. Caspase 9 is activated via the mitochondrial pathway with formation of the apoptosome through Apaf-1 and cytochrome c binding in the presence of dATP. Figure 5.06 shows western blot analysis of caspase 9. Analysis of caspase 9 proved inconclusive as the bands did not appear to represent molecular weights of the active forms of caspase 9, activation of caspase 9 could be investigated using a fluorometric method instead. It has been shown however that caspase 9 can be activated without proteolytic processing (*Stennicke et al (1998)*).

Tables 5.01 and 5.02 show the inhibitory effects of Z-VAD-FMK tested on the mitochondrial pathway model U937 and CAM as well as the death receptor model Jurkat and IgM CD95 incubated for 4 and 24 hours.

U937			Viable cell population	Annexin V positive population	PI permeable population
CAM $\mu$ M	FMK $\mu$ M	Incubation time hours			
0	0	4	86.17% +/- 7.41	4.24% +/- 1.37	8.84% +/- 6.50
		24	88.57% +/- 5.00	3.62% +/- 1.88	6.81% +/- 5.77
5	0	4	40.03% +/- 4.17	51.71% +/- 11.28	7.41% +/- 6.83
		24	10.68% +/- 3.01	14.91% +/- 10.62	50.40% +/- 7.58
5	50	4	86.83% +/- 8.35	3.45% +/- 1.28	9.19% +/- 7.42
		24	35.05% +/- 15.05	6.28% +/- 3.98	41.37% +/- 8.50

**Table 5.01.** Table showing U937 cells incubated with and without 5 $\mu$ M CAM and 50 $\mu$ M Z-VAD-FMK for 4 hours and 24 hours, phosphatidyl serine exposure was assessed with Annexin V measured on a Becton Dickinson FACScan flow cytometer. The data is expressed as the means of n = 4 separate experiments with SD.

Table 5.01 shows how at 4 hours incubation with 5 $\mu$ M CAM the U937 cells increase from 4.24% +/- 1.37 to 51.71% +/- 11.28 Annexin V positive cells, with the addition of 50 $\mu$ M Z-VAD-FMK the percentage of cells with PS exposure is only 3.45% +/- 1.28. This model is shown to be in the early stages of apoptosis with the maintenance of the plasma membrane at 4 hours incubation. After 24 hours the 5 $\mu$ M CAM sample shows a 50.40% +/- 7.68 population of cells with loss of plasma membrane. 24 hours incubation with both 5 $\mu$ M CAM and 50 $\mu$ M Z-VAD-FMK shows the cells to have died by the necrotic route as there was found to be no significant increase in Annexin V positive cells alone. The Jurkat and IgM CD95 model in table 5.02 shows how at 4 hours incubation with 250ng ml<sup>-1</sup> IgM CD95 the Jurkat cells increase from 7.57% +/- 2.85 to 61.24% +/- 3.67 Annexin V positive cells, with the addition of 50 $\mu$ M Z-VAD-FMK the percentage of cells with PS exposure is only 8.06% +/- 3.78. This model is shown to be in the early stages of apoptosis with the maintenance of the plasma membrane at 4 hours incubation. After 24 hours the 250ng ml<sup>-1</sup> IgM CD95 sample shows a 31.33% +/- 10.16 population of cells with loss of plasma membrane.

Jurkat			Viable cell population	Annexin V positive population	PI permeable population
IgM CD95 ng/ml	FMK $\mu$ M	Incubation time hours			
0	0	4	87.84% +/- 3.64	7.57% +/- 2.84	4.33% +/- 1.37
		24	91.65% +/- 1.76	6.01% +/- 1.19	2.24% +/- 0.71
250	0	4	33.97% +/- 4.18	61.24% +/- 3.67	4.47% +/- 2.92
		24	4.04% +/- 3.62	64.40% +/- 10.24	31.33% +/- 10.16
250	50	4	87.73% +/- 4.27	8.06% +/- 3.78	4.09% +/- 1.30
		24	86.34% +/- 0.93	9.52% +/- 0.98	4.08% +/- 1.57

**Table 5.02.** Table showing Jurkat cells incubated with and without 250ng ml<sup>-1</sup> IgM CD95 and 50 $\mu$ M Z-VAD-FMK for 4 hours and 24 hours, phosphatidyl serine exposure was assessed with Annexin V measured on a Becton Dickinson FACScan flow cytometer. The data is expressed as the means of n = 4 separate experiments with SD.

After 24 hours with both the death receptor and 50 $\mu$ M Z-VAD-FMK cells with externalised PS are shown to be 9.52% +/- 0.98 and cells permeable to PI to be 4.08% +/- 1.57. This would suggest that during IgM CD95 induced apoptosis caspase activation precedes other apoptotic events. During CAM induced apoptosis in U937 cells however the death of the cells by necrosis would suggest that some factor in the apoptotic sequence happens before caspase activation, a possible candidate for this is cytochrome c release from the mitochondria to the cytosol.

### 5.2.3 Cytochrome c release

Cytochrome c is required for the formation of the apoptosome leading to activation of caspase 9 and the consequential caspase cascade. Fluorescent microscopy suggested that cytochrome c release occurs early at 4 hours during Ara-C and CD95 activating antibody induced apoptosis in Jurkat cells preceding other early apoptotic events such as PS externalisation and loss of the  $\Delta\Psi_m$ . In order to determine whether cytochrome c release is upstream or downstream of caspase activation in these two apoptotic models, 50 $\mu$ M of the general caspase inhibitor Z-VAD-FMK was also added. As these experiments were set up on the same day both sets of data share the same control. Figure 5.07 shows Jurkat cells incubated with and without 5 $\mu$ M Ara-C and 50 $\mu$ M Z-VAD-FMK.

The control slides (A and E) show intact, round nuclei fluorescing blue with distinct groups of green fluorescing cytochrome c. Slide (B) shows Jurkat cells after 4 hours incubation with 5 $\mu$ M Ara-C where there is some indication of the green fluorescence becoming dispersed showing evidence of cytochrome c release, although the nucleus remains round and intact. With the addition of 50 $\mu$ M Z-VAD-FMK to the sample there is still a suggestion of green fluorescence appearing diffuse showing that cytochrome c release precedes caspase activation during Ara-C treatment on Jurkat cells. Although the addition of Z-VAD-FMK does not stop cytochrome c release it does appear to slow the signs of nuclear blebbing which in non Z-VAD-FMK treated cells occurs after 24 hours. Attempts were made to back this data up by producing cytosolic and mitochondrial fractions to be probed using antibody to cytochrome c on western blots. This method proved difficult however in obtaining pure fractions due to the fragility of the cells used.



**Figure 5.07**

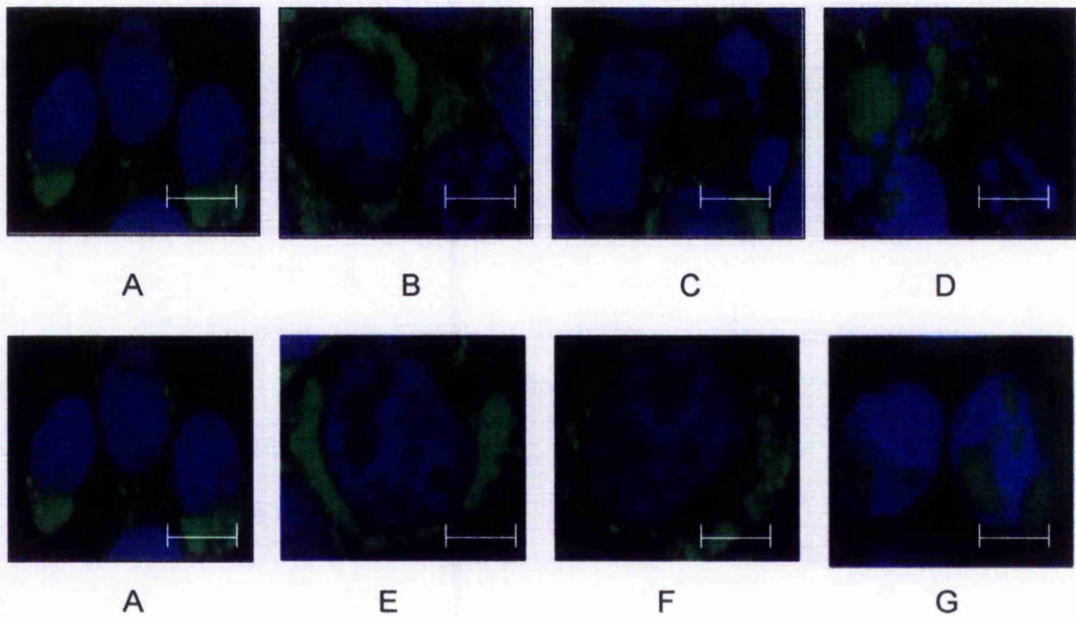


**Figure 5.07.** Jurkat cells treated with and without Ara-C and Z-VAD-FMK, used to measure cytochrome c release and nuclei blebbing with fluorescent imaging. A = control cells, B = 5 $\mu$ M Ara-C treated for 4 hours, C = 5 $\mu$ M Ara-C treated for 24 hours, D = 5 $\mu$ M Ara-C treated for 48 hours, E = 5 $\mu$ M Ara-C + 50 $\mu$ M FMK treated for 4 hours, F = 5 $\mu$ M Ara-C + 50 $\mu$ M FMK treated for 24 hours and G = 5 $\mu$ M Ara-C + 50 $\mu$ M FMK treated for 48 hours. Scale bar: 10 $\mu$ m.

Figure 5.08 shows that during IgM CD95 induced apoptosis in Jurkat cells cytochrome c release is inhibited by the addition of Z-VAD-FMK. This suggests that caspase activation precedes cytochrome c release in this model of apoptosis. Green fluorescence appears to remain in tight discrete groups with round intact nuclei over the 4 hours and 24 hours incubation with the addition of both 250ng ml<sup>-1</sup> IgM CD95 and 50µM Z-VAD-FMK. This finding is supported by the inhibition of the other apoptotic events measured such as the maintenance of the  $\Delta\Psi_m$  and ADP:ATP ratios and there are no measurable signs of PS externalisation or fragmented DNA confirmed by figure 5.08 (E) with round intact nuclei.

**Figure 5.08**

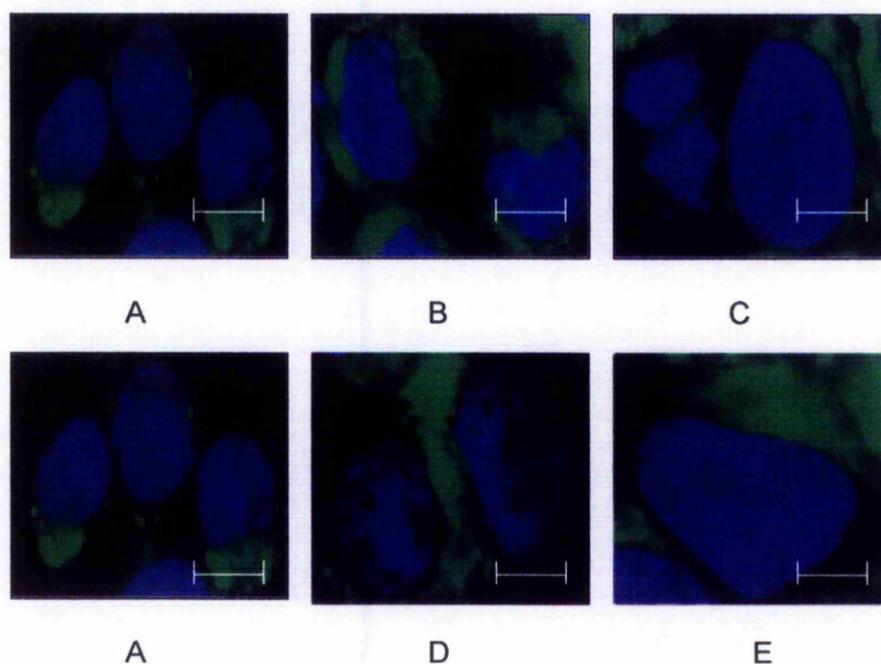


**Figure 5.08.** Jurkat cells treated with IgM CD95 and Z-VAD-FMK, used to measure cytochrome c release and nuclei blebbing with fluorescent imaging. A = Control cells, B =  $250\text{ng ml}^{-1}$  IgM CD95 treated for 4 hours, C =  $250\text{ng ml}^{-1}$  IgM CD95 treated for 24 hours, D =  $250\text{ng ml}^{-1}$  IgM CD95 and  $50\mu\text{M}$  FMK treated for 4 hours, E =  $250\text{ng ml}^{-1}$  IgM CD95 and  $50\mu\text{M}$  FMK treated for 24 hours. Scale bar:  $10\mu\text{m}$ .

## 5.2.4 Apoptotic regulators

As the opening of permeability transition (PT) pores play such a critical role during apoptosis allowing for the release of such apoptogenic molecules as cytochrome c and the apoptosis inducing factor (AIF) from the mitochondria, it could be assumed this process would be carefully monitored. A candidate for the regulation of the formation of these PT pores seems to be Bcl-2 which is localised to the membranes of the mitochondria, nucleus and endoplasmic reticulum.

The hamster fibrosarcoma cell line Met B was stably transfected with a vector expressing either neomycin (G418) selection (neo) or expression vectors for both Bcl-2 and a neomycin (G418) selection vector (Bcl-2). These cells were induced to undergo apoptosis with camptothecin. Table 5.03 shows the comparison between Met B cells expressing normal or elevated levels of Bcl-2 analysed for the percentage of cells with fragmented DNA and decrease in the levels of ATP.

CAM/ $\mu$ M	Neo		Bcl-2	
	% hypodiploid	ATP/RLUs	% hypodiploid	ATP/RLUs
0	3.57	4396.0	1.87	5033.5
500	21.32	1176.1	11.52	1636.7
1000	30.50	820.7	13.57	1544.7
1500	36.74	696.4	15.33	1222.6

**Table 5.03.** Comparison between the ATP/RLUs measured using ApoGlow™ on the Micro Beta Jet (Wallac) and the analysis of the sub G<sub>0</sub> peak was measured using PI on fixed cells. The results are representative data of one Met B experiment expressing normal or elevated levels of Bcl-2 induced to undergo apoptosis with CAM incubated for 48 hours.

Cells showing fragmented DNA were seen to increase from 3.57% in the control sample to 36.74% in the 1500 $\mu$ M CAM concentration in the neo cells which was reflected in the decrease in the levels of ATP falling from 4396.0 in the control to 696.4 in the 1500 $\mu$ M treated sample. The protective properties of Bcl-2 was observed in the Bcl-2 cells showing only a slight increase in cells with fragmented DNA increasing from 1.87% in the control to 15.33% in the 1500 $\mu$ M treated sample which was again reflected in the higher levels of ATP in the Bcl-2 samples. Table 5.04 shows the protective properties of Bcl-2 when the two cell lines were induced to undergo apoptosis with the calcium ionophore Ionomycin.

	Neo		Bcl-2	
Ionomycin/nM	% hypodiploid	ATP/RLUs	% hypodiploid	ATP/RLUs
0	4.43	4683.8	2.15	5163.6
100	3.36	4574.2	2.97	4541.1
500	18.63	1161.1	10.53	1430.9
1000	59.53	178.7	19.71	662.4

**Table 5.04.** Comparison between the ATP/RLUs measured using ApoGlow™ on the Micro Beta Jet (Wallac) and the analysis of the sub G<sub>0</sub> peak was measured using PI on fixed cells. The results are representative data of one Met B experiment expressing normal or elevated levels of Bcl-2 induced to undergo apoptosis with Ionomycin incubated for 48 hours.

Cells showing fragmented DNA were seen to increase from 4.43% in the control sample to 59.53% in the 1000nM Ionomycin concentration in the neo cells which was reflected in the decrease in the levels of ATP falling from 4683.8 in the control to 178.7 in the 1500 $\mu$ M treated sample. The protective properties of Bcl-2 was observed in the Bcl-2 cells showing only a slight increase in cells with fragmented DNA increasing from 2.15% in the control to 19.71% in the 1500 $\mu$ M treated sample which was again reflected in the higher ATP levels.

### 5.3 Discussion

The protective properties of immediate drug removal from HL60 and U937 cells induced to undergo apoptosis with 5 $\mu$ M CAM, varied from complete protection in the HL60 cells to reducing the effects of the drug by half in the U937 cells. Immediate drug removal and 30 minutes exposure to the drug in the Jurkat and Ara-C cytotoxicity model showed significant difference from one another, where 30 minutes exposure to the drug increased the signs of apoptosis. Both the U937 and CAM and Jurkat and Ara-C models showed how the cells were committed to die upon immediate addition of the drug whereas HL60 cells and CAM showed how immediate removal of the drug inhibited the signs of apoptosis. The first sign of apoptosis in Jurkat and Ara-C treated cells has been found to be cytochrome c release from the mitochondria to the cytosol and this may explain the cells commitment to die.

Jurkat and IgM CD95 treated cells with and without 50 $\mu$ M of the general caspase inhibitor Z-VAD-FMK showed in those samples with added Z-VAD-FMK that cytochrome c release was inhibited, there were neither signs of death by the apoptotic route or the necrotic pathway. However in the Jurkat and Ara-C model where cytochrome c release preceded caspase activation Z-VAD-FMK could no longer protect the cells from dying although the measured signs of apoptosis had been reduced. This data suggests that cytochrome c release is upon immediate addition of the drug in U937 and CAM and Jurkat and Ara-C cytotoxicity models but occurs later in HL60 and CAM and Jurkat and IgM CD95 induced apoptosis. Caspase inhibitors have been observed in numerous apoptotic models to be unable to stop cytochrome c release including UV irradiation and staurosporine. An exception to this seems to be when cells are induced to undergo apoptosis by the death receptor pathways, such as CD95L or TNF $\alpha$  induced killing (*Green and Reed (1998)*). This confirms the opinion that activation of caspase 8 is upstream of mitochondrial intervention during this pathway. Jurkat and Ara-C treated cells with Z-

VAD-FMK still died by the apoptotic pathway showing a population of cells with externalised PS but with an intact plasma membrane. Cells treated with CAM and Z-VAD-FMK were protected from the signs of apoptosis at 4 hours incubation but eventually died by the necrotic pathway after 24 hours incubation in the U937 cell line. It has been suggested that in cells containing high levels of caspase inhibitors the release of cytochrome c fails to induce caspase dependent apoptosis and instead is driven towards a necrotic death by the eventual disruption of the electron transport chain (*Green and Reed (1998)*). This is supported by research showing whilst programmed cell death requires energy in the form of ATP it is not a necessary requirement during necrosis (*Tsujimoto (1997)*). There is evidence to suggest that proteins are cleaved to different sized cleavage products depending upon the mechanism by which the cell died. PARP was found to be cleaved to a 50-62kDa substrate when the cells died by the necrotic pathway (*Casiano et al (1998)*). Perhaps this explains the finding during western blot analysis of caspase 3 where an extra band was detected in the sample containing both CAM and Z-VAD-FMK, as these cells were later shown to finally die by a necrotic death.

Research has shown that microinjection of cytochrome c into the cell does not always induce apoptosis. Smac Diablo is a pro-apoptotic protein, which also resides within the mitochondria, its release into the cytosol is thought to be at around the same time as cytochrome c. Smac Diablo supports the onset of apoptosis by binding to and inhibiting the IAPs, which are effective in blocking the activation of the caspases. It appears in some cases that cytochrome c release is not enough to induce apoptosis and that Smac Diablo release from the mitochondria is also required to free bound caspases from the IAPs (*McCarthy et al (2002)*). Apoptosis inducing factor (AIF) is also released from the mitochondria at this time along with some caspases such as caspase 2, caspase 3 and caspase 9 (*Mancini et al (1998)*, *Susin et al (1999)* and *Samali et al (1999)*).

When the hamster fibrosarcoma cell line Met B stably transfected with a vector expressing either neomycin (G418) selection (neo) or an expression vector for both Bcl-2 and a neomycin (G418) selection vector (Bcl-2), were induced to undergo apoptosis with either CAM or Ionomycin the Bcl-2 transfected cells were shown to have reduced apoptotic signs. It has been proposed that the sensitivity of leukaemia cells to cytochrome c release due to  $\text{TNF}\alpha$  exposure, is due to the ratio between the pro and anti apoptotic members of the Bcl-2 family of proteins. The CEM/VLB cell line used in the previously mentioned study was shown to contain a higher level of the pro apoptotic proteins Bcl-x<sub>s</sub> and Bad than CEM cells and as a result were found to be more susceptible to apoptosis (*Li Jia et al (1999)*). This could explain the results obtained with immediate drug removal. If the drug is removed from the cells immediately so as not to give a continuous hit then perhaps not enough of the death promoting family members are activated and so therefore the ratio between the pro and anti apoptotic proteins lies in favour of Bcl-2 and therefore the cells are less susceptible to the drug.

The role of the caspases as the proteases of DNA was evident from the Jurkat and Ara-C treated cells with 50 $\mu\text{M}$  of the general caspase inhibitor Z-VAD-FMK where the upstream release of cytochrome c was able to induce the other signs of apoptosis without the requirement of the caspases such as PS externalisation, loss of the  $\Delta\Psi_m$ , decrease in ATP synthesis and increase in ADP:ATP ratios and eventual plasma membrane permeability. DNA cleavage was shown to be greatly reduced in these samples, confirming the role of the caspases as the activators of the proteases of DNA. It has been suggested that not all apoptotic deaths require caspase activation, loss of the  $\Delta\Psi_m$  or cytochrome c release (*McCarthy (2002)*). Overall this data suggests that there is no one factor that is totally responsible for the cells commitment to apoptosis and that it is both cell and stimulus dependent.



## **Chapter 6 – General Discussion**

The use of bioluminescence as a measurement of ATP and ADP has been proven in this study to be a reliable, sensitive and quick alternative to the conventional methods of the measurement of cell viability. The bioluminescent kits ViaLight HS and ApoGlow™ were found to be highly sensitive both in detecting standards and low cell numbers with excellent reliability. The ViaLight HS kit was able to measure a 96 well white walled luminometer plate in 5 minutes (dependent upon the transport mechanism of the luminometer used) and the ApoGlow™ kit could measure 96 samples in 20 minutes showing detection limits of 50 cells per well for the K562 cell line. The ViaLight HS and ApoGlow™ kits offer many benefits over conventional assays by avoiding the use of radioisotopes and showing greater sensitivity and reproducibility over traditional methods.

By measuring and comparing the relative amounts of ADP to ATP within a population of cells, it was found that by the use of the ApoGlow™ assay, it was possible to screen for all outcomes in a cell viability study. An increase in ATP values above that of the control sample would indicate proliferation in the cell sample, samples giving similar ATP/RLUs to the control and showing no increase in the levels of ADP would indicate growth arrest. The kinetic profile of cells dying by necrosis is one where the ATP/RLUs are greatly reduced compared to that of the control sample, but show a dramatic increase in the levels of ADP. The expected ADP:ATP ratios of a healthy population and a necrotic population of suspension cells is between 0.10 and 1.0. Apoptotic ratios for the suspension models used in this study routinely fell within these limits depending upon whether they were in the early or late stages of apoptosis.

The ApoGlow™ assay was found to be able to monitor the transition from early to late apoptosis to secondary necrosis within a population of cells

and was shown to correlate significantly with the more conventional methods of their analysis. A good example of this was the analysis of phosphatidyl serine (PS) exposure with Annexin V in conjunction with propidium iodide (PI), in Jurkat cells induced to undergo apoptosis with the IgM CD95 activating antibody. After 4 hours incubation the cells were shown to have intact plasma membranes but exposing varying amounts of PS correlating well with the observed ADP:ATP ratios. After 24 hours exposure to the receptor, cells were showing approximately 60% PS 'flip' in all samples. This time the increase in the ADP:ATP ratios were shown to correlate significantly with PI uptake in cells with loss of membrane integrity which is indicative of secondary necrosis. The ADP:ATP ratios showed better correlation with the later stages of apoptosis, which suggests that ATP levels are maintained during programmed cell death to drive the processes of the apoptotic cascade. The formation of the apoptosome during caspase 9 activation for example requires ATP to stabilise the conformational change that occurs due to the binding of cytochrome c to Apaf-1 (*Zamzami et al (2002)*).

The breakdown of the mitochondrial transmembrane potential ( $\Delta\psi_m$ ), measured by the dual potential sensitive dye 5,5',6,6'-tetrachloro-1,1',3,3'-tetraethylbenzimidazolcarbocyanine iodide (JC-1) (*Salvioli et al (1997)*) were shown to correlate with the loss in ATP/RLUs. This significant correlation was evident in all cytotoxic models employed within this study including Jurkat cells and Ara-C, CEM-7 and DEX and HL60 and CAM. At lower drug concentrations during DEX treatment on CEM-7 cells the ATP/RLUs were seen to increase which correlated with an increase in JC-1 uptake. The cell counts that were carried out on these samples showed no proliferation over the control sample suggesting therefore either an increase in ATP production or mitochondrial proliferation. The data presented supported the proliferation of the mitochondria over increased production of ATP due to the increase in red fluorescence detected. It has been suggested that the proliferation of mitochondria during programmed cell death is an integral part of the apoptotic cascade

(*Eliseev et al (2003)*). The FSC-H and SSC-H dot plots obtained from the flow cytometer on the CEM-7 and DEX model showed a population of cells of normal size but with increased granularity. This population of cells eventually made the transition into the apoptotic cell population. Apoptosis is represented by a population of cells with a decrease in cell size and increased granularity. This suggests that the increase in ATP/RLUs and increased activity of the mitochondria is linked with the condensation of the chromatin which occurs early during apoptosis (*McCarthy et al (2002)*). This increase in  $\Delta\psi_m$  has also been witnessed during camptothecin treatment of Jurkat cells (*Sánchez-Alcázar et al (2000)*) and in Ara-C treatment of Jurkat cells in our lab.

The increase in green fluorescence measured with JC-1 is indicative of the loss of the  $\Delta\psi_m$  and was found to correlate well with the ADP:ATP ratios in all of the cytotoxic assays carried out within this study. This suggests a role for both the ViaLight HS and ApoGlow assays as indicators of mitochondrial state. Possible causes for the loss of the  $\Delta\psi_m$  are the irreversible opening of the permeability transition (PT) pores during apoptosis (*Susin et al (1996) and Zamzami et al 2002*). The opening of these pores allows for the entry of water and solutes into the matrix and eventual rupture of the mitochondrial membrane. Closure of the voltage dependent anion channel (VDAC) would result in disruption of the exchange of ATP and ADP across the mitochondrial membrane, leading to hyperpolarisation and subsequent matrix swelling (*Zörnig et al (2001)*). Rupture of the mitochondrial membrane not only disrupts the  $\Delta\psi_m$  but also leads to the release of apoptogenic factors from the mitochondria to the cytosol including apoptosis inducing factor (AIF), Smac Diablo (second mitochondria derived activator of caspases direct IAP binding protein with low pI) and cytochrome c (*Loeffler and Kroemer (2000), Wang (2001) and Zamzami et al 2002*)).

The release of cytochrome c during Ara-C treatment on Jurkat cells was suggested to precede other apoptotic events such as PS exposure, loss

of  $\Delta\psi_m$  and decrease in ATP levels. These findings do not support the theory that mitochondrial rupture occurs upstream of cytochrome c release but rather the formation of pores. Bax is a prime candidate for the formation of such pores either alone or in conjunction with the VDAC to form cytochrome c conducting channels (Zörnig *et al* (2001)). With the release of cytochrome c it would follow that ATP synthesis would cease but as neither  $\Delta\psi_m$  or ATP synthesis were affected in the Jurkat and Ara-C model it would suggest that either enough cytochrome c remained within the inner mitochondrial membrane to allow for the electron transport chain to continue, or the cell switches to another method for the production of ATP. A candidate for this would be a switch from oxidative phosphorylation to glycolysis where it has been observed to occur in malignant cells and some IL-3-dependent cell lines (Chen (1988) and Garland and Halestrap (1997)). As the detection of cytochrome c within the cytosol, loss of ATP and increase in ADP:ATP ratios coincided with the other early apoptotic events in the Jurkat and IgM CD95 model, it would suggest that in death receptor induced killing that this switch between the mechanisms of ATP production can not occur. Future work into this field should include observations of these theories in the apoptotic models used successfully in this study.

The two apoptotic models Jurkat and Ara-C incubated for 48 hours and Jurkat and IgM CD95 treated for 24 hours showed similar percentages to one another of cells undergoing secondary necrosis as measured by PI uptake and loss of  $\Delta\psi_m$ . These two models however illustrated differing ADP:ATP ratios which would suggest that as it was the same cell line but induced to apoptose with different agents, that drug treatment affects the metabolism of the cells in different ways. These differences may be a reflection of the time of release of cytochrome c from the inner mitochondrial membrane to the cytosol. When 50 $\mu$ M of the general caspase inhibitor Z-VAD-FMK was added to the Jurkat and IgM CD95 activating antibody treated cells, cytochrome c release appeared to be inhibited along with the other signs of apoptosis, which suggests that

caspase activation is upstream of cytochrome c release in this model. However in the Jurkat and Ara-C model where cytochrome c release preceded caspase activation Z-VAD-FMK could no longer protect the cells from dying although the measured signs of apoptosis had been reduced.

When 50 $\mu$ M of Z-VAD-FMK was added to the cytotoxicity model U937 and CAM the cells were protected from the signs of apoptosis at 4 hours incubation but were eventually seen to die by the necrotic pathway after 24 hours incubation. During drug induced apoptosis of murine B lymphocytes the addition of Z-VAD-FMK was shown to inhibit the initial signs of apoptosis but failed to maintain cell viability and only succeeded in switching the mechanism of death from apoptosis to necrosis (*Lemaire et al (1999)*). The data in this study seems to support the idea that cytochrome c plays a critical role on the cells commitment to die. It has been suggested that in cells containing high levels of caspase inhibitors that the release of cytochrome c fails to induce caspase dependent apoptosis and instead is driven towards a necrotic death by the eventual disruption of the electron transport chain (*Green and Reed (1998)*). This is supported by research showing whilst programmed cell death requires energy in the form of ATP it is not a necessary requirement during necrosis (*Tsujimoto (1997)*). Caspase inhibitors have been observed in numerous apoptotic models to be unable to stop cytochrome c release including UV irradiation and staurosporine. An exception to this seems to be when cells are induced to undergo apoptosis by the death receptor pathways, such as CD95L or TNF $\alpha$  induced killing (*Green and Reed (1998)*). Activation of the caspases, especially caspase 8, is supported by these findings to be upstream of cytochrome c release. During CAM induced apoptosis in U937 cells the 41kDa intermediate cleavage product and not the active form of caspase 8 was expressed suggesting that caspase 8 is not an integral caspase during this apoptotic pathway. Selective inhibition of caspase 3, caspase 8 and caspase 9 on the Jurkat and IgM CD95 and U937 and CAM apoptotic models would be an

excellent way to clarify the involvement of these caspases and the paths which they take during apoptosis. Another caspase that has been found to act upstream of mitochondria to promote cytochrome c release during Etoposide induced apoptosis in Jurkat cells is caspase 2 (*Robertson et al (2002)*).

The ratio between pro and anti apoptotic members of the Bcl-2 family of proteins has been found to balance the release of apoptogenic factors from the mitochondria (*Li Jia et al (1999)*). This finding could explain the results obtained with immediate drug removal. If the drug is removed from the cells immediately so as not to give a continuous hit then perhaps not enough of the death promoting family members are activated and so therefore the ratio between the pro and anti apoptotic proteins lies in favour of Bcl-2 and therefore the cells are less susceptible to the drug. When the hamster fibrosarcoma cell line Met B stably transfected with a vector expressing either neomycin (G418) selection (neo) or an expression vector for both Bcl-2 and a neomycin (G418) selection vector (Bcl-2), were induced to undergo apoptosis with either CAM or Ionomycin the Bcl-2 transfected cells were shown to have reduced DNA fragmented cells and increased ATP levels. These higher ATP/RLUs are possibly due to enough cytochrome c remaining bound within the mitochondria to maintain the electron transport chain.

The avoidance of an inflammatory response during apoptosis by the maintenance of the cell membrane is the main distinguishing feature of apoptosis from necrosis. ApoGlow™ was seen to correlate significantly with three methods of measuring the loss of plasma membrane integrity including uptake of PI, adenylate kinase (AK) release and loss of lactate dehydrogenase (LDH) from the cell during IgM CD95 induced cell death in Jurkat cells after 24 hours incubation. The bioluminescent method of measuring cytolysis compared well with the conventional methods and may prove useful in combination with ApoGlow™ to give a clearer picture of apoptotic and necrotic cells whereby cells with a loss of ATP and

increase in ADP:ATP ratios but no detectable AK would indicate apoptosis, where cells with detectable AK would indicate cells in necrosis.

As most of the work carried out within this study was performed on suspension cell lines it would be interesting to observe the effects on adherent cells. Preliminary work carried out on the human lung carcinoma A549 induced to undergo apoptosis with CAM showed very little ADP conversion when analysed using ApoGlow™. Adherent cell models require higher drug concentrations and longer incubation times as seen from the 5µM CAM and four hours incubation in the suspension cell line U937 compared to the 1.5mM and 48 hours incubation of CAM in the adherent hamster fibrosarcoma cell line Met B. As adherent cells have only one side exposed to the drug, it seems that a larger dose of drug and extended incubation times are required to overcome the cell to cell interactions and eventual 'round' up of the cell and detachment from the culture flask. The lack of measurable ADP in adherent cells may be a reflection of the involvement of a different metabolic pathway where ATP is degraded to AMP as opposed to ADP. However a difference between the amount of detectable ADP was also observed during Ara-C and IgM CD95 activating antibody treatment on Jurkat cells. Cells induced to undergo apoptosis with Ara-C showed lower ADP:ATP ratios than that of cells treated with CD95 activating antibody. The extended incubation times of the Ara-C treated cells seems to allow for further degradation of ATP which may account for the lower ADP:ATP ratios as the initial ATP values between the two models are similar.

DNA insult initiates the synthesis of poly (ADP-ribose) polymerase (PARP) for DNA repair. As Ara-C affects cellular DNA it may be working to stimulate the PARP mediated suicidal pathway (*Virág (2002)*). Over activation of PARP can lead to decreased levels of NAD<sup>+</sup> and ATP that leads to a necrotic death (*Virág (2002)*). This is evident in the data shown in this study where the Jurkat and Ara-C model shows greater signs of necrotic death as opposed to apoptotic with increased cell membrane permeability than that of the Jurkat and CD95 activating antibody model.

Overall the use of the bioluminescent ATP and ADP assay ApoGlow™ correlated well with the more conventional methods of measuring both early and late markers of apoptosis. It was capable of monitoring the transition from viable to early apoptotic to secondarily necrotic cell populations and showed its self to be a good indicator of mitochondrial state in the apoptotic models used. The assay proved itself to be fast, reliable and reproducible and when used in conjunction with other markers for apoptosis was a useful tool. The main application of ApoGlow™ could be as a screening tool due to the ability to process large numbers of samples in a short time period. The fact that the assay produces a definitive ratio from ATP and ADP RLU's which is not liable to subjective analysis may lead to the possibility of high throughput screening of potential apoptosis inducing agents with predetermined "cut off" ratios. As a tool in drug and medical research this application may prove invaluable.



## References

- Alberts, B., Bray, D., Lewis, J., Raff, M., Roberts, K., Watson, D. (1989). Molecular biology of the cell. **Second edition**, 62-70.
- Bajorath, J., and Aruffo, A. (1997). Prediction of the three dimensional structure of the human Fas receptor by comparative molecular modelling. *J. Comput. Aided Mol. Des.*, **11**, 3.
- Becton Dickinson Diagnostic Systems. Facscalibur Training Manual. (1997).
- Belzacq, A., Viera, H. L. A., Verrier F., Vandecasteele. G., Cohen, I., Prevost, M., et al. (2003). Bcl-2 and Bax modulate adenine nucleotide translocase activity. *Cancer Research*, **63**, 541-546.
- Biron, K. (2003). Weblink,  
<http://bioteach.ubc.ca/Journal/V01101/1926bioluminescence.htm>
- Bradbury, D. A., Simmons, T. D., Slater, K. J., and Crouch, S. P. M. (2000). Measurement of the ADP:ATP ratio in human leukaemic cell lines can be used as an indicator of cell viability, necrosis and apoptosis. *Journal of immunological methods*, **240**, 79-92.
- Brenner, C., Cadiou, H., Vieira, H. L. A., Zamzami, N., Marzo, I., Xie, Z., Leber, B., Andrews, D., Duclouhier, H., Reed, J. C., and Kroemer, G. (2000). Bcl-2 and Bax regulate the channel activity of the mitochondrial adenine nucleotide translocator. *Oncogene*, **19**, 329-336.
- Casiano, C. A., Ochs, R. L., and Tan, E. M. (1998). Distinct cleavage products of nuclear proteins in apoptosis and necrosis revealed by autoantibody probes. *Cell Death Differ.*, **5**, 183-190.
- Chen, L. B. (1988). Mitochondrial membrane potential in living cells. *Annu. Rev. Cell. Biol.*, **4**, 155-181.
- Chittenden, T., Flemington, C., Houghton, A. B., Ebb, R. G., Gallo, G. J., Elangovan, B., et al. (1995). A conserved domain in Bak, distinct from BH1 and BH2, mediates cell death and protein binding functions. *EMBO J.*, **14**, 5589.
- Clarke, P. R. (2002). Apoptosis: lessons from cell-free systems. *Apoptosis the molecular biology of programmed cell death*.
- Crook, N. E., Clem, R. J., and Miller, L. K. (1993). An apoptosis inhibiting baculovirus gene with a zinc finger like motif. *J. Virol.* **67**, 2168-2174.

- Crouch, S. P. M., Kozlowski, R., Slater, K. J., and Fletcher, J. (1993). The use of ATP bioluminescence as a measure of cell proliferation and cytotoxicity. *Journal of Immunological Methods.*, **160**, 81-88.
- Cohen, G. M. (1997). Caspases: the executioners of apoptosis. *Biochem. J.*, **326**, 1-16.
- Darzynkiewicz, Z. Bruno, S. Bino, G. D. Gorczyca, W. Hutz, M. Lassota, P. Traganos, F. (1992). Features of apoptotic cells measured by flow cytometry. *Cytometry*, **13**, 795-808.
- Decker, R.H., Levin, J., Kramer, L. B., Dai, Y., and Grant, S. (2003). Enforced expression of the tumor suppressor p53 renders human leukemia cells (U937) more sensitive to 1-[beta-D-arabinofuranosyl]cytosine (ara-C)-induced apoptosis. *Biochem Pharmacol*, **15;65(12)**, 1997-2008.
- DeLange, A. M., Carpenter, M. S., Choy, J., and Newsway, V. E. (1995). An Etoposide induced block in vaccinia virus telomere resolution is dependent on the virus encoded DNA ligase. *Journal of Virology*, **69(4)**, 2082-2091.
- DeLuca, M., Wannlund, J., and McElroy, W. D. (1979). Factors affecting the kinetics of light emission from crude and purified firefly luciferase. *Anal. Biochem*, **95**, 194-198.
- Desagher, S., Osen-Sand, A., Nichols, A., Eskes, R., Montessuit, S., Lauper, S., Maundrell, K., Antosson, B., and Martinou, J. (1999). Bid-induced conformational change of Bax is responsible for mitochondrial cytochrome c release during apoptosis. *J. Cell Biol.*, **144(5)**, 891-901.
- Deshmukh, M. and Johnson, E. M. J. (1998). Evidence of a novel event during neuronal death: Development of competence-to-die in response to cytoplasmic Cytochrome c. *Neuron*, **21**, 695-705.
- De Wet, J. R., Wood, K. V., Helinski, D. R., and DeLuca, M. (1985). Cloning of firefly luciferase cDNA and the expression of active luciferase in *Escherichia coli*. *Biochemistry*, **82**, 7870-7873.
- Ekert, G., Silke, J., and Vaux, D. L. (1999). Caspase inhibitors. *Cell Death Differ.*, **6**, 1081-1086.
- Eliseev, R. A., Gunter, K. K., and Gunter, T. E. (2003). Bcl-2 prevents abnormal mitochondrial proliferation during Etoposide induced apoptosis. *Exp Cell Res*, **2**, 275-281.
- Ellis, H. M., and Horvitz, H. R. (1986). Genetic control of programmed cell death in the nematode *C. elegans*. *Cell*, **44**, 817-829.

- Eskes, R., Desagher, S., Antonsson, B., and Martinou, J. C. (2000). Bid induces the oligomerisation and insertion of Bax into the outer mitochondrial membrane. *Mol. Cell. Biol.*, **20**, 929-935.
- Fadok, V. A., Voelker, D. R., Cammpbell, P. A., Cohen, J. J., Bratton, D. L., and Henson, P. M. (1992). Exposure of phosphatidylserine on the surface of apoptotic lymphocytes triggers specific recognition and removal by macrophages. *J. Immunol.*, **148**, 2207-2216.
- Finucane, D. M., Bossy-Wetzel, E., Waterhouse, N. J., Cotter, T. G., and Green, D. R. (1999). Bax-induced caspase activation and apoptosis via Cytochrome c release from mitochondria is inhibitable by Bcl-x<sub>L</sub>. *J. Biol. Chem.*, **274**(4), 2225-2233.
- Garland, J., Halestrap, A. (1997). Energy metabolism during apoptosis. *J. Biol. Chem.* **272**, 4680-4688.
- Garland, J. M., and Rudin, C. (1998). Cytochrome c induces caspase-dependent apoptosis in intact hematopoietic cells and overrides apoptosis suppression mediated by Bcl-2, growth factor signalling, MAP-kinase-kinase, and malignant change. *Blood*, **92**, 1235-1236.
- Gorman, A., McCarthy, J., Finucane, D., Reville, W., and Cotter, T. (1994). Morphological assessment of apoptosis. Techniques in apoptosis - a users guide, Portland press, 1-20.
- Green, D. R., and Reed. J. C. (1998). Review: Mitochondria and apoptosis. *Science*, **281**, 1309-1312.
- Hirata, H., Takahashi, A., Kobayashi, S., Yonehara, S., Sawai, H., Okazaki, T., *et al.* (1998). Caspases are activated in a branched protease cascade and control distinct downstream processes in Fas-induced apoptosis. *J. Exp. Med.*, **187**, 587-600.
- Horvitz, H. R. (1999). Genetic control of programmed cell death in the nematode *Caenorhabditis elegans*. *Cancer Res*, **59**, 1701-1706.
- Hsu, Y. T., Wolter, K. G., and Youle, R. J. (1997). Cytosol-to-membrane redistribution of Bax and Bcl-X(L) during apoptosis. *Proc. Natl Acad. Sci. USA*, **94**, 3668-3672.
- Huang, D. C., Adams, J. M., and Cory, S. (1998). The conserved N-terminal BH4 domain of Bcl-2 homologues is essential for inhibition of apoptosis and interaction with CED-4. *EMBO J.*, **17**, 1029.
- Jones, C. B., Clements, M. K., Wasi, S., and Daoud, S. S. (2000). Enhancement of camptothecin-induced cytotoxicity with UCN-01 in breast cancer cells: abrogation of S/G<sub>2</sub> arrest. *Cancer chemotherapy and Pharmacology*, **45**(3), 252-258.

- Kerr, J. F., Wyllie, A. H., and Currie, A. R. (1972). Apoptosis: a basic biological phenomenon with wide-ranging implications in tissue kinetics. *Br. J. Cancer*, **26**, 239-237.
- Koopman, G., Reutelingsperger, C. P., Kuijten, G. A., Keehned, R. M., et al. (1994). Annexin V for flow cytometric detection of phosphatidylserine expression on B cells undergoing apoptosis. *Blood*, **84**, 1415-1420.
- Kroemer, G., Zamzami, N., and Susin, S. A. (1997). Mitochondrial control of apoptosis. *Immunol. Today*, **18**, 44-51.
- Kuhnel, J. M., Perrot, J. Y., Faussat, A. M., Marie, J. P., and Schwaller, M. A. (1997). Functional assay of multidrug resistant cells using JC-1, a carbocyanine fluorescent probe. *Leukemia*, **11**, 1147-1155.
- Kumar, S. (1999). Mechanisms mediating caspase activation in cell death. *Cell Death Differ.*, **6**, 1060-1066.
- Leist, M., Single, B., Castoldi, A. F., Kuhnle, S., and Nicotera, P. (1997). Intracellular adenosine triphosphate (ATP) concentration: a switch in the decision between apoptosis and necrosis. *J. Exp. Med.*, **8**, 1481-1486.
- Leist, M., Single, B., Naumann, H., Fava, E., Simon, B., Kuhnle, S., and Nicotera, P. (1999). Inhibition of mitochondrial ATP generation by nitric oxide switches apoptosis to necrosis. *Exp. Cell Research.*, **249**, 396-403.
- Lemaire, C., Andréau, K., Sidoti-de Fraisse, C., Adam, A., and Souvannavong, V. (1999). IL-4 inhibits apoptosis and prevents mitochondrial damage without inducing the switch to necrosis observed with caspase inhibitors. *Cell death and Differentiation*, **6**, 813-820.
- Li Jia., Macey, M. G., Yuzhi Yin., Newland, A. C., and Kelsey, S.M. (1999). Subcellular distribution of Bcl-2 family proteins in human leukaemia cells undergoing apoptosis. *Blood.*, **93(7)**, 2353-2359.
- Li, P., Nijhawan, D., Budihardjo, I., Srinivasula, S. M., Ahmed, M., Alnmri, E. S., et al. (1997). Cytochrome c and dATP-dependent formation of Apaf-1/caspase-9 complex initiates an apoptotic protease cascade. *Cell*, **91**, 479-489.
- Lieberthal, W., Menza, S. A., Levine, J. S. (1998). Graded ATP depletion can cause necrosis or apoptosis of cultured mouse proximal tubular cells. *Am J Physiol*, **274(2 Pt 2)**, F315-F327.
- Loeffler, M., and Kroemer, G. (2000). The mitochondrion in cell death control: Certainties and incognita. *Experimental cell research*, **256**, 19-26.
- Lundin, A. (1990). Clinical applications of luminometric ATP monitoring.

- Majno, G., and Joris, I. (1995). Apoptosis, oncosis, and necrosis. An overview of cell death. *Am J Pathol*, **146**(1), 3-15.
- Mancini, M., Nicholson, D. W., Roy, S., Thornberry, N. A., Peterson, E. P., Casciola-Rosen, L. A., *et al.* (1998). The caspase-3 precursor has a cytosolic and mitochondrial distribution: implications for apoptotic signalling. *J. Cell Biol*, **140**, 1485-1495.
- Martin, S. J., Reutelingsperger, C. P., McGahon, A. L., Radar, J. A., *et al.* (1995). Early redistribution of plasma membrane phosphatidylserine is a general feature of apoptosis regardless of the initiating stimulus: inhibition by overexpression of Bcl-2 and Abl. *J. Exp. Med.*, **182**, 39-51.
- Martinou, J. C., Desagher, S., and Antonsson, B. (2000). *Nat. Cell Biol*, **2**, E41-E43.
- McCarthy, N. J. (2002). Why be interested in death? *Apoptosis the molecular biology of programmed cell death*.
- McCarthy, N. J., and Bennett, M. R. (2002). Death signalling by the CD95/TNFR family of death domain containing receptors. *Apoptosis the molecular biology of programmed cell death*.
- Mignotte, B., and Vayssiere, J. (1998). Review: Mitochondria and apoptosis. *Eur. J. Biochem.*, **252**, 1-15.
- Miller, L. J., Marx, J. (1998). Review: Apoptosis. *Science*, **281**, 130-1326.
- Montani, M. S., Tuosto, L., Giliberti, R., Stefanini, L., Cundari, E., Piccolella E. (1999). Dexamethasone induces apoptosis in human T cell clones expressing low levels of Bcl-2. *Cell Death Differ*, **6**(1), 79-86.
- Morris, R. G., Hargreaves, A. D., Duvall, E., and Wyllie, A. H. (1984). Hormone-induced cell death. 2. Surface changes in thymocytes undergoing apoptosis. *Am. J. Pathol.*, **115**, 426-436.
- Muchmore, S. W., Sattler, M., Liang, H., Meadows, R. P., Harlan, J. E., Yoon, H. S., *et al.* (1996). X-ray and NMR structure of human Bcl-x<sub>L</sub>, an inhibitor of programmed cell death. *Nature*, **381**, 3351.
- Newmeyer, D. D., Bossy-Wetzel, E., Kluck, R. M., Wolf, B. B., Beere, H. M., and Green, D. R. (2000). Bcl-X<sub>L</sub> does not inhibit the function of Apaf-1. *Cell death and differentiation*. **7**, 402-407.
- Nicholson, D. W., Ali, A., Thornberry, N. A., Vaillancourt, J. P., Ding, C. K., Gallant, M., Gareau, Y., Griffin, P. R., Labelle, M., Lazebnik, Y. A., Munday, N. A., Raju, S. M., Smulson, M. E., Yamin, T. T., Yu, V. L., and Miller, D. K. (1995). Identification and inhibition of the ICE/CED-3 protease necessary for mammalian apoptosis. *Nature*, **376**, 37-43.

- Nicholson, D. W. (1999). Review: Caspase structure, proteolytic substrates, and function during apoptotic cell death. *Cell Death Differ.*, **6**, 1028-1042.
- Nicoletti, I., Migliorati, G., Pagliacci, M. C., Grignani, F., and C, Riccardi. (1991). A rapid and simple method for measuring thymocyte apoptosis by propidium iodide staining and flow cytometry. *Journal of Immunological Methods*, **139**, 271-279.
- Nijhawan, L. P., Budihardjo, I., Srinivasula, S. M., Ahmad, M., Alnemri, E. S., et al. (1997). Cytochrome c and dATP-dependent formation of Apaf-1 / caspase-9 complex initiates an apoptotic protease cascade. *Cell*, **91**, 479-489.
- Olson, M., Kornbluth S. (2001). *Curr Mol Med*, **1**, 91-122.
- Oltvai, Z. N., Milliman, C. L., and Korsmeyer, S. J. (1993). Bcl-2 heterodimerises in vivo with a conserved homolog, Bax, that accelerates programmed cell death. *Cell*, **74**, 609.
- Ormerod, M. G. (1998). Review: The study of apoptotic cells by flow cytometry. *Leukemia*, **121**, 1013-1025.
- Osborne, B. A. (1996). *Curr Opin Immunol*, **8**, 245-254.
- Pazzagli, M., Cadenas, E., Kricka, L. J., Roda, A., and Stanley, P. E. (1988). *Journal of bioluminescence and chemiluminescence studies and applications in biology and medicine*.
- Petty, R., Sutherland, L., Hunter, E., and Cree, I. (1995). Comparison of MTT and ATP-based assays for the measurement of viable cell number. *J Biolumin Chemilumin*, **10(1)**, 29-34.
- Robertson, J. D., Enoksson, M., Suomela, M., Zhivotovsky, B., and Orrenius, S. (2002). Caspase-2 acts upstream of mitochondria to promote Cytochrome c release during etoposide-induced apoptosis. *J. Biol. Chem.*, **33**, 29803-29809.
- Roy, N., and Cardone, M. H. (2002). The caspases: consequential cleavage. *Apoptosis the molecular biology of programmed cell death*.
- R&D Systems. Apoptosis Detection Kits: Kit Insert For Kits TA4638, TA5532.
- Salvioli, S., Ardizzoni, A., Franceschi, C., and Cossarizza, A. (1997). JC-1 but not DiOC<sub>6</sub>(3) or rhodamine 123, is a reliable fluorescent probe to assess  $\Delta\Psi$  changes in intact cells: implications for studies on mitochondrial functionality during apoptosis. *FEBS Letters*, **411**, 77-82.

- Salvioli, S., Barbi, C., Dobrucki, J., Moretti, L., Pinti, M., Pedrazzi, J., *et al.* (2000). Opposite role of changes in mitochondrial membrane potential in different apoptotic processes. *FEBS Letters*, **469**, 186-190.
- Samali, A., Cai, J., Zhivotovsky, B., Jones, D. P., and Orrenius, S. (1999). Presence of a pre-apoptotic complex of pro-caspase-3, hsp60, and hsp10 in the mitochondrial fraction of Jurkat cells. *EMBO J.*, **18**, 2040-2048.
- Sánchez-Alcázar, J.A., Ault, J.G., Khodjakov., Schneider, E. (2000). Increased mitochondrial cytochrome c levels and mitochondrial hyperpolarisation precede camptothecin-induced apoptosis in Jurkat cells. *Cell Death Differ.*, **7**, 1090-1100
- Savill, J., Fadok, V., Henosn, P., and Haslett, C. (1993). Phagocyte recognition of cells undergoing apoptosis. *Immunol. Today*, **14**(3), 131-136.
- Seleger, H. H., and McElroy, W. D., (1960). Spectral emission and quantum yield of Firefly bioluminescence. *Arch Biochem Biophys.*, **88**, 136-41
- Shimizu, S., Eguchi, Y., Kamiike, W., Itoh, Y., Hasegawa, J. I., Yamabe, K., Ohtsuki, Y., Matsuda, H., and Tsujimoto, Y. (1996). Induction of apoptosis as well as necrosis by hypoxia and predominant prevention of apoptosis by bcl-2 and bcl-xL. *Cancer Res*, **56**, 2161-2166.
- Silke, J., Verhagen, A. M., Ekert, P. G., and Vaux, D. L. (2000). Sequence as well as functional similarity for DIABLO/Smac and Grim, Reaper and Hid? *Cell Death Differ.*, **12**, 1274.
- Slee, E. A., Harte, M.T., Kluck, R. M., Wolf, B. B., Casiano, C. A., Newmeyer, D. D., *et al.* (1999). Ordering the Cytochrome c-initiated caspase cascade: hierarchical activation of caspases-2, -3, -6, -7, -8 and -10 in a caspase-9-dependent manner. *J. Cell Biol.*, **144**, 281-292.
- Slee, E. A., Adrain, C., and Martin, S. J. (1999). Serial killers: ordering caspase activation events in apoptosis. *Cell Death Differ.*, **6**, 1067-1074.
- Solange, D., Osen-Sand, A., Nichols, A., Eskes, R., Montessuit, S., Lauper, S., *et al.* (1999). Bid-induced conformational change of Bax is responsible for mitochondrial cytochrome c release during apoptosis. *J. Cell Biol.*, **144**, 891-901.
- Song, Q., Lees-Miller, S. P., Kumar, S., Zhang, N., Chan, D. W., Smith, G. C., *et al.* (1996). DNA-dependent protein kinase catalytic subunit: a target for an ICE-like protease in apoptosis. *EMBO J.*, **15**, 3238.
- Spence, A. P., Mason, E. B. (1992). Human anatomy and physiology. **Fourth edition.** 804-809.

- Steck, K, McDonnell, T, Sneige, N, el-Nagger, A. (1996). A flow cytometric analysis of apoptosis and Bcl-2 in primary breast carcinomas: clinical and biological implications. *Cytometry*, **24**, 116-122.
- Stefanelli, C., Bonavita, F., Stanic, I., Farruggia, G., Falcieri, E., Robuffo, I., *et al.* (1997). ATP depletion inhibits glucocorticoid-induced thymocyte apoptosis. *Biochem. J.*, **322**, 909-917.
- Stennicke, H. R., Deveraux, Q. L., Humke, E. W., Reed, J. C., Dixit, V. M., and Salvesen, G. S. (1999). Caspase-9 can be activated without proteolytic processing. *J. Biol. Chem.*, **274**, 8359-8362.
- Srinivasula, S. M., Ahmed, M., Fernandes-Alnemri, T., and Alnemri, E. S. (1998). Autoactivation of procaspase-9 by Apaf-1-mediated oligomerisation. *Mol. Cell*, **1**, 949-947.
- Susin, S. A., Zamzami, N., and Kroemer, G. (1996). The cell biology of apoptosis: Evidence for the implication of mitochondria. *Apoptosis.*, **1**, 231-242.
- Susin, S. A., *et al.* (1998). *Biochimica et Biophysica Acta*, **1366**, 151-165.
- Susin, S. A., Lorenzo, H. K., Zamzami, N., Marzo, I., Snow, B. E., Brothers, G. M., *et al.* (1999). Molecular characterisation of mitochondrial apoptosis-inducing factor (AIF). *Nature*, **397**, 441-446.
- Susin, S. A., Lorenzo, H. K., Zamzami, N., Marzo, I., Larochette, N., Alzari, P. M., *et al.* (1999). Mitochondrial release of caspases-2 and -9 during the apoptotic process. *J. Exp. Med.*, **189**, 383-391.
- Takahashi, A., Alnemri, E. S., Lazebnik, Y. A., Fernandes-Alnemri, T., Litwack, G., Moir, R. D., Goldman, R. D., Poirier, G. G., Kaufmann, S. H., and Earnshaw, W. C. (1996). Cleavage of lamin A by Mch2 alpha but not CPP32: multiple interleukin 1 beta-converting enzyme-related proteases with distinct substrate recognition properties are active in apoptosis. *Proc. Natl. Acad. Sci. USA*, **93**, 8395-8400.
- Thornberry, N. A., Rano, T. A., Peterson, E. P., Rasper, D. M., Timkey, T., Garcia-Calvo, M., *et al.* (1997). A combinatorial approach defines specificities of members of the caspase family and granzyme B. Functional relationships established for key mediators of apoptosis. *J. Biol. Chem.*, **272**, 17907-17911.
- Tomei, L. D., Shapiro, J. P., and Cope, F. O. (1993). *Proc. Natl. Acad. Sci. U.S.A.*, **90**, 853-857.
- Trump, B. F., Valigorsky, J. M., Dess, J. H., Mergner, J. W., Kim, K. M., Jones, R. T., *et al.* (1973). Cellular change in human disease: A new method of pathological analysis. *Hum. Pathol.*, **4**, 89-109.



- Tsujimoto, Y. (1997). Apoptosis and necrosis: Intracellular ATP level as a determinant for cell death modes. *Cell death and differentiation.*, **4**, 429-434.
- Tsujimoto, Y. (1998). Role of Bcl-2 family proteins in apoptosis: apoptosomes or mitochondria? *Genes Cells*, **3**, 697.
- Tsujimoto, Y. (2002). Regulation of apoptosis by the Bcl-2 family of proteins. *Apoptosis the molecular biology of programmed cell death*.
- Turnerbiosystems application notes (2004).
- Verhoven, B., Schlegel, R. A., and Williamson, P. (1995). Mechanisms of phosphatidylserine exposure, a phagocyte recognition signal, on apoptosis T lymphocytes. *J. Exp. Med*, **182**, 1597-1601.
- Virág, L. (2002), web link, <http://www.earn.dote.hu/parp.html>.
- Walker, P. R., and Sikorska, M. (1997). New aspects of the mechanism of DNA fragmentation in apoptosis. *Biochem. Cell Biol*, **75(4)**, 87-299.
- Wang, X. (2001). The expanding role of mitochondria in apoptosis. Review. *Genes and development.*, **15**, 2922-2933.
- Whitley, G., Ashton, S., Balarajah, G., Cartwright, J., Dash. P., Johstone. A., and Prefumo. F. (2004). Reproductive and cardiovascular disease research group, department of biochemistry and immunology at St. George's hospital Medical School, London.  
Weblink, <http://www.sghms.ac.uk/depts/immunology/~dash/apoptosis/caspases.html>.
- Wills, P., Hickey, R., Ross, D., Cuddy, D., and Malkas, L. (1996). A novel in vitro model system for studying the action of ara-C. *Cancer Chemother Pharmacol.* **38(4)**, 366-372.
- Wolf, B. B., and Green, D. R. (1999). *J. Biol. Chem.*, **274**, 200049-200052.
- Wyllie, A. H., Kerr, J. F., and Currie, A. R. (1980). Cell death: the significance of apoptosis. *Int. Rev. Cytol.*, **68**, 251-306.
- Wyllie, A. H., Morris, R. G., Smith, A. L., Dunlop, D. (1984). Chromatin cleavage in apoptosis: association with condensed chromatin morphology and dependence on macromolecular synthesis. *J. Pathol*, **142**, 67-77.
- Wyllie, A. H. (1987). Apoptosis: cell death in tissue regulation. *J. Pathol.*, **153**, 313-316.

Yasuhara, N., Eguchi, Y., Tachibana, T., Imamoto, N., Yoneda, Y., Tsujimoto, Y. (1997). Essential role of active nuclear transport in apoptosis. *Genes cells*, **2**, 55-64.

Zamzami, N., Susin, S. A., and Kroemer, G.. (2002). Mitochondria in apoptosis: Pandora's Box. *Apoptosis the molecular biology of programmed cell death*.

Zheng, T. S., Hunot, S., Kuida, K., and Flavell, R. A. (1999). Caspase knockouts: matters of life and death. *Cell Death Differ.*, **6**, 1043-1053.

Zörnig, M., Hueber, A., Baum, W., Evan, G. (2001). Apoptosis regulators and their role in tumorigenesis. Review. *Biochimica et Biophysica Acta*, **1551**, F1-F37.